Title
The development of topographic maps in the mammalian central visual system

Author
Owens, Melinda Tsaoying

Publication Date
2011

Peer reviewed|Thesis/dissertation

The development of topographic maps in the mammalian central visual system

by

Melinda Tsaoying Owens

DISSERTATION

Submitted in partial satisfaction of the requirements for the degree of

DOCTOR OF PHILOSOPHY

in

Neuroscience

in the

GRADUATE DIVISION

of the

UNIVERSITY OF CALIFORNIA, SAN FRANCISCO

Acknowledgements

I would like to thank my research advisor, Dr. Michael P. Stryker; my scientific collaborators, Dr. David Feldheim and Dr. Jason Triplett at the University of California, Santa Cruz and Dr. Mark Henkemeyer and Dr. Sonal Thakar at the University of Texas, Southwestern; my committee and everyone who has read and commented on the work published in this dissertation; and finally my parents James Owens and Yulin Tsao and my husband Corin Anderson.

Chapter 1 of this thesis has not been published but is being prepared for submission. For this project, Sonal Thakar and Mark Henkemeyer bred, and genotyped all mouse mutants.

Chapter 2 is a reprint of the material as it appears in the journal *Cell*. Jason Triplett, with the assistance of Jena Yamada, bred and genotyped the mice, performed all injections of anatomical tracers, and did all histology. Greg Lemke was the original creator of the mice, and Jianhua Cang was the first person to image a mouse of the genotype described in this paper. David Feldheim and Michael Stryker supervised and directed the research.

The research done in Chapter 3 was a collaboration with Jason Triplett and David Feldheim. They bred and genotyped mice, performed retinal injections, and did all histology.

Chapter 4 has not been published but is being prepared for submission. For this project, Jason Triplett bred and genotyped most of the mice, performed all injections of anatomical tracers, and did all histology. David Feldheim and Michael Stryker supervised and directed the research.

The development of topographic maps in the mammalian central visual system

Melinda T. Owens

Abstract

Connections between sensory areas are often organized using topographic maps, which preserve in the target the neighbor-neighbor relations present in the source. In this dissertation, I use functional imaging, anatomical tracing, and computational modeling to investigate how neural activity and molecular guidance cues interact during neural development to form orderly, precise topographic maps.

The first chapter describes the role of EphB/ephrin-B signaling in shaping topographic maps in the superior colliculus (SC) and primary visual cortex (V1). These molecules have been widely hypothesized to pattern the SC's elevation axis. Functional imaging of EphB signaling mutants did not reveal disruptions in map precision in either area. However, I found changes in the rotation of the maps, suggesting a role for EphB signaling in specifying the overall axes of the map.

The second chapter details the development of the projection from V1 to the SC. In wildtype animals, the corticocollicular projection aligns with the SC's retinotopic map. We use the *Isl2-EphA3*$^{ki/ki}$ mouse, which has a single map of space in V1 and a doubled map in SC, to show that retinal activity early in life is instructive for the proper alignment of this projection.

In the third chapter, we show that the *Isl2-EphA3*$^{ki/ki}$ mutant has a single instead of a doubled cortical map because the projection from the retina to the dorsolateral geniculate nucleus contains only a single map of space.

The fourth chapter reveals unexpected heterogeneity in the functional collicular maps of the *Isl2-EphA3*$^{wt/ki}$ mutant. We show that the EphA levels of this animal are such that it exists at a point of instability, where stochastic processes during development can push map formation locally into one of two structures. Patterned retinal activity, which encourages the maps to be smooth, is necessary for expressing this variability. We propose a general model for how EphA signaling and retinal activity interact in collicular mapping.

Overall, these results illustrate how functional imaging can reveal unexpected aspects of topographic map development. They show that together, neural activity and molecular guidance cues shape many of aspects of map formation in several different visual brain areas.

Table of Contents

Page

Acknowledgements ……. iii

Abstract …… v

Introduction …….. 1

Chapter 1: Knockout of EphB/ephrin-B signaling alters the orientation of the retinotopic map in primary visual cortex without changing the precision of topography ……. 7

Chapter 2: Retinal input instructs alignment of visual topographic maps ……..… 34

Supplemental Information for Chapter 2 …….. 45

Chapter 3: Differences between cortical and collicular map development in *Isl2-EphA3* knock-in mice …… 53

Chapter 4: The origins of structural and functional heterogeneity in a topographic map mutant …… 61

Conclusions ……. 95

List of References …….. 106

List of Figures and Illustrations

Chapter 1: Knockout of EphB/ephrin-B signaling alters the orientation of the retinotopic map in primary visual cortex without changing the precision of topography

Figure 1 …… 28

Figure 2 …… 29

Figure 3 …… 30

Figure 4 …… 31

Figure 5 …… 32

Figure 6 …… 33

Chapter 2: Retinal input instructs alignment of visual topographic maps

Figure 1 …… 35

Figure 2 …… 36

Figure 3 …… 37

Figure 4 …… 38

Figure 5 …… 39

Figure 6 …… 40

Supplemental material for Chapter 2: Retinal input instructs alignment of visual topographic maps

Figure S1 …… 49

Figure S2 …… 50

Figure S3 …… 51

Figure S4 …… 52

Chapter 3: Differences between cortical and collicular map development in *Isl2-EphA3* knock-in mice

Figure 1 …… 60

Chapter 4: The origins of structural and functional heterogeneity in a topographic map mutant

Figure 1 …… 86

Figure 2 …… 87

Figure 3 …… 88

Figure 4 …… 89

Figure 5 …… 90

Figure 6 …… 91

Figure 7 …… 92

Figure 8 …… 93

Figure 9 …… 94

Introduction

The proper functioning of the adult brain depends on events that happen early in development, when each of the billions of neurons that comprise the nervous system must correctly find its partners and make appropriate synapses. In sensory areas, these connections are often organized using topographic maps, which preserve in the target the neighbor-neighbor relations that are present in the source. In the visual system, topographic organization begins naturally in the retina and is maintained in its target structures because neighboring retinal ganglion cells (RGCs) project to neighboring targets in the superior colliculus (SC) (called the optic tectum in non-mammals) or dorsal lateral geniculate nucleus (dLGN). In turn, neighboring dLGN neurons project to neighboring neurons in primary visual cortex (V1), preserving the retina's continuous topographic representation of the visual world through three levels of organization.

Because a projecting structure may be physically quite distant from its targets and the topographic order of neighboring axons is not preserved over such distances, this topographic organization must be created anew in each target structure. This process occurs under the influence of several cues, some of which are activity-dependent and some of which are molecular. Type II retinal waves, which are spontaneous bursts of spiking activity that spread in a wave-like fashion across the developing retinal ganglion cells during the first week of life, act to refine both collicular and cortical topographic maps and contribute to their precision (Cang et al., 2005a). Mice that lack the β2 subunit of the nicotinic acetylcholine receptor (nAChR) have both abnormal retinal waves and deficits in cortical and collicular mapping, particularly in the azimuth (nasotemporal) axis (Bansal et al., 2000; Cang et al., 2005b). The EphA/ephrin-A signaling pathway is also

crucial for guiding axons to the correct positions in the retinocollicular and retino-geniculocortical pathways (Cang et al., 2008b; Cang et al., 2008a; Cang et al., 2005a; Feldheim and O'Leary, 2010). The tyrosine kinase receptors EphAs and their membrane-bound ligands the ephrin-As are present across the nasotemporal axis of the eye, the anterior-posterior axis of the SC, and the mediolateral axis of V1 as opposing counter-gradients and act as positional labels to guide incoming axons to their approximate positions (Marcus et al., 1996; Flenniken et al., 1996; Flanagan, 2006; Cang et al., 2008b; Cang et al., 2005a). Together, the EphA/ephrin-As and retinal waves explain almost the entirety of the map of the azimuth axis in the colliculus and cortex (Cang et al., 2008a; Cang et al., 2008b).

Although the factors that influence the formation of the azimuth axis are well understood, there is considerable debate and uncertainty about the mechanisms most important for mapping of the elevation (dorsoventral) axis. Even in mutants with very little or no topographic order in the azimuth axis, the map of the elevation axis is little affected, implying that mapping of these two axes is independent (Cang et al., 2008a; Cang et al., 2008b). It is known that axons in the optic tract are already somewhat presorted along the elevation but not the azimuth axis (Plas et al., 2005). Several studies have proposed candidates for the molecules responsible for elevation mapping in the SC/ optic tectum, including Wnt3a, Sema3, and ALCAM and its receptor L1 (Schmitt et al., 2006; Liu et al., 2004; Buhusi et al., 2008; Buhusi et al., 2009). However, by far the most popular hypothesis has been that elevation signaling is controlled by signaling through EphBs and their ligands, the ephrin Bs. Mice express these molecules in a mediolateral gradient across the developing SC, consistent with a role in elevation mapping, and

mutants that are deficient in the EphBs may exhibit ectopic laterally-located termination zones in the SC, showing that loss of the molecules affects RGC branching within the colliculus (Hindges et al., 2002; McLaughlin et al., 2009). In the experiments described in chapter 1, we probed the role of EphBs and ephrin-Bs in SC map formation by performing functional imaging of the SCs of various mutant mice with compromised EphB or ephrin-B signaling. Given that EphA/ephrin-A signaling is important for both retinocollicular and retinogeniculocortical mapping, we also wanted to know whether topographic mapping was disrupted in the V1 of these mice. Contrary to expectations, we found no quantitative change in the precision of topographic maps of the superior colliculus of animals with even severe disruptions of EphB signaling. Map precision in primary visual cortex was similarly unaffected. However, the overall structure of the maps in superior colliculus and V1 was altered: disrupting EphB signaling altered the angles the azimuth and the elevation maps made with each other. In V1, elevation maps were frequently rotated abnormally far towards the midline, opposite to the direction in which cortical maps are rotated in mice lacking ephrin-As (Cang et al, 2005a). These results suggest that the overall role of EphB and ephrin-B signaling is to influence the global orientation of these maps instead of the precision of topography.

The most studied models of visual map formation, the retinocollicular/retinotectal projection and to a lesser extent the retinogeniculocortical projections, have looked at the creation of maps that receive feed-forward input from the retina. However, higher visual areas also make connections with each other; such links are important for integrating information from various brain areas and allow organisms to analyze multiple visual attributes of objects and comprehend the outside world (Mesulam, 1998). The

corticocollicular projection, which goes from V1 to the SC, provides a link between two major streams of visual processing: the retinocollicular pathway, used for some reflexive visual behaviors, and the retinogeniculocortical pathway involved in conscious vision. The SC, which is an integrative midbrain center, is organized into several layers, each of which has distinct sources of innervation and afferent targets (May, 2006). RGCs project to the most dorsal layer of the SC, the upper stratum griseum superficiale (SGS), while axons from V1 terminate in a deeper layer of the SGS (lower SGS). The V1 projection is organized so that it is in register with the retinocollicular map (Drager and Hubel, 1976). In the second chapter, we explore how the corticocollicular projection aligns with the SC's retinotopic map by using the *Isl2-EphA3*$^{ki/ki}$ mouse. This mouse possesses two copies of the *Isl2-EphA3* knock-in allele, which means that it over-expresses EphA3 in the spatially random subset of its RGCs that express *Isl2* (Brown et al., 2000). Because mapping is based on relative, not absolute, levels of EphAs, in this mouse, the Isl2^{+} RGCs project to one end of the colliculus and the Isl2^{-} neurons go to the other, creating two maps of space (Brown et al., 2000). We established that this mutant has a single map of space in the cortex, which meant that we could study its corticocollicular projection to distinguish between molecular-gradient-based and retinal-matching-based models of map alignment. We found that the cortical projection in the *Isl2-EphA3*$^{ki/ki}$ mouse splits so it can innervate both maps in the SC, suggesting that input from the retina is instructive for its proper development. In support of this hypothesis, we see that alignment occurs after the retinal map is established but before eye opening and that reduction or removal of retinal input alters corticocollicular mapping. Most importantly, we show that disrupting retinal waves in this mouse by knocking out β2 prevents map alignment, leaving the

cortical projection to terminate abnormally broadly but centered in the position that would be normal in wildtype mice. Taken together, these data suggest that the V1 projection aligns with a pre-existing retinocollicular map by matching activity patterns.

The third chapter is an investigation of why the cortical and collicular maps in *Isl2-EphA3*$^{ki/ki}$ mouse are so different. By performing retrograde labeling from the cortex to the dLGN and anterograde tracing from the retina to the dLGN, we show that the origin of the cortex's single map is the presence of only a single map of space in the retinogeniculate projection. We conclude that despite similarities in how they create topographic maps, the development of the retinogeniculate and the retinocollicular projections must engage different mechanisms, at least with respect to RGCs that express *Isl2*.

In wildtype animals, retinotopic maps are smooth, precise, and stereotyped. Map variability occurs when the projections to a structure are grossly abnormal, as in the case of primary visual cortex of the Siamese cat, or when major guidance cues are missing, as in the collicular maps of mice lacking all of the ephrin-As present in SC: the inputs to a map overwhelm the ability of the cues present in those maps to corral them into a smooth, regular organization (Cang et al., 2008b; Kaas and Guillery, 1973). In the last chapter, we use functional imaging to uncover unexpected map heterogeneity in the *Isl2-EphA3*$^{wt/ki}$ mouse. This mouse is heterozygous for the *Isl2-EphA3* allele and thus expresses only half as much EphA3 as the *Isl2-EphA3*$^{ki/ki}$ mouse used in the previous chapters. The heterogeneity in maps could not be explained by purely genetic factors, since multiple map structures could be present within one animal or even one map. Using functioning imaging and computational modeling, we also showed that the heterozygous *Isl2-EphA3*

knock-in mouse exists at a point of instability: changing the over-expression levels of EphA3 even slightly caused map structures to be much less diverse. Retinal waves were also necessary for the presence of map variability. We develop an account of collicular map formation that describes how a precise combination of molecular guidance cues and patterned neural activity can reveal the stochastic process inherent in map formation and lead to map heterogeneity

In this dissertation, I study how patterned retinal activity and Eph/ephrin signaling shape topographic projections and maps in a number of different models: the retino-collicular projection, the retinogeniculocortical pathway, and the corticocollicular projection. Using optical intrinsic signal imaging, I characterize for the first time the functional topographic maps of several different mutant mice with altered Eph and ephrin signaling. By crossing some of those mutants with β2 knockout mice, I analyze how those Eph and ephrin mutations affect mapping in the presence and absence of retinal waves. I combine these results from functional imaging with those from anatomical tracing techniques and computational modeling to form a fuller picture of topographic map development in these systems, shedding light on how long-range connections are organized in the brain as a whole.

Knockout of EphB/ephrin-B signaling alters the orientation of the retinotopic map in primary visual cortex without changing the precision of topography

Melinda T. Owens[1,2], Sonal Thakar[3], Mark Henkemeyer[3], Michael P. Stryker[1,2] *

[1]Neuroscience Graduate Program, [2]Physiology, UCSF, San Francisco, CA;

[3]Developmental Biology, UT Southwestern, Dallas, TX

SUMMARY

EphBs and their ligands the ephrin-Bs have been hypothesized to control the mapping of the elevation axis of topographic visual maps in the superior colliculus. Here, we use functional imaging of intrinsic signals to show that in superior colliculus, even severe disruptions of EphB and ephrin-B signaling do not change the precision of the map. Map precision in primary visual cortex was similarly unaffected. However, in both superior colliculus and cortex, such disruptions can cause a novel rotation of the elevation map towards the midline. These findings indicate that the role of EphB/ephrin-B signaling in visual topographic mapping is to guide the formation of the structure of the visual map as a whole without affecting the creation of precise topography within the map.

INTRODUCTION

During development, each of the billions of neurons that make up the human brain must correctly find its partners and make appropriate synapses. In sensory areas,

these connections are often organized using topographic maps, which preserve in the target the neighbor-neighbor relations that are present in the source. As an example, in the visual system, topographic organization begins naturally in the retina, and it is maintained in its target structures because neighboring retinal ganglion cells (RGCs) project to neighboring targets in the superior colliculus (SC) (called the optic tectum in non-mammals) or dorsal lateral geniculate nucleus (dLGN). In turn, neighboring dLGN neurons project to neighboring neurons in primary visual cortex (V1), preserving the retina's continuous topographic representation of the visual world through three levels of organization.

Because a projecting structure may be physically quite distant from its targets and the topographic order of neighboring axons is not preserved over such distances, this topographic organization must be created anew in each target structure. This process occurs under the influence of several cues, some of which are activity-dependent and some of which are molecular. In both the retinocollicular and the retinogeniculocortical pathways, spontaneous waves of spiking activity that spread across the developing retinal ganglion cells during the first week of life act to refine topographic maps and contribute to their precision (Cang et al., 2005b). In addition, in both of these pathways, the EphA /ephrin-A signaling pathway is also important for guiding axons to the correct positions (Cang et al., 2008b; Cang et al., 2008a; Cang et al., 2005b; Feldheim and O'Leary, 2010).These molecules are present in opposing gradients in sources and targets, guiding incoming axons to arborize at appropriate locations (McLaughlin and O'Leary, 2005).Together, the EphA/ephrin-As and retinal waves explain almost the entirety of the map of the azimuth (nasotemporal) axis (Cang et al., 2008a; Cang et al., 2008b).

However, even in mutants with very little or no topographic order in the azimuth axis, the map of the elevation (dorsoventral) axis is almost unaffected, implying that mapping of these two axes is independent (Cang et al., 2008a; Cang et al., 2008b).There is considerable debate and uncertainty about the mechanisms most important for mapping of the elevation axis. Axons in the optic tract are already somewhat presorted along the elevation but not the azimuth axis (Plas et al., 2005). For the retinal projection to the SC/optic tectum, in which the elevation axis is represented mediolaterally, there is evidence that a mediolateral gradient of Wnt3a controls mapping through the Ryk and Frizzled receptors, that a gradient of Sema3 encourages RGCs to terminate laterally, and that interfering with either the cell adhesion molecule ALCAM or its receptor L1's interaction with ankyrin causes ectopic, laterally-located termination zones in mice with normal retinas (Schmitt et al., 2006; Liu et al., 2004; Buhusi et al., 2008; Buhusi et al., 2009). However, by far the most popular hypothesis has been that elevation signaling is controlled by signaling through EphBs and their ligands, the ephrin Bs. Mice express ephrin-B1, EphB1, EphB2, and EphB3 in a mediolateral gradient across the developing SC, consistent with a role in elevation mapping (Hindges et al., 2002). Mice that are deficient in EphB1, EphB2, and/or EphB3 may exhibit ectopic laterally-located termination zones in the SC in early life, showing that loss of the molecules affects RGC branching within the colliculus (Hindges et al., 2002; McLaughlin et al., 2009).

Mapping methods based on anatomical tracers are useful for showing topographic disturbances at a small number of positions or at a particular range of length scales. However, only functional techniques such as optical imaging of intrinsic signals (OIS) can reveal the structure of an entire SC or V1 map at once at a range of length scales

(Cang et al., 2008a; Cang et al., 2008b). We have begun to test the hypothesis that EphB and ephrin-B signaling plays a role in topographic mapping in the SC by imaging the SCs of various mutant mice with compromised EphB or ephrin-B signaling. Given that EphA/ephrin-A signaling is important for both retinocollicular and retinogeniculocortical mapping, we also wanted to know whether topographic mapping was disrupted in the V1 of these mice. Contrary to expectations, we found no quantitative change in the precision of topographic maps of the superior colliculus of animals with even severe disruptions of EphB signaling. Map precision in primary visual cortex was similarly unaffected. However, the overall structure of the maps in superior colliculus and V1 were altered: disrupting EphB signaling altered the angles the azimuth and the elevation maps made with each other. In V1, elevation maps were frequently rotated abnormally far towards the midline. These results suggest that the overall role of EphB and ephrin-B signaling is to influence the global orientation of these maps instead of the precision of topography.

RESULTS

EphB and ephrin-Bs in the mammalian brain

The EphBs form a family of tyrosine kinases that bind to the transmembrane ligands the ephrin-Bs. Mammals express five EphBs (EphB1-4 and EphB6) and three ephrin-Bs (ephrin-B1-3); for the most part, any EphB can bind to any ephrin-B, and vice versa, making the functions of each protein partially redundant. Since the EphBs are crucial for aspects of development as disparate as blood vessel morphogenesis and cell positioning in the gastrointestinal tract, it is not surprising that they play a role in the formation of the nervous system, including the visual system (Pitulescu and Adams,

2010). Previous work has showed that ephrin-Bs and EphBs are expressed in the retina and superior colliculus in a gradient fashion. EphB1, EphB2, and EphB3 are all expressed most strongly in the ventral part of the retina, while ephrin-B1 and B2 are expressed most strongly dorsally (Hindges et al., 2002; Williams et al., 2003). In the SC, where the elevation axis is represented mediolaterally, EphB2 and EphB3 are expressed most strongly laterally in the SC, as opposed to the expression of ephrin-B1 and B3, which are expressed most strongly medially (Hindges et al., 2002). Therefore, opposing gradients of EphBs and ephrin-Bs are present in the visual system in a way that is consistent with their directing topographic mapping in the elevation axis.

Maps in the superior colliculus of EphB mutants are of normal quality but are rotated

The presence of a gradient does not mean that the molecule in question is necessary for map formation. Therefore, to look at the functional effect of EphB signaling in forming the topographic map of the superior colliculus, we performed optical imaging of intrinsic signals in various EphB mutants and their wildtype littermates. To visualize functional maps, we showed anesthetized mice drifting bars on a computer monitor 25cm away from the eye contralateral to the hemisphere being imaged (Fig 1A). The bars were swept along the D-V or N-T axes to stimulate constant lines of elevation or azimuth, respectively. By extracting the optical signal at the stimulus frequency using a Fourier method, we computed the response magnitude and timing in relation to the stimulus cycle, which can then be converted to the location in visual field (Cang et al., 2008a; Kalatsky and Stryker, 2003). Using this method, we found that all collicular maps, even those from animals that were missing four out of the five EphBs present in

mammals (quadruple knockouts missing EphBs 1, 2,3 and 6; hereafter, qKOs), were of grossly normal shape and topography (Fig 1D-G). We quantitatively compared the SC maps of wildtype mice from the EphB mutant mouse colony to those from qKOs, which had the least remaining EphB signaling of all the mutants we analyzed and thus ought to have the most impairment. Neither SC map size nor peak amplitude differed between the elevation maps of qKOs and wildtypes (Fig. 1H,I). The SC size of wildtypes (n=3) was 1.13± 0.04 mm^2 versus 1.15± 0.05 mm in qKOs (n=4); the peak amplitude in the elevation maps of wildtypes was 1.6± 0.7 $x10^{-4}$ fractional change in reflection versus 1.9± 0.6 $x10^{-4}$ in qKOs. To quantitatively analyze topography, we computed map scatter, which is a measure of how much the phase of the average pixel in the map derived from functional imaging differs from its neighbors. We found that qKOs and wildtype animals also did not differ in the amount of scatter in their maps, even their elevation maps (Fig. 1J). Wildtypes had an average azimuth map scatter of 10.3± 7.1 degrees and an average elevation scatter of 3.3±2.1 degrees, while qKOs had an azimuth scatter of 7.7± 3.3 degrees and an elevation scatter of 2.7± 2.1 degrees. (Scatters derived from azimuth maps is larger and more variable than those derived from elevation maps because the template used for analysis of both maps was based on the strongest pixels of the elevation maps.) The lack of change in map scatter in these qKO animals, which are missing most of their EphBs throughout their bodies, strongly indicates that the EphBs do not affect topographic mapping on a large scale in the superior colliculus.

However, in some mutants, another anomaly was present: the horizontal and vertical meridians did not lie at the usual angle to each other. In wildtype animals, the representations of the horizontal and vertical meridians of the maps are close to

orthogonal, with a mean angle of 83± 4^{O} between them. However, in qKOs animals, the mean angle is significantly different, 73± 4^{O} (p=0.01) (Fig. 1K). The disruption of three of these EphBs, 1, 2, and 3, caused a difference in mean angle, to 73± 6^{O}, that just barely missed significance (p=0.06, n=3). However, the rotation was dependent on the loss of at least three three EphBs: animals with disruptions of only two, EphB2 and EphB3, had inter-meridian angles that were not significantly different from those in wildtype, 80± 8^{O} (p=0.50, n=4). (Note: In these latter two types of mutant, the disruption in the EphB2 was not achieved with a null allele but instead with an allele of EphB2, EphB2-lacZ, that is missing its cytoplasmic tail (Henkemeyer et al., 1996).) These results suggest that although loss of EphBs does not influence the precision of the map, it does change its overall structure.

Rotations of the cortical map in mice missing EphB2 and EphB3

Given that mapping mechanisms may not be the same in the superior colliculus and in visual cortex (Triplett et al., 2009), we also looked in primary visual cortex to see whether alterations of EphB signaling affected topographic mapping there. We found that qKOs had maps in V1 of normal size, peak amplitude, and map scatter (Fig 2A-C), indicating that even severe disruptions of EphB signaling did not affect these parameters. (In qKOs (n=4), mean size was 2.40± 0.16mm^2, peak amplitude of the elevation map was 1.4± 0.4x10^{-4}, and elevation map scatter was 2.4± 2.2^{O}, while in wildtypes (n=8), mean size was 2.19± 0.62 mm^2, peak amplitude was 1.8± 0.6, and scatter was 2.5± 2.6^{O}.) However, some individuals presented with rotated elevation maps. In the primary visual cortex of wildtype animals, the horizontal and vertical meridians of the maps are present

at a mean angle of 78 ±6^{O} (n=22) between them (Fig. 3A,B). In contrast, many mutant animals that had disrupted EphB2 and EphB3 signaling had a much smaller angle between the horizontal and vertical meridians, with inter-median angles as low as 55^{O} (Fig C-F). The angle that the vertical meridian made compared to the midline seemed to be what changed the most; the angle of the horizontal meridian altered comparatively little. In addition, several of these mutants had other alterations in map structure, such as a split near the rostral end of V1, which were never seen in wildtype mice. (The map split is circled in red in Fig 3H.)

We defined a "rotated map" as one with an inter-median angle of less than 67.1^{O}, which is two standard deviations below the mean seen in wildtype animals (Fig 4A, in black). Using this definition, we found that greater disruption of EphB signaling was generally correlated with a higher frequency of rotated maps. Single knockouts of EphB2 or EphB3 alone never had rotated maps (n=3 and n=5, respectively) (Fig 4A, in purple and blue, respectively). However, the loss of four EphBs (1, 2, 3, and 6) increased the frequency of rotated maps to around 50% (3 of 6 animals) (Fig. 4A, in red). Intermediate levels of disruptions of EphB signaling gave intermediate frequencies of rotations. One of the two double knockouts of EphB2 and EphB3 had a rotated map (Fig. 4A in green). Animals missing EphB1 and 3 and with the EphB2-lacZ allele showed a rotation frequency of rotation of 2 of 6 (Fig. 4A in orange). Importantly, the level of EphB signaling disruption did not affect the degree of rotation, only the frequency of getting rotated maps. Indeed, one of the largest amounts of rotation (53^{O}) was seen in an animal that was only an EphB2/3 double knockout.

Loss of forward signaling by EphB2 is necessary for map rotation

Although rotated maps were seen in EphB1/B2-lacZ/B3 mutants and in EphB1/2/3/6 qKOs, no rotated maps were seen in EphB1/3/6 knockouts (n=6), implying that loss of EphB2 is necessary for rotated maps (Fig. 4A, in gray). Because the EphB receptors can signal in both the forward (into the receptor-expressing cell) and reverse (into the ligand-expressing cell) directions, and because signaling in different directions may have different roles, we wanted to know whether the cortical rotation phenotype depended on forward or reverse signaling (Pitulescu and Adams, 2010; Cowan and Henkemeyer, 2002). To that end, we analyzed the cortical maps of EphB3 knockout mice that also had mutations in EphB2 that disabled specific protein domains. We chose mutants bred on an EphB3 null background because cortical rotation was never seen with the loss of EphB2 alone. Animals that homozygous for the EphB2-lacZ allele, which is missing its cytoplasmic tail and thus lacks all forward signaling but can still bind to ephrin-Bs and activate reverse signaling, had a high frequency of map rotation (3 of 8 mice imaged) (Fig 4B, in brown) (Henkemeyer et al., 1996). Since this result implies that forward signaling by EphB2 is necessary for correct cortical orientation, we explored different aspects of that forward signaling. The cytoplasmic tail of EphB2 contains, among other domains, a tyrosine kinase domain, which is responsible for kinase activity, and a PDZ binding motif, which is responsible for the recruiting and binding of other proteins in the cell that contain PDZ domains; in some systems, these domains have distinct roles (Genander et al., 2009). Mice homozygous for the EphB2^{K661R} allele, which contains a point mutation that inactivates the kinase domain, also displayed map rotation (2 of 5 animals imaged) (Fig. 4B, in blue) (Genander et al., 2009). In contrast, mice

homozygous for the EphB2$^{\Delta VEV}$ allele, which lacks the last three amino acids of the cytoplasmic tail and cannot bind to PDZ-containing proteins (Genander et al., 2009), never display map rotation (n=4) (Fig. 4B, in red). Curiously, mice with an allele, EphB2^{KVEV}, that has both of these mutations also do not display map rotation (n=9) (Fig. 4B, in purple) (Genander et al., 2009). Overall, it appears that loss of the kinase activity component of forward signaling is specifically responsible for cortical map rotation, although additional loss of the PDZ domain can rescue this phenotype.

Loss of Ephrin-B1 is important for map rotation

Given that loss or disruption of EphBs leads to map rotation, we wanted to know which of their ligands, the ephrin-Bs, was most important for this phenotype. We analyzed mutants of ephrin-B1, -B2, and -B3. To delete ephrin-B1, mice carrying ephrin-B1-loxP alleles were crossed with a Krox20-Cre line expressing Cre recombinase in the germline, ensuring that ephrin-B1 was missing in every cell in the body (Davy et al., 2004). Complete knockouts of ephrin-B2 die early in embryonic development because of ephrin-B2's role in angiogenesis (Wang et al., 1998). Instead, we looked at two lines of mice with a reduced capacity for ephrin-B2 reverse signaling. One line was heterozygous for ephrin-B2-lacZ, an allele of ephrin-B2 that has no capacity for reverse signaling because it lacks most of ephrin-B2's cytoplasmic tail, and the other line possessed one copy of the ephrin-B2-lacZ allele and one copy of the ephrin-B2$^{6YF\Delta V}$ allele, which is missing the part of the intracellular domain that interacts with SH2 and PDZ domains (Dravis and Henkemeyer, 2011; Dravis et al., 2004). For ephrin-B3, we used a simple knockout (Yokoyama et al., 2001). Ephrin-B1 knockout mice had a high frequency of

cortical map rotation, with 3 of 6 animals imaged being affected (Fig 4C, in blue.). In contrast, neither the ephrin-B3 knockouts nor either line of ephrin-B2 mutants had a high frequency of rotation (1 of 5 for the ephrin-B3 null, 0 of 6 for the ephrin-B2-lacZ/+ line, and 1 of 9 for the more severely mutated ephrin-B2-lacZ/ ephrin-B2$^{6YF\Delta V}$ line) (Fig. 4C, in light green, dark green, and red, respectively). Therefore, loss of ephrin-B1, while not affecting the quality of topographic mapping, is most likely to lead to rotation of the cortical map.

Alterations in cortical mapping do not correlate with defects in collicular mapping

Because of the redundancy present among the EphBs and ephrin-Bs, phenotypes involving the loss of these genes rarely have full penetrance. For example, in no genotype analyzed did the proportion of animals displaying a cortical rotation defect exceed 50%. We wanted to find out whether individual animals with a rotated cortical map, which we know have enough of a functional deficit in EphB or ephrin-B signaling to display a cortical phenotype, were more likely to display a collicular map precision phenotype as well. Analysis of this question was possible because all animals whose colliculi were imaged had previously undergone cortical imaging. We compared the map size, peak amplitude, and map scatter of maps from wildtype animals to those from any animals with a cortical rotation defect regardless of genotype. We found no difference in any of these measures (Fig. 5A-C). (For wildtypes (n=3), average size was 1.13± 0.04mm^2, peak amplitude in elevation was 1.6± 0.7 x10^{-4}, and scatter in elevation was 3.3± 2.1 degrees; for animals with rotated cortical maps (n=8), size was 1.10± 0.10mm^2, peak amplitude was 1.9± 1.0 x10^{-4}, and scatter was 3.4± 2.2 degrees.) These results, which show no

collicular map precision deficits even in the animals that possess another EphB or ephrin-B-related phenotype, imply that disruptions in EphB or ephrin-B signaling truly do not affect the precision of topographic mapping in the SC.

We saw that altered EphB/ephrin-B signaling could change the inter-meridian angle in both collicular and cortical maps. Theoretically, defects in the optics of the eye could account for the distorted maps. However, if EphB/ephrin-B signaling were acting through this mechanism, individual animals should have similar inter-meridian angles in both their collicular and cortical maps. To see if this were the case, we measured the correlation between the inter-meridian angles of the collicular and cortical maps of each individual animal (Fig 6). We included all individuals of the genotypes analyzed in this paper that had both collicular and cortical maps (32 animals in total). The correlation of the inter-meridians angles was not significantly different from zero (r^2 of 0.01, p=0.56), showing that the loss of EphB or ephrin-B signaling acts independently on the collicular and cortical maps and implying that EphB's site of action is downstream of the retina.

DISCUSSION

The orderly and organized way the continuous topographic representation of the visual world present in the retina is preserved throughout the visual system is a key model for the study of axon guidance and topographic map formation. In our experiments, we have analyzed the role of EphB and ephrin-B signaling in the development of visual topographic projections to the superior colliculus and to primary visual cortex. Using functional imaging, we found that although disruption of EphB and ephrin-B signaling did not affect topographic precision in the superior colliculus or primary visual cortex, it

could cause an abnormal rotation of these maps. In cortex, the penetrance of this phenotype increases as more signaling is disrupted through the loss of more EphBs, and its presence depends the most on the loss of ephrin-B1 and the loss of kinase activity from EphB2.

Presence of ectopic termination zones in animals with ordered functional maps

Although this study did not look for the presence of ectopic termination zones in the superior colliculi of these mutant animals, extensive previous work has shown that such zones are common in knockouts of multiple EphBs (Hindges et al., 2002). Those studies use animals from the same source as the ones used in this paper, making it unlikely that our animals would lack these ectopic termination zones. It seems logical that improper anatomical mapping on the local scale of individual RGC axons would, when multiplied across the entire SC, lead to altered large-scale functional mapping. Indeed, BMPR mutant mice, which have ectopic termination zones because of alterations of dorsoventral specification in the retina, have abnormal collicular receptive fields, and mutants with disrupted signaling in the EphA/ephrin-A pathway have both ectopic termination zones anterior or posterior to the correct site of termination and disorganized functional maps of azimuth (Plas et al., 2008; Chandrasekaran et al., 2009; Cang et al., 2005a; Feldheim et al., 2000). However, in EphB and ephrin-B mutants, the presence of ectopic termination zones does not seem to be linked to the precision of topographic mapping, implying that some other factors must ensure that an orderly, large-scale functional map arises despite abnormalities in the underlying anatomy.

A previous study showed that alterations in EphB signaling particularly affect axons from the ventral retina, which go to the medial part of the superior colliculus (McLaughlin et al., 2009). The techniques used in the present experiments, however, reveal the full mediolateral extent of the rostral SC, so topographic mapping disruptions present only in the medial part of the SC would still be expected to be visible. It has also been shown that the ectopic termination zone phenotype is not fully penetrant. However, animals with increasing numbers of mutant EphB alleles are increasingly likely to have ectopic termination zones, with animals possessing five mutant alleles of either EphB1, 2, or 3 having a frequency of these close to 90% (McLaughlin et al., 2009). The quadruple knockout mice we imaged each had eight mutant alleles (two null alleles each of EphB1, 2, 3, and 6), making it very likely that nearly every one of them had such ectopic termination zones. Therefore, the fact that clear, ordered maps were found in the SC of qKOs cannot be blamed on regional variations in ectopic termination zone formation or the low penetrance of the ectopic termination zone phenotype.

Instead, it is likely that these ectopic termination sites are not contributing to the functional image. One possibility is that the ectopic termination sites are pruned later in life. Anatomical tracing studies are generally done around postnatal day 8 (P8), while functional imaging studies cannot be performed earlier than eye-opening and are usually postponed until after P40, when the visual system is mature. Although we did not look for ectopic termination zones in our older mice, it is known that under normal conditions, the refinement of contralaterally-projecting RGC axon arbors in the SC is finished by P8 and that in at least in one other mapping mutant, pruning of ectopic branches does not occur after this point (McLaughlin et al., 2003; Dhande et al., 2011). Therefore, it is less

likely that these ectopic sites are physically pruned. Another possibility is that neural signals from these ectopic termination sites are ignored or functionally suppressed when the map as a whole is activated. It is known that the V1 cortical maps of "Midwestern" Siamese cats can suppress large amounts of aberrant geniculate input in order to form smooth and precise maps, but little is known about functional suppression in SC (Kaas and Guillery, 1973). However, it is known that collicular receptive fields in another mutant with elevation mapping defects, the BMPR knockout mouse, can respond to the wrong location in elevation and can be split, patchy, or distorted (Chandrasekaran et al., 2009). It would be interesting to monitor the output of individual collicular neurons in EphB and ephrin-B mutant animals, perhaps by using single-unit recording techniques, to tell whether they get input from one or two locations in the visual field and then to model how responses of the individual neurons add up to the full map.

Origin of elevation mapping

If the EphB/ephrin-B signaling system is not responsible for the precision of topographic mapping in the elevation axis, what is? Very little is known about the mechanisms that govern elevation mapping in V1. On the other hand, several candidates for mapping in the SC have put forward, including Sema 3, Wnt3a and its receptors Ryk and Frizzled, and L1 and its ligand ALCAM (Schmitt et al., 2006; Liu et al., 2004; Buhusi et al., 2008; Buhusi et al., 2009). Although these molecules all are present in mediolateral gradients across the SC and their manipulation can alter the places where and how RGCs terminate, this study shows that the presence of ectopic termination zones does not necessarily imply that the large-scale functional map is disordered. More work is

needed to see whether disruptions of any of these other candidates alters the precision of topographic mapping on a wide scale, whether in the SC alone or also in cortex.

Orientation of visual maps

This study has found that disruption of EphB signaling can cause changes in the inter-meridian angle in superior colliculus and abnormal rotation of the topographic map in primary visual cortex towards the midline. Even though the vertical and horizontal meridians are orthogonal to each other in the real world, their representations in the maps of some EphB or ephrin-B mutant mice are not. The fact that these rotated maps with non-orthogonal axes are still orderly and precise suggests that neural activity, which refines maps, operates on a local scale even when a map is disturbed in its overall structure (Cang et al., 2005b). Curiously, while cortical elevation maps in EphB mutants are rotated towards the midline, cortical maps in ephrin-A2/3/5 triple knockouts are rotated abnormally in the opposite direction (Cang et al., 2005a). Our findings are consistent with the hypothesis that the normal alignment of visual maps is a compromise between distinct molecular gradients for the azimuth and elevation axes that are not at right angles. Under the influence of neural activity, such a map would become coherent and assume an intermediate orientation. In cortex, we would presume that the two opposing gradients would consist of EphB/ephrin-B and EphA/ephrin-A. In the superior colliculus, one of the gradients would be EphB/ephrin-B, but its opposing gradient is currently unknown.

The rotation phenotype in cortex is not fully penetrant, as only 50% of quadruple knockouts display a rotated map. In addition, for any given genotype that displays rotated

maps, the range of map rotations can be very broad. The EphBs are highly redundant, and it is possible that the remaining EphB, EphB4, might be able to compensate for the lack of the other EphBs in the qKOs. According to the Allen Brain Atlas, EphB4 is not highly expressed in visual cortex during adulthood or in the telencephalon before birth or in the first week of life; nevertheless, its expression might be upregulated when the other EphBs are missing (Allen Developing Mouse Brain Atlas, 2009). Another possibility is that EphB/ephrin-B signaling is not the only factor that resists the rotation of the map towards the midline, although so far no other candidates have been found that rotate the cortical map in that direction. The extent to which EphB4 or the unknown other factors are upregulated or utilized in each animal may determine the presence and extent of rotation. Investigating these possibilities will have to await the breeding of quintuple EphB knockouts or the creation of a dominant-negative reagent against the EphBs that can be applied *in vivo* over the first week of life, when the axons from the dLGN grow into V1 to form the topographic map (Lopez-Bendito and Molnar, 2003).

The presence of a rotated cortical map, which is a visible consequence of disrupted EphB or ephrin-B signaling, did not imply the presence of an imprecisely-mapped collicular map. Individuals with rotated cortical maps had collicular maps of the same size, peak amplitude, and scatter as wildtype mice. In addition, the inter-meridian angles of individual animal's collicular and cortical map did not correlate, suggesting that retinotopic map formation in each of these areas proceeds independently. This finding echoes that of (Triplett et al., 2009), which found that mice with severely altered maps of space in the colliculus could have normal cortical maps. Our study confirms that despite sharing a dependence on ephrin-A signaling, the processes of topographic mapping in V1

and in the SC are not identical and can be affected independently of each other (Cang et al., 2008a; Cang et al., 2005a).

Conclusions

These experiments provide strong evidence that EphB/ephrin-B signaling does not play a role in achieving topographic map precision in either primary visual cortex or in the superior colliculus. They do, however, reveal a role for these molecules in determining the orientation of these visual maps. Our data illustrate how using functional measures of topographic mapping that can capture the organization of a whole structure at once complements the use of traditional anatomical tracers in elucidating map structure and development.

METHODS

Mice

Mice used in this study included *EphB1* knockouts (Williams et al., 2003), *EphB2* knockouts, *EphB2*-lacZ mice (Henkemeyer et al., 1996), *EphB2*^{K661R}, *EphB2*$^{\Delta VEV}$, *EphB2*^{KVEV} point mutants (Genander et al., 2009), *EphB3* knockouts (Orioli et al., 1996), *EphB6* knockouts (Shimoyama et al., 2002), *ephrin-B1* conditional mutants (Davy et al., 2004), *ephrin-B2*-lacZ mice (Dravis et al., 2004), *ephrin-B2*$^{6YF\Delta V}$ mice (Dravis and Henkemeyer, 2011), and *ephrin-B3* knockouts (Yokoyama et al., 2001). To generate mice missing ephrin-B1, ephrin-B1-loxP mice were crossed with a Krox20-Cre line that expresses Cre in the germline, ensuring that ephrin-B1 was knocked out everywhere in the animal. Mice were maintained on a mixed 129/CD1/ C57Bl6 background. Roughly

60% of mice with EphB and 20% of mice with ephrin-B disruptions were imaged and analyzed blind to genotype. Findings from blind and witting experiments were similar. All mouse protocols were performed in accordance with the University of Texas Southwestern and University of California San Francisco IACUC standards.

Functional Imaging

Imaging of intrinsic optical signals was performed as described previously in adult mice older than 40 days of age (Cang et al., 2008a; Kalatsky and Stryker, 2003). For imaging of the cortex, two anesthesia regimens were used. Mice were either anesthetized with isoflurane (0.8%) supplemented with chlorprothixene (0.003 mg/kg) given intramuscularly and imaged through the skull, or they were injected intraperitoneally with urethane (1.0 g/kg in 10% saline solution) supplemented with chlorprothixene (0.03 mg/kg) and given a tracheotomy and a craniotomy over the left hemisphere. With either anesthesia regimen, animals were also given atropine (0.3 mg/kg) and dexamethasone (2 mg/kg) subcutaneously. Animals anesthetized with isoflurane were generally revived after cortical imaging, and some underwent further imaging another day. Animals anesthetized with urethane were either euthanized after cortical imaging or prepared for collicular imaging. Collicular imaging was preceded by aspiration of the overlying cortex. Electrophysiological studies demonstrate that ablating or silencing visual cortex does not change receptive field properties of superficial SC neurons (Drager and Hubel, 1976; Schiller et al., 1974). Optical images of the cortical intrinsic signal were obtained at the wavelength of 610 nm, using a Dalsa 1M30 CCD camera (Dalsa, Waterloo, Canada) controlled by custom software. A high-refresh-rate monitor (Nokia Multigraph 4453, 1024 × 768 pixels at 120 Hz) was placed 25 cm away from the animal where it subtended

70° of the contralateral visual field. Drifting thin bars (2° width and full-screen length) were displayed on the monitor. Animals were presented with horizontal or vertical bars drifting orthogonal to the axis corresponding to either the dorsal-ventral or nasal-temporal axis of the animal in order to stimulate the constant lines of elevation or azimuth, respectively.

Analysis of Retinotopic Maps

Topographic maps were analyzed using custom software in Matlab. Size was taken to be the response area of the elevation map within 30% (for cortex) or 15% (for SC) of the peak magnitude. To measure map quality, we measured both peak amplitude and map "scatter." To calculate scatter, we identified the 20,000 pixels (representing 1.6mm^2), for cortex, or the 10,000 pixels (representing 0.80mm^2), for the SC, with the strongest response in the elevation map. For each of these pixels, we calculated the difference between its phase value and the mean phase value of its surrounding 25 pixels (including itself). For maps of high quality, the phase differences are quite small because of smooth phase progression. To measure map "rotation," we approximated the representation of the vertical and horizontal meridians as lines and calculated the smaller of the two angles the lines made as they crossed. Statistical tests were performed as indicated in the figure legends.

REFERENCES

Please refer to the global list of references in this dissertation.

ACKNOWLEDGEMENTS

This work was supported by grants from the NIH (R01-EY02874 to M.P.S. and R01-EY017434 to M.H.). M.T.O was supported by an NSF Graduate Research Fellowship and an NIH Training Program for the Visual Sciences (T32-EY007120). We thank Sam Pleasure, Erik Ullian, and members of the Stryker and Henkemeyer labs for discussion and critical reading of the manuscript.

Figure 1

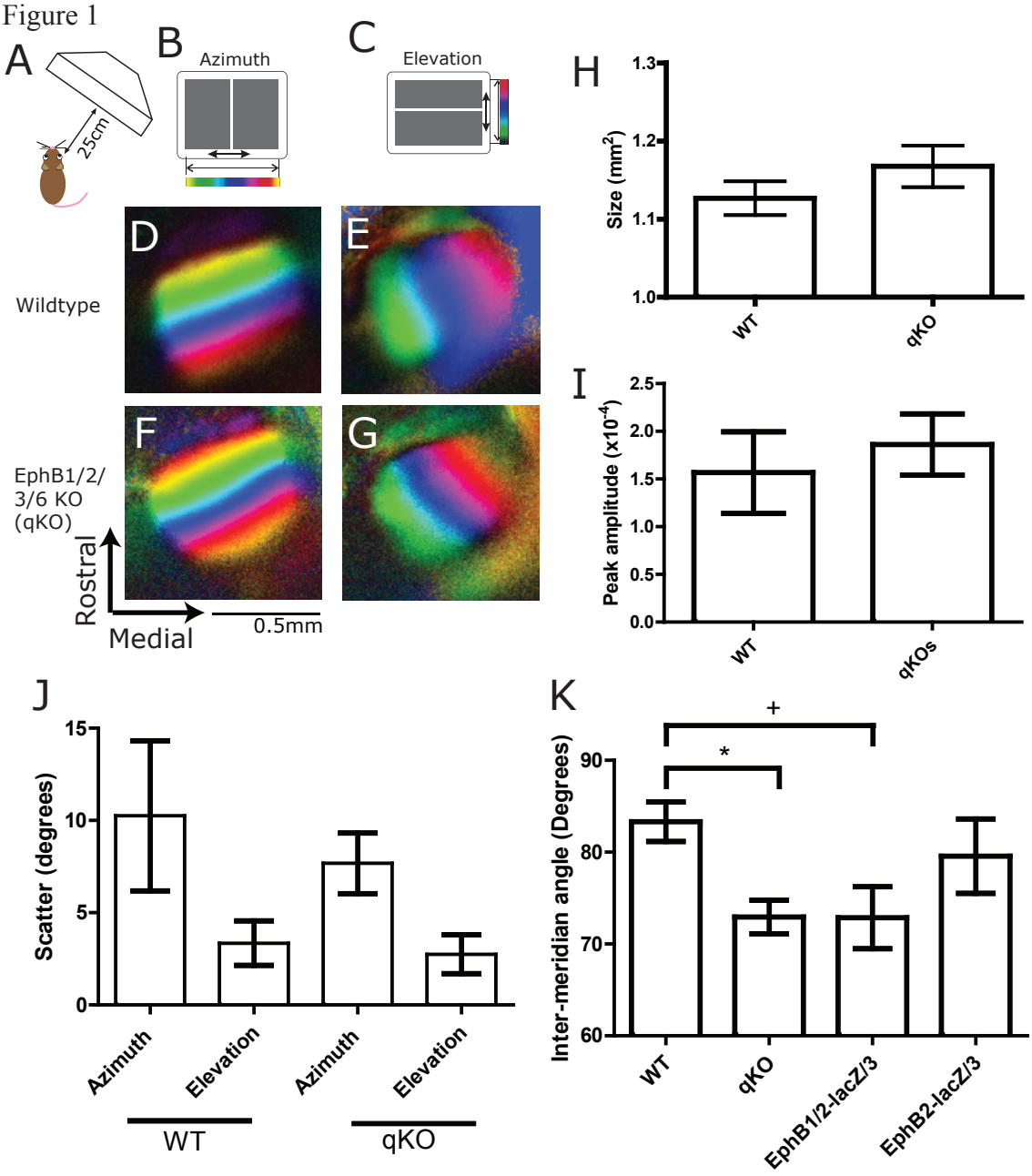

Figure 1: A. A stimulus monitor is placed 25cm away from the anesthetized mouse, contralateral to the hemisphere being imaged. B-E. Collicular azimuth (D) and elevation (E) maps of a wildtype mouse. The color code used to represent positions of different lines on the stimulus monitor is illustrated in panel B for azimuth and C for elevation. F-G. Azimuth (F) and elevation (G) maps of a representative EphB1/2/3/6 qKO mouse. H. Size of SC map in WT vs. qKO animals. I. Peak amplitude as a fractional change of reflection in the elevation maps of WT vs. qKO mice. J. Map scatter in the azimuth and elevation maps of WT vs. qKO mice. K. Inter-meridian angle for WT, qKO, EphB1/B2-lacZ/B3, and EphB2-lacZ/B3 mice. * is significant at the p=0.05 level. + is not significant, p=0.06. All significances tested with a two-tailed Student's t-test.

Figure 2

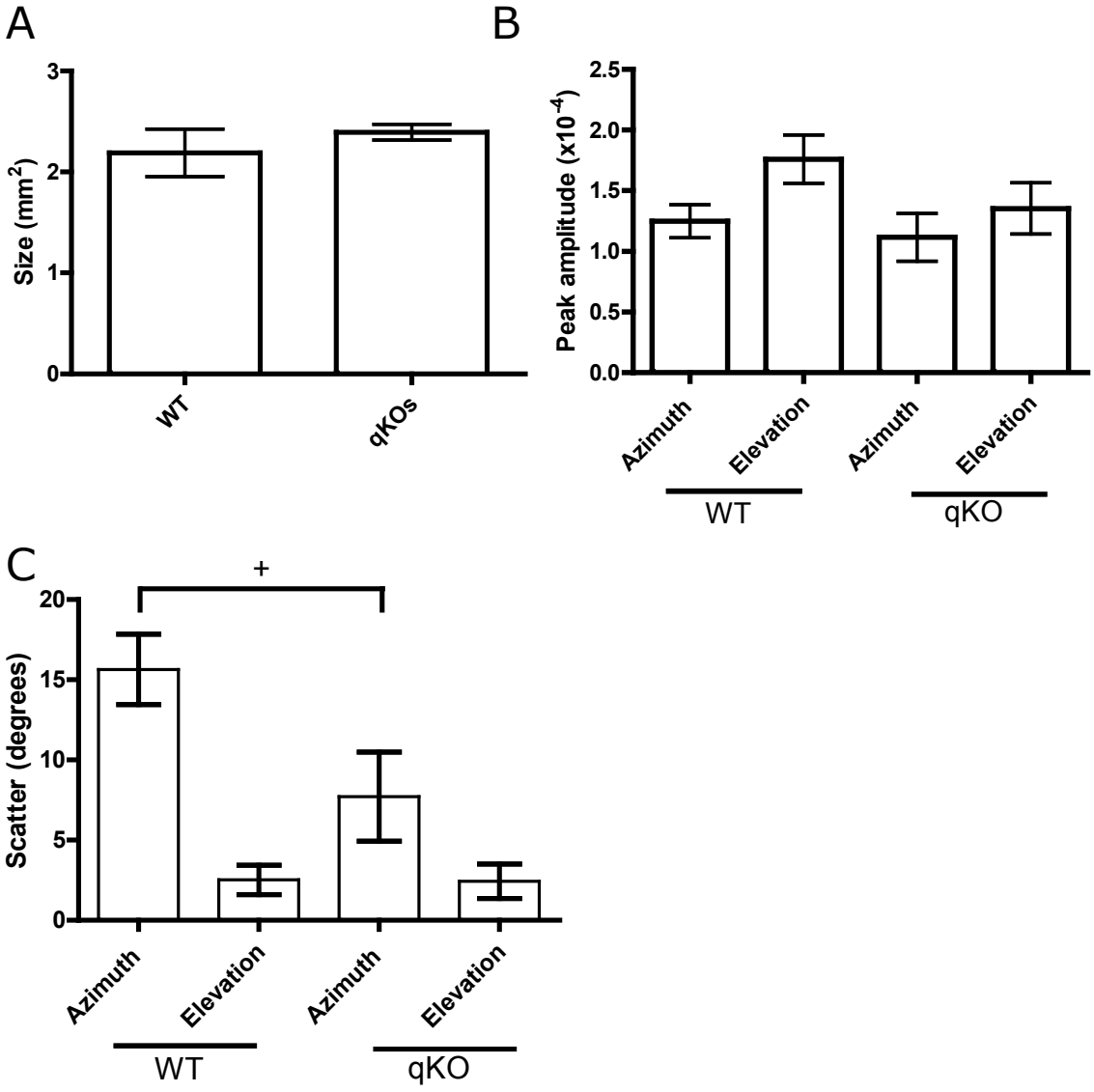

Figure 2: A. Size of V1 map in WT vs. qKO animals. B. Peak amplitude of the azimuth and elevation maps as a fractional change of reflection in WT vs. qKO mice. C. Map scatter in the azimuth and elevation maps of WT vs. qKO mice. + is non-significant (p=0.06). All significances tested with a two-tailed Student's t-test.

Figure 3

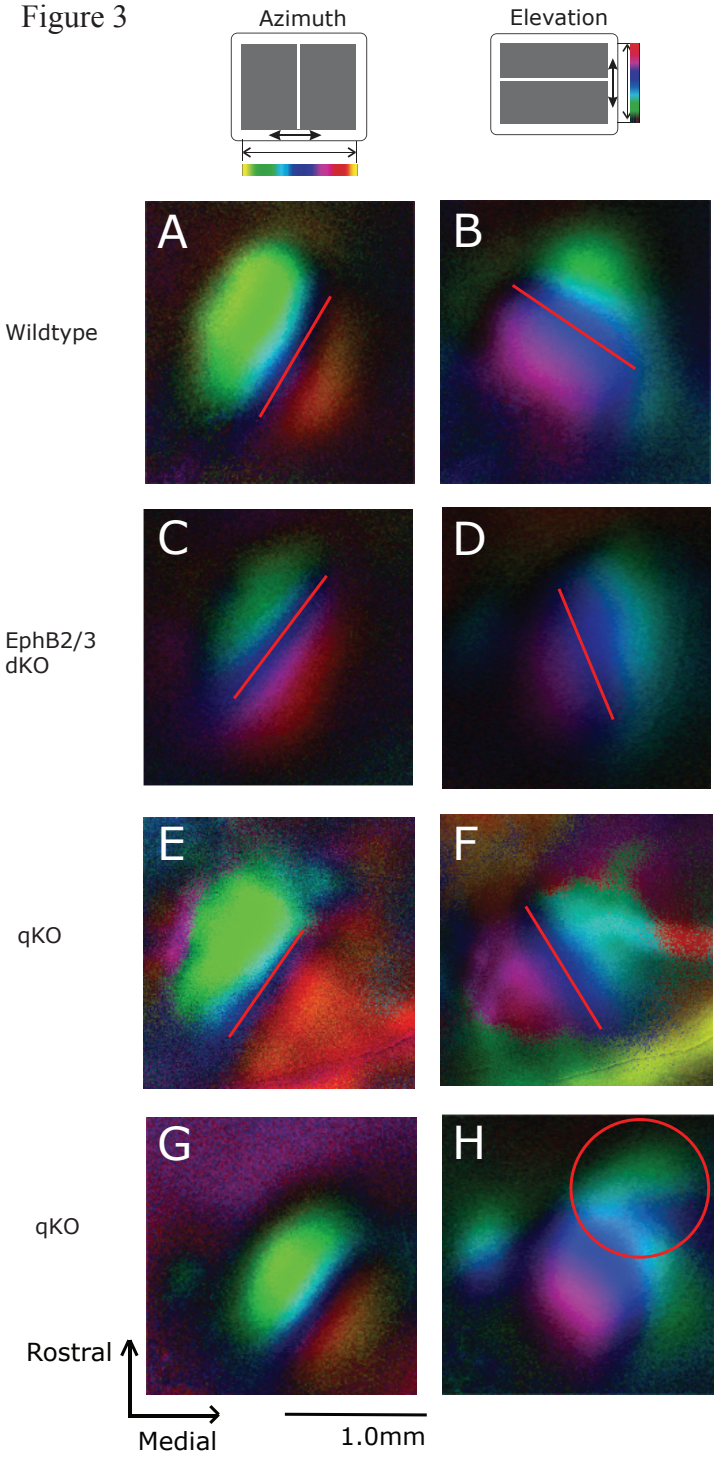

Figure 3: A-B. Azimuth (A) and elevation (B) maps of the V1 of a wildtype mouse. The horizontal (in A) and vertical (in B) meridians are outlined in red for better visualization. C-D. The azimuth (C) and elevation (D) maps of the V1 of an EphB2/3 double knockout mouse with a rotated cortical map. E-F. The azimuth (E) and elevation (F) maps of the V1 of a qKO mouse with a rotated map. G-H. The azimuth (G) and elevation (H) maps of another qKO mouse. The area of elevation map abnormality is circled in red in H.

Figure 4

A

EphB	1	2	3	6
Wildtype				
B2 KO		X		
B3 KO			X	
B2/3 dKO		X	X	
B1/B2-lacZ/B3 KO	X	lacZ*	X	
B1/2/3/6 qKO	X	X	X	X
B1/3/6	X		X	X

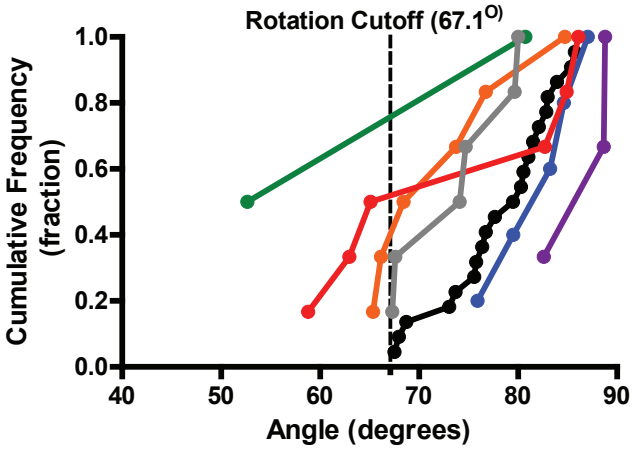

B

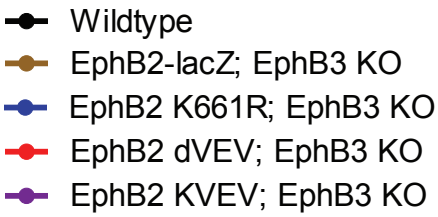

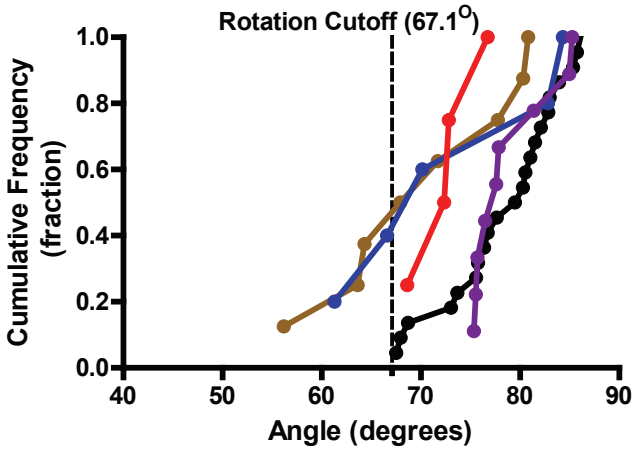

C

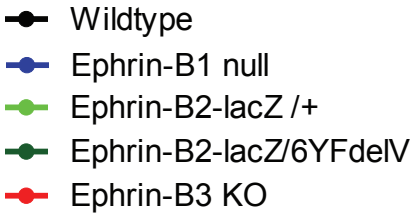

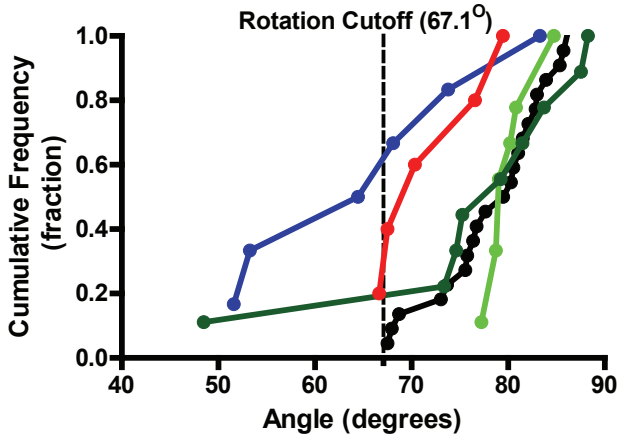

Figure 4: A. Inter-meridian angles of the cortical maps of various EphB knockouts and mutants, shown as a cumulative frequency plot. Line at 67.1° shows the cutoff for determining whether a map is "rotated." Legend on the left illustrates which EphBs are deleted in each mutant. *: EphB2-lacZ allele lacks EphB2's cytoplasmic tail. B. Inter-meridian angles of cortical maps of various EphB2 mutants. C. Inter-meridian angles of various ephrin-B mutants.

Figure 5

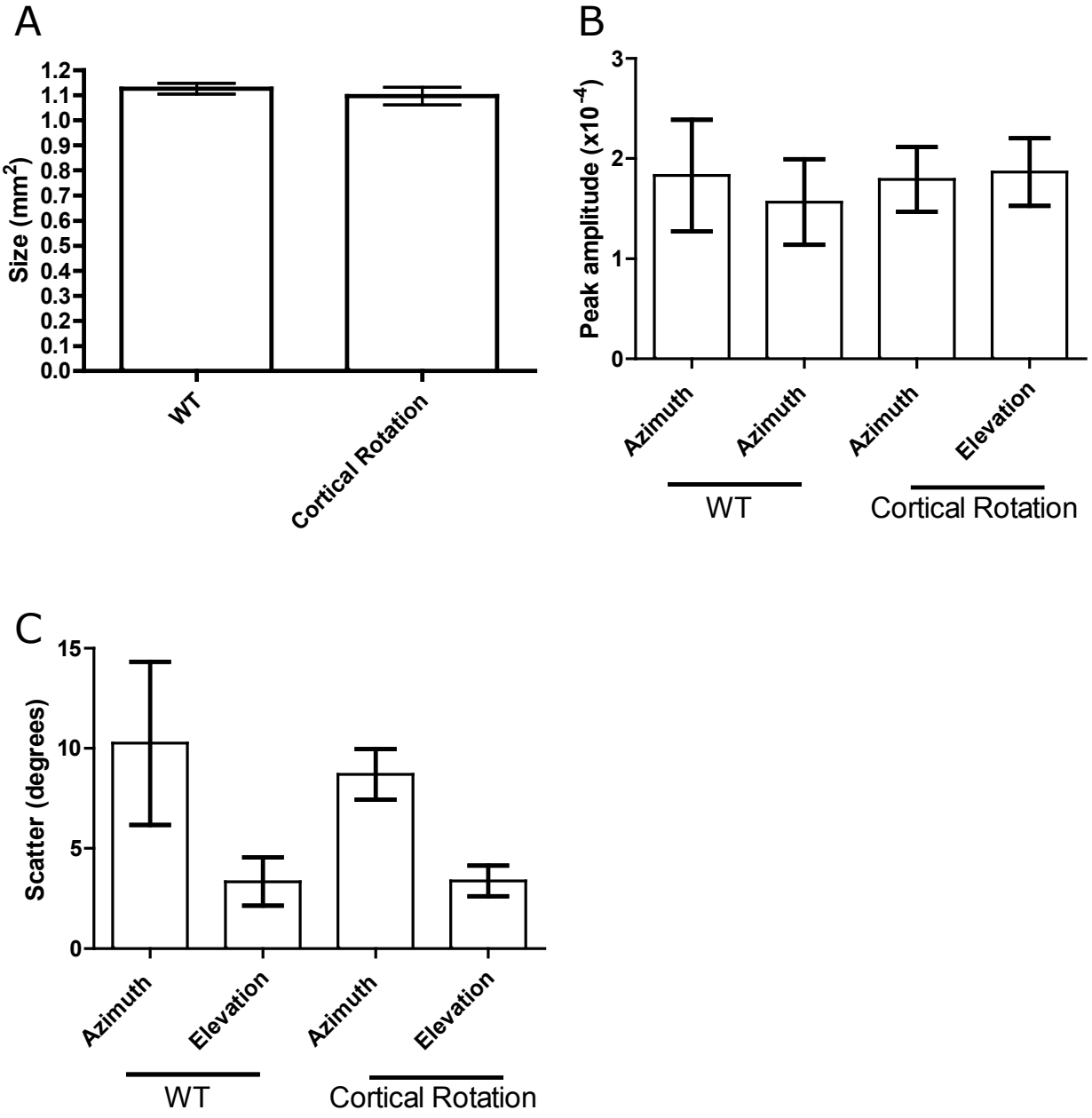

Figure 5: A. Size of the SC in wildtype mice compared to all mice with a rotated cortical map. B. Peak amplitude as a fractional change of reflection in the azimuth and elevation maps of WT mice vs. mice with a rotated cortical map. C. Map scatter in the azimuth and elevation maps of WT mice vs. mice with a rotated cortical map. All significances are tested with a two-tailed Student's t-test.

Figure 6

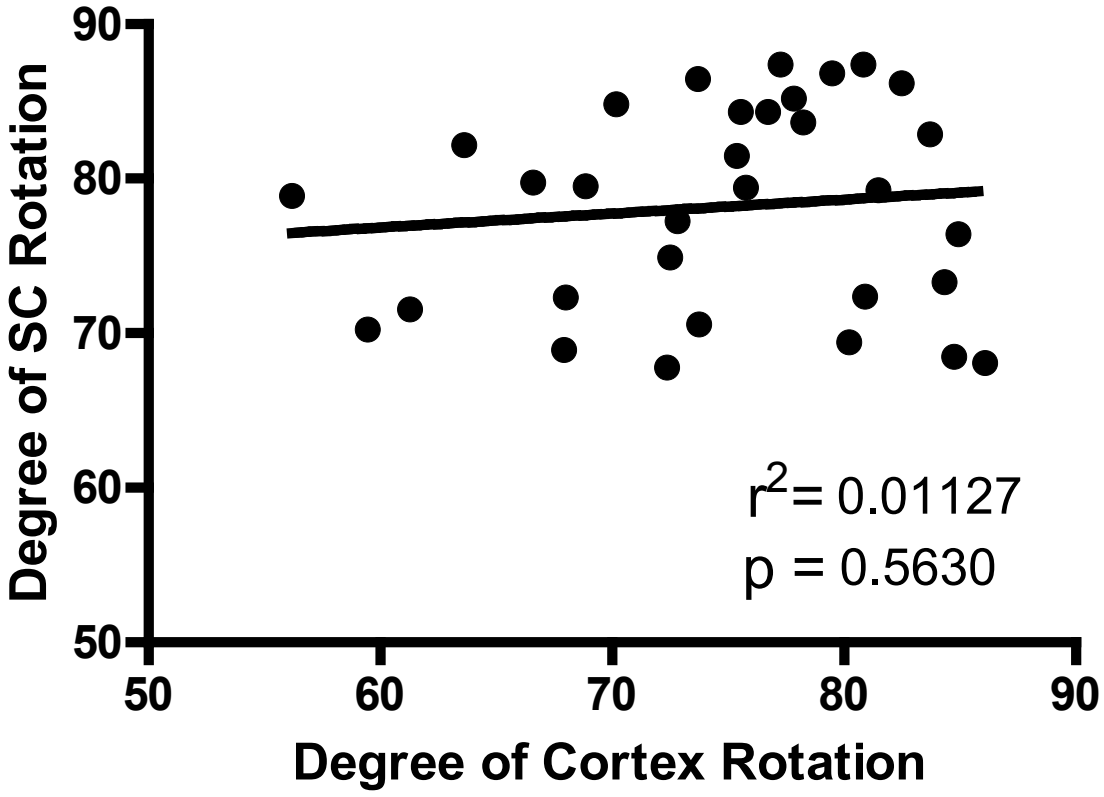

Figure 6: Plot of the inter-meridian angle in cortex vs. the inter-meridian angle in the superior colliculus. Each data point is an individual animal. The p value is from a test of whether the slope is significantly different from zero.

Cell

Retinal Input Instructs Alignment of Visual Topographic Maps

Jason W. Triplett,[1] Melinda T. Owens,[2] Jena Yamada,[1] Greg Lemke,[3] Jianhua Cang,[4] Michael P. Stryker,[2] and David A. Feldheim[1,*]
[1]Department of Molecular, Cell, and Developmental Biology, University of California, Santa Cruz, Santa Cruz, CA 95064, USA
[2]W.M. Keck Foundation Center for Integrative Neuroscience, Department of Physiology, University of California, San Francisco, San Francisco, CA 94143, USA
[3]Molecular Neurobiology Laboratory, The Salk Institute for Biological Studies, La Jolla, CA 92037, USA
[4]Department of Neurobiology and Physiology, Northwestern University, Evanston, IL 60208, USA
*Correspondence: feldheim@biology.ucsc.edu
DOI 10.1016/j.cell.2009.08.028

SUMMARY

Sensory information is represented in the brain in the form of topographic maps, in which neighboring neurons respond to adjacent external stimuli. In the visual system, the superior colliculus receives topographic projections from the retina and primary visual cortex (V1) that are aligned. Alignment may be achieved through the use of a gradient of shared axon guidance molecules, or through a retinal-matching mechanism in which axons that monitor identical regions of visual space align. To distinguish between these possibilities, we take advantage of genetically engineered mice that we show have a duplicated functional retinocollicular map but only a single map in V1. Anatomical tracing revealed that the corticocollicular projection bifurcates to align with the duplicated retinocollicular map in a manner dependent on the normal pattern of spontaneous activity during development. These data suggest a general model in which convergent maps use coincident activity patterns to achieve alignment.

INTRODUCTION

The ability to analyze multiple attributes of the external environment allows for a robust comprehension of the outside world, but the means by which attributes from distinct sources are bound together in the brain presents a significant challenge for neuroscience (Mesulam, 1998; Treisman, 1996). Vision provides information about the size, shape, color, and motion of perceived objects, and each of these qualities may be processed in separate areas prior to integration (Felleman and Van Essen, 1991; Wolfe and Cave, 1999). Neuronal connections responsible for processing visual information are often organized as orderly topographic maps, in which neighbor-neighbor relationships are maintained between brain areas (Chklovskii and Koulakov, 2004; Luo and Flanagan, 2007). Over the past decade, a great deal of work has elucidated many of the molecular and activity-dependent mechanisms responsible for the development of topographic maps (Huberman et al., 2008a). However, little is known about how topographic maps from different brain regions are merged in associative areas.

The mouse superior colliculus (SC) is an integrative midbrain center that controls reflexive head and eye movements. The SC is organized into several layers, each of which has distinct sources of innervation and afferent targets (May, 2005). Retinal ganglion cells (RGCs) project to the dorsal-most layer of the SC, the upper stratum griseum superficiale (SGS), and are organized topographically, such that the nasal-temporal (N-T) axis of the retina projects to the anterior-posterior (A-P) axis of the SC and the dorsal-ventral (D-V) axis of the retina projects along the medial-lateral (M-L) axis of the SC. The SC also receives visual input from the primary visual cortex (V1). V1 axons terminate in a deeper layer of the SGS (lower SGS) and are organized such that they are in register with the retinocollicular map (Dräger and Hubel, 1976). This corticocollicular projection provides a link between the two major streams of visual processing, the retinocollicular pathway, used for some reflexive visual behaviors, and the retino-geniculo-cortical pathway involved in conscious vision.

Two distinct models can explain how the retinocollicular and corticocollicular maps become aligned in the SC (Figure 1). A gradient-matching model postulates that gradients of molecules expressed by both V1 and RGC axons match graded labels expressed in the SC to specify each map (Figure 1A). In this case, corticocollicular mapping is independent of retinocollicular mapping, but because both projections use information provided by the same target molecules, they become aligned. Consistent with this model, there are complementary gradients of expression of EphAs and ephrin-As along the axes corresponding to the azimuth representation: the N-T axis of the retina, the M-L axis of V1, and the A-P axis of the SC. These countergradients direct topographic mapping, such that areas of high EphA expression project to areas with low ephrin-A expression, and areas of high ephrin-A expression project to areas of low EphA expression (Cang et al., 2005a; Feldheim et al., 1998; Frisén et al., 1998; Luo and Flanagan, 2007; Rashid et al., 2005; and Figure 1A). Therefore, temporal RGCs and lateral V1 projection neurons would project to the same A-P location in the SC because they express similar amounts of EphA receptors.

A retinal-matching model for map alignment proposes that Hebbian-type mechanisms (Hebb, 1949) or direct axon-axon

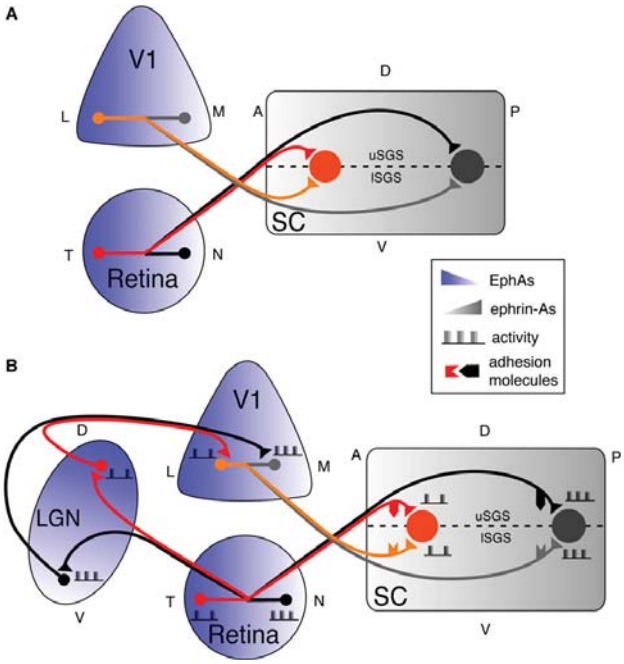

Figure 1. Models of Visual Map Alignment in the Superior Colliculus of the Wild-Type Mouse

(A) Gradient-matching model. Graded expression of EphA receptors (blue) in both the retina and primary visual cortex (V1) are used to guide topographic mapping in the superior colliculus (SC), which expresses repulsive ephrin-A ligands (gray) in a gradient in both recipient layers. N, nasal; T, temporal; A, anterior; P, posterior; D, dorsal; V, ventral; L, lateral; M, medial; uSGS, upper stratum griseum superficiale; lSGS, lower stratum griseum superficiale.

(B) Retinal-matching model. Retinocollicular mapping is established first through the use of graded EphAs and ephrin-As. Then, V1 projection neurons terminate in areas with similar activity patterns or with RGCs expressing complementary cell surface molecules.

interactions are used to direct V1 and RGC axons that monitor the same point in space to terminate in the same region of the SC (Figure 1B). In this model, the retinocollicular map is first established by a gradient-matching mechanism. V1 axons would then form synapses with SC neurons onto which RGCs that share common activity patterns or cell surface molecules synapse. In support of this model, it has been shown that retinal input can be instructive for the alignment of auditory and visual maps in the owl tectum and ferret SC (King et al., 1988; Knudsen and Brainard, 1991). Additionally, in the peripheral nervous system, axon-axon signaling is used to direct the convergent innervation of motor and sensory neuron axons onto a common muscle target (Gallarda et al., 2008).

Here, we show that *Islet2-EphA3* knockin ($EphA3^{ki/ki}$) mice (Brown et al., 2000), have two functional maps in the SC, but a single functional map in V1, providing a tool to distinguish between these models. We find that corticocollicular projections align with both of the duplicated retinocollicular maps in $EphA3^{ki/ki}$ mice, suggesting that retinal input is instructive for corticocollicular topography and map alignment. In support of this, we find that alignment occurs after the retinal map is established but before eye opening, and that reduction or removal of retinal input alters corticocollicular mapping. Furthermore, we show that disruption of spontaneous cholinergic retinal waves in $EphA3^{ki/ki}$ mice prevents map alignment. Taken together, these data suggest that the V1 projection aligns with a pre-existing retinocollicular map by matching activity patterns.

RESULTS

Islet2-EphA3 Knockin Mice Have a Duplicated Azimuth Map in the SC, but Not V1

One of the most striking experiments that demonstrated the importance of EphA receptors in topographic mapping of the retinocollicular projection comes from Brown and colleagues, who showed that $EphA3^{ki/ki}$ mice have duplicated anatomical maps in the SC (Brown et al., 2000). $EphA3^{ki/ki}$ mice ectopically express EphA3 from an internal-ribosome-entry-site cDNA expression cassette placed in the 3′ untranslated region of the *Islet2* gene. This drives expression of EphA3 in about 40% of RGCs scattered in a salt-and-pepper fashion across the retina (Brown et al., 2000), and results in the retina having two populations of RGCs: (1) an $Islet2^{-}$ population that expresses endogenous EphA levels, and (2) an $Islet2^{+}$ population that has EphA3 expression superimposed on top of the endogenous EphA levels. Because RGCs sort topographically along the A-P axis of the SC based on relative EphA levels, these mice have duplicated azimuth maps in the SC, as assessed by anatomical tracing (Brown et al., 2000; Reber et al., 2004).

We asked if the duplicated anatomical maps in these mice were functional, or if instead one of the maps became silenced. To distinguish between these possibilities we used a Fourier method for imaging of intrinsic optical signals of neural activity to visualize the functional maps in the mouse SC (Cang et al., 2008b; Kalatsky and Stryker, 2003). In this method, drifting thin bars are presented on a video monitor placed 25 cm away from an anesthetized mouse, contralateral to the SC being imaged. The bars were swept along the D-V or N-T axes to stimulate constant lines of elevation or azimuth, respectively. By extracting the optical signal at the stimulus frequency, we

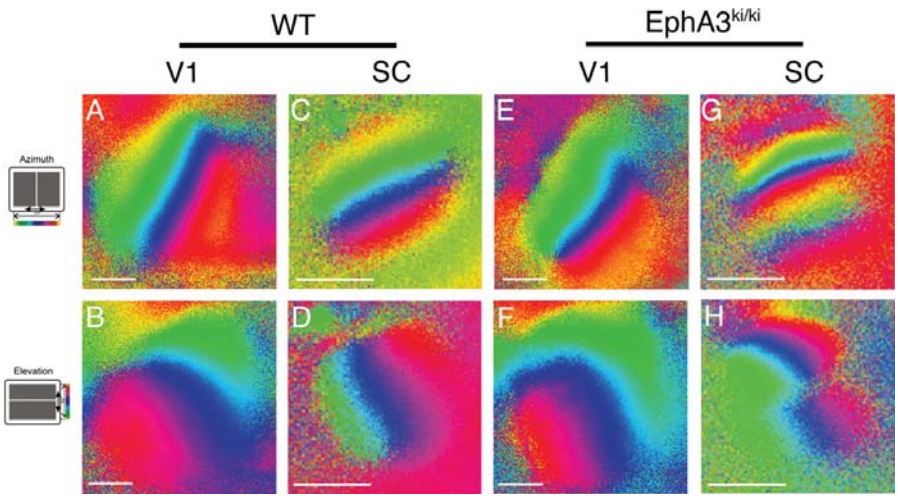

Figure 2. EphA3$^{ki/ki}$ Mice Have Duplicated Functional Maps in the SC and a Single Functional Map in V1

(A–D) Intrinsic optical imaging signal obtained from V1 (A and B) and SC (C and D) of WT adult mice presented a drifting bar stimulus along the azimuth (A and C) or elevation (B and D) axis. Scale bar represents 500 μm.

(E–H) Intrinsic optical imaging signal obtained from V1 (E and F) and SC (G and H) of EphA3$^{ki/ki}$ animals presented a drifting bar stimulus along the azimuth (E and G) or elevation (F and H) axis. Scale bar represents 500 μm.

computed the response magnitude and timing in relation to the stimulus cycle, which can then be converted to the location in visual field. Using this method, we found that wild-type (WT) mice have functional topography along both the azimuth and elevation axes to form single, continuous maps in both the SC and V1 (Figures 2A–2D). By contrast, in EphA3$^{ki/ki}$ mice there were two complete and continuous maps of azimuth (along the A-P axis of the SC) (Figure 2G), which are generally consistent with the anatomical maps of Brown et al. (2000). Each of the maps occupied about half of the SC; however, we detected a stronger signal from the anterior compared to the posterior map (see Figure S1 available online). Imaging of the elevation axis (along the M-L axis of the SC) showed that its map did not duplicate, but a discontinuity in the representation of elevation was observed at the border between the two azimuthal maps (Figure 2H). As a result, the SCs of EphA3$^{ki/ki}$ mice contain two complete maps of the visual field, each with a full representation of azimuth and elevation.

We next asked if the functional V1 map is duplicated in EphA3$^{ki/ki}$ mice. To determine this, we used the same imaging procedure and found that there was always a single topographic map in V1 of EphA3$^{ki/ki}$ mice, similar to those observed in WT animals (Figure 2A, 2B, 2E, and 2F). Therefore, while EphA3$^{ki/ki}$ mice have a duplicated functional map along the N-T mapping axis of the visual field in the SC, they have a single functional map in V1.

In theory, a single functional map in V1 could arise if an early anatomically duplicated map were somehow repaired by the intrinsic connections in the cortex or if one map were silenced, resulting in a single functional map when one measures the responses of cortical cells. To test this possibility, we performed anatomical tracing experiments to determine whether the retinogeniculate and geniculo-cortical projections were duplicated anatomically. We anterogradely labeled subsets of RGCs projecting to the lateral geniculate nucleus (LGN) of the thalamus, and retrogradely labeled LGN cells by injection of tracer in their terminal arbors in V1. In neither case did we find a duplication of the maps (Figure S2). These anatomical findings are consistent with the functional data, showing that RGC axons in EphA3$^{ki/ki}$ mice do not form a duplicated map in the retino-geniculo-cortical pathway.

V1 Projections Split to Align with a Duplicated SC Map in EphA3$^{ki/ki}$ Mice

The fact that EphA3$^{ki/ki}$ mice have a single map in V1 but a duplicated map in the SC allowed us to test models of map alignment in the SC. Because there is ectopic EphA3 expression in RGCs, but not in either V1 or the SC, a gradient-matching model predicts that a single injection of DiI into V1 would trace axons that terminate in the topographically appropriate position of the SC, which would result in a misalignment of the V1 and SC maps. However, a retinal-matching model for alignment predicts that V1 terminations in the SC will align with those of RGC terminations that monitor the identical region of visual space. In this model, a single injection of DiI into V1 of EphA3$^{ki/ki}$ mice would result in two termination zones (TZs) in the SC, with neither TZ

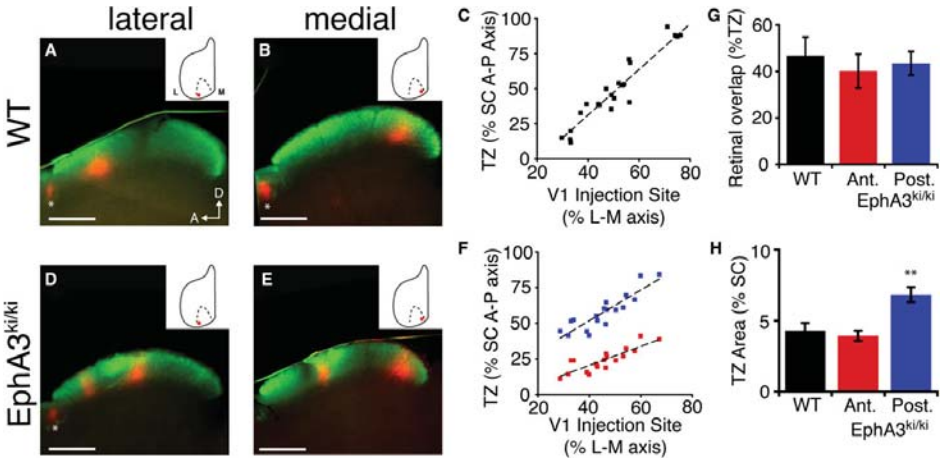

Figure 3. V1-SC Projections Form Two Termination Zones in EphA3$^{ki/ki}$ Mice

(A and B) Parasagittal sections of the SC after focal injection of DiI (red) in V1 and whole eye fill with CTB-488 (green) in the contralateral eye, which labels all RGCs. In WT mice lateral V1 injections result in TZs in the anterior SC, while medial V1 injections give rise to TZs in the posterior SC. *Inserts*: Schematic of V1 injection site; scale bar represents 500 μm; L, lateral; M, medial; A, anterior; D, dorsal; *, pretectal nucleus.

(C) Corticocollicular TZ location expressed as a percent of SC anterior-posterior axis plotted against the V1 injection site, expressed as percent of the lateral-medial axis of the cortical hemisphere. Line represents best-fit regression, $R^2 = 0.9135$, n = 23.

(D and E) Parasagittal SC sections after focal injection of DiI (red) in V1 and whole eye fill with CTB-488 (green) in the contralateral eye, which labels all RGCs. In EphA3$^{ki/ki}$ mice lateral V1 injections result in two termination zones in the anterior and central SC, whereas medial injections result in two termination zones in the central and posterior SC. *Inserts*: Schematic of V1 injection site; scale bar represents 500 μm; *, pretectal nucleus.

(F) Corticocollicular TZ location expressed as a percent of SC anterior-posterior (A-P) axis plotted against the V1 injection site expressed as percent of the lateral-medial (L-M) axis of the cortical hemisphere. Line represents best-fit regression, $R^2 = 0.7828$ and 0.7131 for posterior (blue) and anterior (red) TZs, respectively; n = 18.

(G) Quantification of corticocollicular TZ overlap with the retinal recipient layer in WT and EphA3$^{ki/ki}$ mice. Data are represented as mean and standard error of the mean (SEM), n > 10.

(H) Quantification of corticocollicular TZ area expressed as a percent of SC area in WT and EphA3$^{ki/ki}$ mice. Data are represented as mean ± SEM, n = 18. **p < 0.01 by ANOVA and Tukey's HSD post-hoc analysis.

in the position that would normally be topographically appropriate. To distinguish between these possibilities, we injected DiI focally into V1 of adult (>postnatal day 40 or P40) mice and visualized the V1 terminations in parasagittal SC sections that reveal the N-T mapping axis. In some mice we also labeled all of the contralateral RGC inputs into the SC by injecting fluorescein-conjugated cholera toxin B (CTB-488) into the eye. Corticocollicular TZs were observed in the lower SGS, but we found they overlapped significantly with projections from the retina, because nearly half (46.8% ± 8.0%) of corticocollicular TZ area fell within the region of retinal input (Figure 3G). In adult WT mice, we found that V1 projection neurons map topographically within the SC such that neurons in medial, central, and lateral V1 project to the posterior, central, and anterior SC, respectively, with a linear relationship between V1 injection site and SC TZ location ($R^2 = 0.9135$, N = 23) (Figures 3A–3C).

In contrast to the findings in WT mice, a single injection into V1 of EphA3$^{ki/ki}$ mice always resulted in two TZs in the SC rather than one (18/18 mice) (Figures 3D–3F). Quantification of injection site and TZ locations revealed that V1 axons split into two topographic maps ($R^2_{ant} = 0.7131$, $R^2_{post} = 0.7828$) (Figure 3F). Interestingly, the posterior TZs were approximately twice the area (1.89 ± 0.21-fold) of the anterior TZs, which were similar in size to WT TZs (Figure 3H), suggesting that refinement of the posterior map was incomplete. This difference was consistent with the weaker signal from the posterior map as compared with the anterior map observed during our functional imaging experiments (Figure S1), suggesting there might also be a correlation between retinal input strength and corticocollicular refinement. However, posterior-projecting V1 neurons did not make errors in laminar localization, because overlap with the retinal input layer was similar to that seen in anterior TZs and WT TZs (Figure 3G).

Retinal Input Is Required for Precise Topographic Mapping and Refinement of Corticocollicular Projections

Our functional imaging and anatomical tracing studies in EphA3$^{ki/ki}$ mice suggest an instructive role for RGC input in the alignment of retinocollicular and corticocollicular maps. Previous

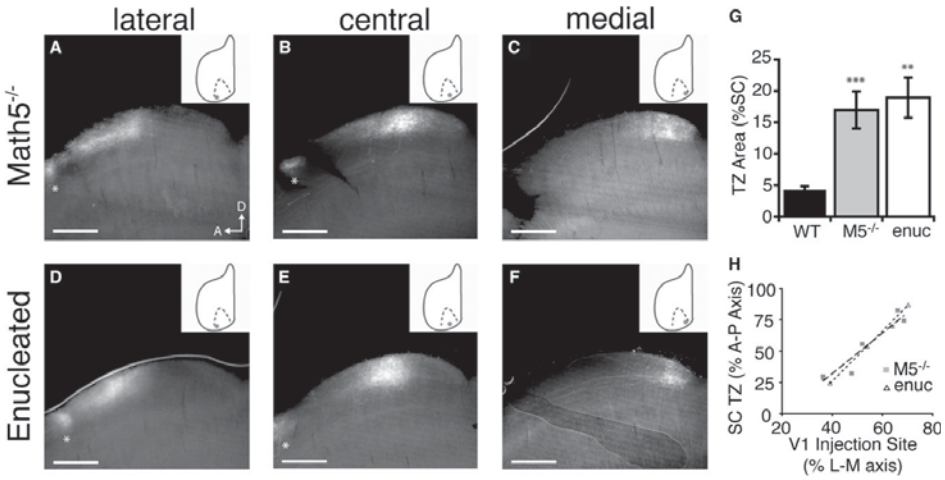

Figure 4. Retinal Input Is Required for Precise Topography of the Corticocollicular Projection

(A–C) Parasagittal SC sections after focal injection of DiI (white) in V1. In Math5$^{-/-}$ mice, injections in lateral, central, and medial V1 result in broad TZs in anterior, central, and posterior SC, respectively. *Inserts*: Schematic of V1 injection site; scale bar represents 500 μm; *, pretectal nucleus; A, anterior; D, dorsal.

(D–F) Parasagittal SC sections after focal injection of DiI (white) in V1. In adult WT mice that were enucleated at P6, injections in lateral, central and medial V1 result in broad TZs in anterior, central, and posterior SC, respectively. *Inserts*: Schematic of V1 injection site; scale bar represents 500 μm; *, pretectal nucleus; A, anterior; D, dorsal.

(G) Quantification of TZ size as a percent of the SC in WT, Math5$^{-/-}$, and enucleated mice. Data are represented as mean ± SEM, n > 3 for each group; because data from anterior and posterior TZs were not significantly different (p = 0.4, n > 3), these data were pooled. ***p < 0.001 versus WT; **p < 0.01 versus WT, Kolmogorov-Smirnov test.

(H) Corticocollicular TZ location expressed as a percent of SC anterior-posterior (A-P) axis was plotted against the V1 injection site expressed as percent of the lateral-medial (L-M) axis of the cortical hemisphere for Math5$^{-/-}$ (gray squares) and enucleated mice (open triangles). Line represents best-fit regression, R^2 = 0.9139 for Math5$^{-/-}$ and R^2 = 1 for enucleated.

studies have shown that removal of retinal input during development or adulthood results in increased corticocollicular plasticity (García del Caño et al., 2002), and that anophthalmic mice have broader corticocollicular TZs compared with WT controls (Khachab and Bruce, 1999). However, neither of these studies performed a detailed analysis of the topographic organization of V1 projections.

To determine whether retinal input was required for V1 projection topography, we assessed corticocollicular maps in two kinds of mice in which the retinal input to the SC is reduced: (1) mice lacking Math5, a basic-helix-loop-helix transcription factor essential for RGC differentiation (Brown et al., 2001), and (2) monocularly enucleated WT mice. Math5 mutant mice have approximately 5%–10% of wild-type levels of RGCs (Lin et al., 2004). These remaining RGCs project to the anterior medial SC and only fill approximately 35% of the SC (C. Pfeiffenberger, J.W.T., and D.A.F., unpublished data). Corticocollicular TZs were approximately four times as large in Math5$^{-/-}$ and enucleated mice compared with WT controls (17.0% ± 3.0% and 18.9% ± 3.2% versus 4.3% ± 0.5%) (Figures 4A–4G). However, rough topography remained intact in both of these mice, with a linear relationship between V1 injection site and the center of the TZ location in the SC (R^2 = 0.9139, N = 7, Math5$^{-/-}$; R^2 = 1, n = 3, enucleated) (Figure 4H). Taken together, these data suggest that when retinal input is reduced or absent, rough corticocollicular topography remains; however, TZ refinement and precise localization are impaired.

Corticocollicular Mapping Occurs after Retinocollicular Mapping and before Eye Opening

For a retinal-matching mechanism to be used, it is advantageous for the retinocollicular neurons to complete map formation prior to the time when V1 axons refine. Previous studies have shown that many RGC axons initially overshoot their eventual collicular TZ before a process of local branching and pruning refines the axons to their final TZ, which finishes by P8 in the mouse (Hindges et al., 2002; McLaughlin et al., 2003; Figures 5E and 5F). We examined the time course of corticocollicular projection mapping by anatomical tracing. We first observed V1 axons in the SC at P6, where they streamed in without a defined TZ (Figure 5A). Over the next week, V1 axons refine to a final TZ by P12 (Figures 5B–5D and 5G). These data indicate that corticocollicular mapping occurs after the retinocollicular map has formed and before eye opening, which occurs at P14–15. Also, they are

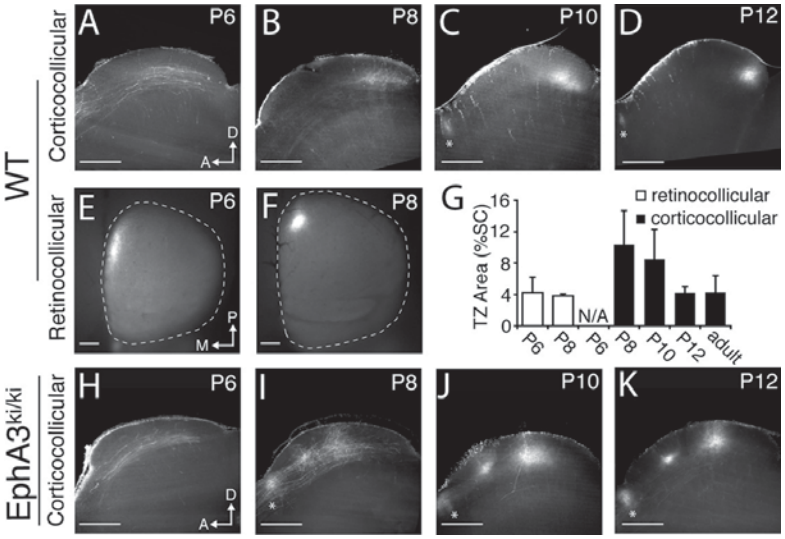

Figure 5. Time Course of Corticocollicular Mapping in WT and EphA3$^{ki/ki}$ Mice

(A–D) Parasagittal SC sections after focal injection of DiI (white) in V1. In WT pups corticocollicular axons were observed as early as postnatal day 6 (P6), and a broad TZ was apparent by P8, which refined further at P10 and completed by P12. Scale bar represents 500 μm; *, pretectal nucleus; A, anterior; D, dorsal.

(E and F) Whole-mount SC images after focal injection of DiI (white) in nasal retina. In WT mice, a broad retinocollicular TZ was apparent at P6 (E), which was fully refined by P8 (F). Scale bar represents 500 μm; M, medial; P, posterior.

(G) Quantification of TZ size as a percent of the SC. Data are represented as mean and standard deviation, n > 3 for each group.

(H–K) Parasagittal SC sections after focal injection of DiI (white) in V1. In EphA3$^{ki/ki}$ pups, corticocollicular axons were observed at P6, and broad TZs were apparent by P8, which refined further at P10 and were complete by P12. Scale bar represents 500 μm; *, pretectal nucleus; A, anterior; D, dorsal.

consistent with the idea that V1 axons sort topographically by matching with a retinocollicular map that is already present.

Cholinergic Activity Is Required for Visual Map Alignment in EphA3$^{ki/ki}$ Mice

Before eye opening, spontaneous activity in the form of correlated bursts of action potentials propagates across the retina in a wave-like manner. Retinal waves progress through three distinct developmental stages that differ in their means of propagation. In mice, the earliest waves begin around embryonic day 16 (E16), propagate quickly, occur with high frequency, and are mediated by gap junctions (Firth et al., 2005; Singer et al., 2001; Syed et al., 2004). Between birth and P10 the middle-stage waves rely primarily upon cholinergic neurotransmission between starburst amacrine cells and RGCs. During this time both wave speed and wave frequency are lower compared with embryonic waves (Bansal et al., 2000; Feller et al., 1996; Syed et al., 2004). Late-stage waves (P10–P15+) depend increasingly on glutamatergic neurotransmission between bipolar cells and RGCs, and coincide with increases in wave speed and frequency (Demas et al., 2006; Wong, 1999). To determine which of these types of activity might be important for map alignment, we examined the time course of corticocollicular projection bifurcation in EphA3$^{ki/ki}$ mice. We found that V1 axons reach the SC by P6 and slowly refine to two termination zones by P12 (Figures 5H–5K), similar to the time course seen in WT mice (Figures 5A–5D). This refinement occurs during the end of the cholinergic middle-stage waves and overlaps the period of the glutamatergic late-stage waves, suggesting that one or both of these types of spontaneous activity patterns could be used for map alignment.

To test the requirement for locally correlated neural activity produced by middle-stage waves in corticocollicular map refinement, we examined whether precise alignment of retinocollicular and corticocollicular maps still occurred in β2 nicotinic acetylcholine receptor subunit knockout (β2$^{-/-}$) mice, in which the pattern of spontaneous retinal activity is dramatically altered (Bansal et al., 2000; McLaughlin et al., 2003; Sun et al., 2008; Xu et al., 1999). We find that the corticocollicular topography is disrupted in these mice almost as much as in Math5$^{-/-}$ and enucleated mice. Single injections of DiI into V1 resulted in diffuse TZs, occupying greater than three times the A-P collicular territory as in WT animals (15.5% ± 1.6% versus 4.3% ± 0.5%) (Figures S3A, S3B, and S3D). Interestingly, we observed that the layer specificity of corticocollicular projections was also disrupted in β2$^{-/-}$ mice, since TZs showed less overlap with

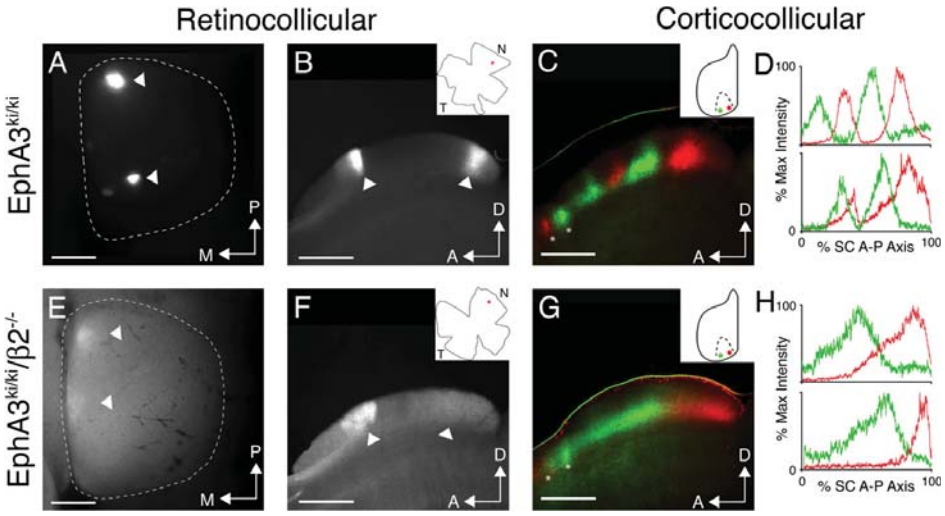

Figure 6. Spontaneous Cholinergic Waves Are Required for Map Alignment in EphA3$^{ki/ki}$ Mice

(A) Whole-mount SC after focal injection of DiI (white) in nasal retina. In EphA3$^{ki/ki}$ mice, two distinct retinocollicular TZs were observed (arrowheads) in the appropriate topographic positions. Scale bar represents 500 μm; M, medial; P, posterior.

(B) Parasagittal section of the SC in (A) revealing two distinct retinocollicular TZs (arrowheads). *Insert*: Schematic of retinal injection site; scale bar represents 500 μm; A, anterior, D, dorsal. Images in (A) and (B) are from the same SC.

(C) Parasagittal SC section after focal injection of DiI (red) and DiA (green) in V1. In EphA3$^{ki/ki}$ mice, each single injection results in two corticocollicular TZs, which are interdigitated. *Insert*: Schematic of V1 injection sites; scale bar represents 500 μm; *, pretectal nucleus; A, anterior; D, dorsal.

(D) Representative intensity profile plots from two EphA3$^{ki/ki}$ mice after focal injection of DiI (red) and DiA (green) in V1.

(E) Whole-mount SC after focal injection of DiI (white) in nasal retina. In EphA3$^{ki/ki}$/β2$^{-/-}$ mice, showing two broad TZs (arrowheads). Scale bar represents 500 μm; M, medial; P, posterior.

(F) Parasagittal section of the SC in (D) showing two broad TZs (arrowheads). *Insert*: Schematic of retinal injection site; scale bar represents 500 μm; A, anterior; D, dorsal. Images in (D) and (E) are from the same SC.

(G) Parasagittal SC section after focal injection of DiI (red) and DiA (green) in V1. In EphA3$^{ki/ki}$/β2$^{-/-}$ mice, each single injection results in a single, broad TZ, which are not interdigitated. *Insert*: Schematic of V1 injection sites; scale bar represents 500 μm; *, pretectal nucleus; A, anterior; D, dorsal.

(H) Representative intensity profile plots from two EphA3$^{ki/ki}$/β2$^{-/-}$ mice after focal injection of DiI (red) and DiA (green) in V1.

retinocollicular projections compared to WT (24.9% ± 6.3% versus 46.8% ± 8.0%) (Figure S3E). However, rough topography was maintained in β2$^{-/-}$ mice (R^2 = 0.9118, n = 10) (Figure S3D), similar to the retinocollicular phenotype observed in these mice (Chandrasekaran et al., 2005).

To determine the precise role of cholinergic spontaneous activity in the alignment of V1 and retinal projections, we crossed the β2$^{-/-}$ mice with EphA3$^{ki/ki}$ mice to create combination mutants (EphA3$^{ki/ki}$/β2$^{-/-}$). Analysis of retinocollicular mapping in these mice revealed that they retained a duplicated map, although each TZ was somewhat broader (Figures 6E and 6F). If map alignment did not depend on the locally correlated activity produced by cholinergic waves and was instead driven by other mechanisms, two broader TZs would be expected from a single V1 labeling. Alternatively, if β2-dependent waves were required for map alignment, we would expect a single rather than a duplicated corticocollicular map, such that labeling of V1 neurons would result in a single, broad TZ in the SC. In every case, we detected only a single, broad TZ for each V1 injection in EphA3$^{ki/ki}$/β2$^{-/-}$ mice (Figures 6G and 6H). Use of two colors to label the origin of two different V1 projection populations revealed that the map was indeed singular, because there was no interdigitation of TZs, as was always observed in EphA3$^{ki/ki}$ mice in which cholinergic activity was not altered (Figures 6C and 6D). These data are consistent with a role for cholinergic middle-stage waves in the retinal instruction of corticocollicular map alignment.

DISCUSSION

In these experiments we have used the projection from V1 to the SC as a model to investigate the mechanisms by which sensory maps become aligned during development. Using a combination of anatomical tracing and functional imaging techniques, we found that the EphA3$^{ki/ki}$ mouse has a duplicated functional map along the azimuth axis in the SC but has only a single

map in V1. Remarkably, the corticocollicular projections in this mouse compensate perfectly for this discrepancy and project to both SC maps to maintain alignment. Both the refinement of the corticocollicular map and its splitting in animals with a duplicated retinocollicular map take place after retinocollicular map refinement and before eye opening. Alignment is blocked in mice that lack the normal pattern of spontaneous retinal activity. Taken together, these results demonstrate that that the visual maps in the cortex and SC are aligned in a multistep process. First, the primary visual connections to the SC and LGN and from the LGN to V1 form topographic maps using a combination of mapping labels, patterned retinal activity, and axon competition, and are well refined by P8 (Cang et al., 2008b; Hindges et al., 2002; McLaughlin et al., 2003; Pfeiffenberger et al., 2006). Following this, V1 neurons project to the SC and are oriented and guided to their normal area of the SC using molecular cues, such as Ephs and ephrins. These axons finally refine to areas of the SC that share similar activity patterns generated by retinal waves.

Functional Duplication of the Azimuth Representation in the SC but Not V1 of EphA3$^{ki/ki}$ Mice

The generation of EphA3$^{ki/ki}$ mice allowed for a detailed understanding of the role of graded labels in the development of the retinocollicular map (Brown et al., 2000; Reber et al., 2004). In these mice, EphA3 is expressed in RGCs that normally express Islet2, which leads to the ectopic expression of EphA3 in about half of all RGCs. As a result, immediately adjacent RGCs can have drastically different total EphA receptor expression levels. These RGCs now project to different SC locations, resulting in an overall duplication of the retinocollicular map. These results demonstrate that RGCs sort topographically based on their relative EphA expression level on axons (Brown et al., 2000; Lemke and Reber, 2005). Here, we used a method of intrinsic-signal optical imaging to show that this duplicated map is functional, with each map maintaining smooth topography. Although the azimuth map was duplicated, the elevation representation in the SC remained singular in these mice. These data clearly demonstrate that each axis is mapped independently, in a Cartesian manner, as originally posited by Sperry in his chemoaffinity hypothesis (Sperry, 1963).

Importantly for this study, we found that, despite the duplicated collicular azimuth map, EphA3$^{ki/ki}$ mice have single, normal anatomical maps in the retinogeniculate and geniculocortical projections and a normal, single, functional map in V1. Why is there no map duplication in the retino-geniculo-cortical pathway? One possibility is that although both the Islet2^{+} and Islet2^{-} RGCs project to the SC, the LGN receives input solely from one of these populations. In this case, one would expect two maps in the SC but only one in the LGN, because the relative EphA receptor gradient expressed by the RGC population projecting to the LGN would not be changed. It is known that Islet2^{+} neurons in WT mice project to both the SC and LGN (Pak et al., 2004). It is possible that either the Islet2^{-} RGCs do not project to the contralateral LGN or that the ectopic EphA3 expression in Islet2^{+} RGCs alters their normal projection pattern. We did not observe any change in the size of the LGN in EphA3$^{ki/ki}$ mice (data not shown), suggesting the latter possibility is unlikely. Another possibility is that activity-dependent mapping mechanisms could fix the anatomical map in the LGN but not the SC, because of a differential dependence of correlated activity in the development of topography (Pfeiffenberger et al., 2006). Future studies will be directed to distinguish between these possibilities.

Our studies also find that the two functional maps occupy an equal portion of the SC, but that visual responses from the posterior map are weaker than those from the anterior or WT maps. In EphA3$^{ki/ki}$ mice, the Islet2^{+} subset of RGCs that project to the anterior half of the SC may be a separate physiological type than Islet2^{-} RGCs. These different classes of RGCs may have different maximal responses to the moving bar stimulus used for functional mapping, which could account for the differences in response seen in the two maps. We also observed that the size of the posterior corticocollicular TZ in EphA3$^{ki/ki}$ mice is always larger than the anterior TZ. Because the posterior functional map is weaker relative to the anterior map, this may be the result of a homeostatic mechanism that regulates corticocollicular synapse formation in the SC, as has been demonstrated previously for retinocollicular input (Chandrasekaran et al., 2007). Future characterization of the electrophysiological RGC subtypes projecting to each half of the SC in these mice is needed.

The Corticocollicular Projection Aligns with the Retinocollicular Map Using a Retinal-Matching Mechanism

The disparate maps in V1 and the SC in the EphA3$^{ki/ki}$ mice allowed us to distinguish between models of topographic map alignment during development. Gradient-matching models postulate that gradients of molecules expressed by both V1 and RGC axons match with graded labels expressed in the SC to specify each map. In this case we would expect that a focal injection of DiI into V1 would lead to a TZ in the same place as it would in WT mice, which would lead to a misalignment between the V1 and SC maps in EphA3$^{ki/ki}$ mice. Instead we find that a single injection into V1 results in two and only two TZs in the SC. This shows that V1 axons change their termination sites in response to the duplicated retinocollicular map by matching retinal input. Furthermore, in mice with reduced retinal input, either through enucleation or genetic reduction of RGC number in Math5$^{-/-}$ mice, corticocollicular mapping was disrupted. In both of these cases, we observed overall rough topography of corticocollicular TZs, showing that corticocollicular neurons may also use SC-derived cues to form rough topography.

Retinal input could, in theory, be matched by using common activity patterns shared by V1 neurons and RGCs or be matched using cell surface proteins expressed on V1 and RGC axons. There is a precedence for molecular interactions between axons playing an important role in axon guidance (Gallarda et al., 2008; Pittman et al., 2008), and corticocollicular projections are located such that it is possible they may interact with RGC axons. One mechanism could involve EphA/ephrin-A interactions between V1 and RGC axons. Nasal RGCs express high levels of ephrin-A, so the collicular ephrin-A gradient would be altered in EphA3$^{ki/ki}$ mice by central-projecting nasal axons.

However, we do not observe an obvious change in EphA or ephrin-A gradients in these mice, suggesting the contribution of RGC axon-localized ephrin-As is minor compared with the SC-derived expression (Figure S4). It is also possible that other, yet unidentified molecules that could serve this function might be duplicated in the SC of EphA3$^{ki/ki}$ mice.

Spontaneous Activity Patterns Are Used to Align the Corticocollicular Projection

The time-course of the establishment of the corticocollicular projection in WT and EphA3$^{ki/ki}$ mice shows that refinement occurs before the emergence of vision and during a period when RGCs fire bursts of patterned, spontaneous activity, called retinal waves. This timing overlaps with the end of cholinergic waves and the beginning of the glutamatergic wave period (Huberman et al., 2008a). Cholinergic waves are required for topographic mapping in the retinocollicular, retinogeniculate, and geniculocortical projections (Cang et al., 2008a; McLaughlin et al., 2003; Pfeiffenberger et al., 2006), suggesting that these bursts carry topographic information that filter through the visual circuit. To test if cholinergic retinal waves are used by the V1 projection to align with the retinocollicular projection, we labeled the V1 projection in EphA3$^{ki/ki}$/β2$^{-/-}$ combination mutants. β2$^{-/-}$ mice have severely altered patterns of spontaneous retinal activity during the first postnatal week, resulting in retinocollicular TZs that fail to refine normally (Chandrasekaran et al., 2005; McLaughlin et al., 2003). In EphA3$^{ki/ki}$/β2$^{-/-}$ mutants, retinocollicular TZs are broad, but still duplicate along the A-P axis of the SC. Remarkably, we find that corticocollicular projections in EphA3$^{ki/ki}$/β2$^{-/-}$ mice do not bifurcate in the SC, indicating they are misaligned with the retinocollicular map and implicating a role for β2-dependent cholinergic activity in map alignment. Because the β2 mutation is a global knockout the exact contributions of retinal and cortical cholinergic activity cannot be distinguished at this time. It is likely that the refinement defects seen in β2$^{-/-}$ mice are due to its action in the retina, since intraocular injection of epibatidine results in a similar phenotype (Cang et al., 2005b; Chandrasekaran et al., 2005). Supporting this view is the observation that transgenic expression of the wild-type β2 gene in the retina of β2$^{-/-}$ mice rescues the retinotopic refinement defects in the SC and LGN (M.C. Crair, personal communication). More broadly, any perturbation to retinal activity is also likely to affect cortical activity, although the visual cortex does maintain spontaneous activity following enucleation (Chiu and Weliky, 2001).

Interestingly, we also observed that corticocollicular TZs in β2$^{-/-}$ mice show significantly less overlap with the retinal recipient layer than do WT TZs. This suggests that corticocollicular lamination is also dependent on cholinergic spontaneous activity. These data are in contrast to recent studies in mammalian and zebrafish models, which found that RGC lamination in the SC/tectum was not changed when activity was altered or blocked (Huberman et al., 2008b; Nevin et al., 2008). Perhaps the shared activity patterns of these axons allow them to overcome barriers of cell adhesion proposed as cues to define lamination profiles in the CNS (Sanes and Yamagata, 1999). A possible consequence of this layering defect could be a reduced ability of retinal and cortical axons to interact in the SC. Thus, we cannot rule out the possibility that our results in EphA3$^{ki/ki}$/β2$^{-/-}$ mice may be caused by a disruption of this interaction during development. Future studies will be directed at determining the molecular cues guiding corticocollicular projections to their appropriate layer(s) and the influence of activity on the expression and function of these cues.

Conclusions

These experiments demonstrate an instructive role for RGCs in the mapping and alignment of a second, cortical visual projection to the SC. Our data demonstrate a role for spontaneous activity that occurs prior to eye opening in providing this instructive signal, which is necessary for both alignment of visual maps and proper lamination of corticocollular projections. Considering previous studies in barn owls and ferrets suggesting a similar instructive role for visual input in auditory mapping in the midbrain (King et al., 1988; Knudsen and Brainard, 1991), it may be a general rule that convergent inputs to a central structure use concomitant activity to align with the primary map. It will be interesting to test this general rule for the mapping of other modalities in the mammalian SC using the genetic models described here.

EXPERIMENTAL PROCEDURES

Mice

CD-1, C57Bl/6, or WT littermate mice were used as controls for each experiment. Math5 mutant, β2 mutant, and Isl2-EphA3 knockin mice were generated and genotyped as previously described (Brown et al., 2000; Brown et al., 2001; Xu et al., 1999). Enucleation experiments were performed on postnatal day 6 mice anaesthetized on ice. All mouse protocols were performed in accordance with the University of California Santa Cruz and San Francisco IACUC standards.

Functional Imaging

Imaging of intrinsic optical signals was performed as described previously (Cang et al., 2008b; Kalatsky and Stryker, 2003). Briefly, adult mice were anesthetized with urethane (1.0 g/kg in 10% saline solution) supplemented with chlorprothixene (0.03 mg/kg), and a craniotomy was made in the left hemisphere. For imaging the SC, the overlying cortex was aspirated. Electrophysiological studies demonstrate that ablating or silencing visual cortex does not change receptive field properties of superficial SC neurons (Dräger and Hubel, 1976; Schiller et al., 1974). Optical images of the cortical intrinsic signal were obtained at the wavelength of 610 nm, using a Dalsa 1M30 CCD camera (Dalsa, Waterloo, Canada) controlled by custom software. A high-refresh-rate monitor (Nokia Multigraph 4453, 1024 × 768 pixels at 120 Hz) was placed 25 cm away from the animal where it subtended 70° of the contralateral visual field. Drifting thin bars (2° width and full-screen length) were displayed on the monitor. Animals were presented with horizontal or vertical bars drifting orthogonal to the axis corresponding to either the dorsal-ventral or nasal-temporal axis of the animal in order to stimulate the constant lines of elevation or azimuth, respectively.

Axon Tracing and Whole Eye Fill

Adult mice were anaesthetized by intraperitoneal injection of 100 mg/kg ketamine and 10 mg/kg xylazine. Juveniles were anaesthetized briefly on ice until tail reflex was absent. For corticocollicular projection labeling, an incision was made in the scalp to expose the skull over V1, and a hole was manually drilled in the skull using a 25-gauge needle over the desired injection site. A small amount of 1,1′-dioctadecyl-3,3,3′,3′-tetramethylindocarbocyanine (DiI) or 4-(4-(dihexadecylamino)styryl)-N-methylpyridinium iodide (DiA) (Invitrogen, Carlsbad, CA, USA) (10% in *N,N*-dimethylformamide) was injected using a handheld picospritzer (Parker Instrumentation, Cleveland) and a pulled glass

needle. For whole-eye fill, fluorescently labeled cholera toxin subunit B (CTB) (Invitrogen) was injected intraocularly. For RGC labeling, DiI was injected at focal regions intraocularly as described previously (Feldheim et al., 2000).

Fluorescent Microscopy

Two days (juveniles) or one week (adults) after injection, animals were sacrificed and intracardially perfused with ice-cold 4% paraformaldehyde in phosphate-buffered saline (PBS). Brains were dissected out, fixed overnight, and embedded in 2% agarose in PBS. Vibratome sections were cut 150 μm thick in the sagittal plane, coverslipped, and imaged using a digital camera through a 2.5X, 5X, or 10X objective on an Axioskop 2 Plus microscope (Zeiss).

Quantification and Statistics

Image quantifications were made using the ImageJ 1.38x program (NIH). For quantification of corticocollicular TZ overlap, images were thresholded by discarding pixels below the 20th percentile in intensity. Areas of retinal input and TZ were obtained from individual images, and overlapping pixels were obtained using the "AND" function. Statistical analyses were performed using the statistical software package R (R Foundation, Vienna). Statistical tests performed are indicated in the figure legends.

SUPPLEMENTAL DATA

Supplemental Data include Supplemental Experimental Procedures and four figures and can be found with this article online at http://www.cell.com/supplemental/S0092-8674(09)01049-6.

ACKNOWLEDGMENTS

This work was supported by grants from the NIH (R01-EY014689 to D.A.F., R01-EY02874 to M.P.S., R01-EY018621 to J.C., R01-NS031249 to G.L.). J.W.T. was supported by an NIH National Research Service Award Postdoctoral Fellowship (F32-EY18531). M.T.O was supported by an NIH Training Program for the Visual Sciences (T32-EY007120). We thank Bin Chen, Yi Zuo, and members of the Feldheim and Stryker labs for discussion and critical reading of the manuscript.

Received: April 10, 2009
Revised: June 23, 2009
Accepted: August 5, 2009
Published: October 1, 2009

REFERENCES

Bansal, A., Singer, J.H., Hwang, B.J., Xu, W., Beaudet, A., and Feller, M.B. (2000). Mice lacking specific nicotinic acetylcholine receptor subunits exhibit dramatically altered spontaneous activity patterns and reveal a limited role for retinal waves in forming ON and OFF circuits in the inner retina. J. Neurosci. *20*, 7672–7681.

Brown, A., Yates, P.A., Burrola, P., Ortuño, D., Vaidya, A., Jessell, T.M., Pfaff, S.L., O'Leary, D.D., and Lemke, G. (2000). Topographic mapping from the retina to the midbrain is controlled by relative but not absolute levels of EphA receptor signaling. Cell *102*, 77–88.

Brown, N.L., Patel, S., Brzezinski, J., and Glaser, T. (2001). Math5 is required for retinal ganglion cell and optic nerve formation. Development *128*, 2497–2508.

Cang, J., Kaneko, M., Yamada, J., Woods, G., Stryker, M.P., and Feldheim, D.A. (2005a). Ephrin-as guide the formation of functional maps in the visual cortex. Neuron *48*, 577–589.

Cang, J., Niell, C.M., Liu, X., Pfeiffenberger, C., Feldheim, D.A., and Stryker, M.P. (2008a). Selective Disruption of One Cartesian Axis of Cortical Maps and Receptive Fields by Deficiency in Ephrin-As and Structured Activity. Neuron *57*, 511–523.

Cang, J., Renteria, R.C., Kaneko, M., Liu, X., Copenhagen, D.R., and Stryker, M.P. (2005b). Development of precise maps in visual cortex requires patterned spontaneous activity in the retina. Neuron *48*, 797–809.

Cang, J., Wang, L., Stryker, M.P., and Feldheim, D.A. (2008b). Roles of ephrin-as and structured activity in the development of functional maps in the superior colliculus. J. Neurosci. *28*, 11015–11023.

Chandrasekaran, A.R., Plas, D.T., Gonzalez, E., and Crair, M.C. (2005). Evidence for an instructive role of retinal activity in retinotopic map refinement in the superior colliculus of the mouse. J. Neurosci. *25*, 6929–6938.

Chandrasekaran, A.R., Shah, R.D., and Crair, M.C. (2007). Developmental homeostasis of mouse retinocollicular synapses. J. Neurosci. *27*, 1746–1755.

Chiu, C., and Weliky, M. (2001). Spontaneous activity in developing ferret visual cortex in vivo. J. Neurosci. *21*, 8906–8914.

Chklovskii, D.B., and Koulakov, A. (2004). Maps in the brain: what can we learn from them? Annu. Rev. Neurosci. *27*, 369–392.

Demas, J., Sagdullaev, B.T., Green, E., Jaubert-Miazza, L., McCall, M.A., Gregg, R.G., Wong, R.O., and Guido, W. (2006). Failure to maintain eye-specific segregation in nob, a mutant with abnormally patterned retinal activity. Neuron *50*, 247–259.

Dräger, U.C., and Hubel, D.H. (1976). Topography of visual and somatosensory projections to mouse superior colliculus. J. Neurophysiol. *39*, 91–101.

Feldheim, D.A., Vanderhaeghen, P., Hansen, M.J., Frisén, J., Lu, Q., Barbacid, M., and Flanagan, J.G. (1998). Topographic guidance labels in a sensory projection to the forebrain. Neuron *21*, 1303–1313.

Feldheim, D.A., Kim, Y.I., Bergemann, A.D., Frisén, J., Barbacid, M., and Flanagan, J.G. (2000). Genetic analysis of ephrin-A2 and ephrin-A5 shows their requirement in multiple aspects of retinocollicular mapping. Neuron *25*, 563–574.

Felleman, D.J., and Van Essen, D.C. (1991). Distributed hierarchical processing in the primate cerebral cortex. Cereb. Cortex *1*, 1–47.

Feller, M.B., Wellis, D.P., Stellwagen, D., Werblin, F.S., and Shatz, C.J. (1996). Requirement for cholinergic synaptic transmission in the propagation of spontaneous retinal waves. Science *272*, 1182–1187.

Firth, S.I., Wang, C.T., and Feller, M.B. (2005). Retinal waves: mechanisms and function in visual system development. Cell Calcium *37*, 425–432.

Frisén, J., Yates, P.A., McLaughlin, T., Friedman, G.C., O'Leary, D.D., and Barbacid, M. (1998). Ephrin-A5 (AL-1/RAGS) is essential for proper retinal axon guidance and topographic mapping in the mammalian visual system. Neuron *20*, 235–243.

Gallarda, B.W., Bonanomi, D., Müller, D., Brown, A., Alaynick, W.A., Andrews, S.E., Lemke, G., Pfaff, S.L., and Marquardt, T. (2008). Segregation of axial motor and sensory pathways via heterotypic trans-axonal signaling. Science *320*, 233–236.

García del Caño, G., Gerrikagoitia, I., and Martínez-Millán, L. (2002). Plastic reaction of the rat visual corticocollicular connection after contralateral retinal deafferentiation at the neonatal or adult stage: axonal growth versus reactive synaptogenesis. J. Comp. Neurol. *446*, 166–178.

Hebb, D. (1949). The Organization of Behavior: A Neurophysiological Theory (New York: Wiley).

Hindges, R., McLaughlin, T., Genoud, N., Henkemeyer, M., and O'Leary, D.D. (2002). EphB forward signaling controls directional branch extension and arborization required for dorsal-ventral retinotopic mapping. Neuron *35*, 475–487.

Huberman, A.D., Feller, M., and Chapman, B. (2008a). Mechanisms underlying development of visual maps and receptive fields. Annu. Rev. Neurosci. *31*, 479–509.

Huberman, A.D., Manu, M., Koch, S.M., Susman, M.W., Lutz, A.B., Ullian, E.M., Baccus, S.A., and Barres, B.A. (2008b). Architecture and activity-mediated refinement of axonal projections from a mosaic of genetically identified retinal ganglion cells. Neuron *59*, 425–438.

Kalatsky, V.A., and Stryker, M.P. (2003). New paradigm for optical imaging: temporally encoded maps of intrinsic signal. Neuron *38*, 529–545.

Khachab, M.Y., and Bruce, L.L. (1999). The development of corticocollicular projections in anophthalmic mice. Brain Res. Dev. Brain Res. *114*, 179–192.

King, A.J., Hutchings, M.E., Moore, D.R., and Blakemore, C. (1988). Developmental plasticity in the visual and auditory representations in the mammalian superior colliculus. Nature *332*, 73–76.

Knudsen, E.I., and Brainard, M.S. (1991). Visual instruction of the neural map of auditory space in the developing optic tectum. Science *253*, 85–87.

Lemke, G., and Reber, M. (2005). Retinotectal mapping: new insights from molecular genetics. Annu. Rev. Cell Dev. Biol. *21*, 551–580.

Lin, B., Wang, S.W., and Masland, R.H. (2004). Retinal ganglion cell type, size, and spacing can be specified independent of homotypic dendritic contacts. Neuron *43*, 475–485.

Luo, L., and Flanagan, J. (2007). Development of continuous and discrete neural maps. Neuron *56*, 284–300.

May, P.J. (2005). The mammalian superior colliculus: laminar structure and connections. Prog. Brain Res. *151*, 321–378.

McLaughlin, T., Torborg, C.L., Feller, M.B., and O'Leary, D.D. (2003). Retinotopic map refinement requires spontaneous retinal waves during a brief critical period of development. Neuron *40*, 1147–1160.

Mesulam, M.M. (1998). From sensation to cognition. Brain *121*, 1013–1052.

Nevin, L.M., Taylor, M.R., and Baier, H. (2008). Hardwiring of fine synaptic layers in the zebrafish visual pathway. Neural Dev. *3*, 36.

Pak, W., Hindges, R., Lim, Y.S., Pfaff, S.L., and O'Leary, D.D. (2004). Magnitude of binocular vision controlled by islet-2 repression of a genetic program that specifies laterality of retinal axon pathfinding. Cell *119*, 567–578.

Pfeiffenberger, C., Yamada, J., and Feldheim, D.A. (2006). Ephrin-As and patterned retinal activity act together in the development of topographic maps in the primary visual system. J. Neurosci. *26*, 12873–12884.

Pittman, A.J., Law, M.Y., and Chien, C.B. (2008). Pathfinding in a large vertebrate axon tract: isotypic interactions guide retinotectal axons at multiple choice points. Development *135*, 2865–2871.

Rashid, T., Upton, A.L., Blentic, A., Ciossek, T., Knoll, B., Thompson, I.D., and Drescher, U. (2005). Opposing Gradients of Ephrin-As and EphA7 in the Superior Colliculus Are Essential for Topographic Mapping in the Mammalian Visual System. Neuron *47*, 57–69.

Reber, M., Burrola, P., and Lemke, G. (2004). A relative signalling model for the formation of a topographic neural map. Nature *431*, 847–853.

Sanes, J.R., and Yamagata, M. (1999). Formation of lamina-specific synaptic connections. Curr. Opin. Neurobiol. *9*, 79–87.

Schiller, P.H., Stryker, M.P., Cynader, M., and Berman, N. (1974). Response characteristics of single cells in the monkey superior colliculus following ablation or cooling of visual cortex. J. Neurophysiol. *37*, 181–194.

Singer, J.H., Mirotznik, R.R., and Feller, M.B. (2001). Potentiation of L-type calcium channels reveals nonsynaptic mechanisms that correlate spontaneous activity in the developing mammalian retina. J. Neurosci. *21*, 8514–8522.

Sperry, R.W. (1963). Chemoaffinity in the orderly growth of nerve fiber patterns and connections. Proc. Natl. Acad. Sci. USA *50*, 703–710.

Sun, C., Warland, D.K., Ballesteros, J.M., van der List, D., and Chalupa, L.M. (2008). Retinal waves in mice lacking the beta2 subunit of the nicotinic acetylcholine receptor. Proc. Natl. Acad. Sci. USA *105*, 13638–13643.

Syed, M.M., Lee, S., Zheng, J., and Zhou, Z.J. (2004). Stage-dependent dynamics and modulation of spontaneous waves in the developing rabbit retina. J. Physiol. *560*, 533–549.

Treisman, A. (1996). The binding problem. Curr. Opin. Neurobiol. *6*, 171–178.

Wolfe, J.M., and Cave, K.R. (1999). The psychophysical evidence for a binding problem in human vision. Neuron *24*, 11–17, 111–125.

Wong, R.O. (1999). Retinal waves and visual system development. Annu. Rev. Neurosci. *22*, 29–47.

Xu, W., Orr-Urtreger, A., Nigro, F., Gelber, S., Sutcliffe, C.B., Armstrong, D., Patrick, J.W., Role, L.W., Beaudet, A.L., and De Biasi, M. (1999). Multiorgan autonomic dysfunction in mice lacking the beta2 and the beta4 subunits of neuronal nicotinic acetylcholine receptors. J. Neurosci. *19*, 9298–9305.

Cell, Volume *139*

Supplemental Data

Retinal Input Instructs Alignment

of Visual Topographic Maps

Jason W. Triplett, Melinda T. Owens, Jena Yamada, Greg Lemke, Jianhua Cang, Michael P. Stryker, and David A. Feldheim

SUPPLEMENTAL EXPERIMENTAL PROCEDURES

Receptor affinity probe *in situ*

EphA3-AP and ephrin-A5-AP *in situ* staining was done essentially as described (Feldheim et al., 1998), with some modifications. Postnatal day 8 brains were dissected and fixed 15 min in 4% paraformaldehyde at 4°C. After washing in PBS, brains were embedded in 5% agarose in PBS on ice. Parasagittal sections were cut 250 μm thick with a manual Vibroslice (World Precision Instruments, Sarasota) and collected in ice-cold PBS. Sections containing the SC were treated with either AP, EphA3-AP or ephrin-A5 AP (Cheng et al., 1995), washed in Hepes buffered saline (HBS, 20 mM Hepes pH 7.0), post-fixed in 40% acetone/10% formalin pH 6.2 for 1 min, washed in HBS, and heat-inactivated in HBS at 65°C overnight. The following morning, sections were washed in HBS and AP reaction was carried out at room temperature.

SUPPLEMENTAL FIGURE LEGENDS

Figure S1. Comparison of anterior and posterior SC functional maps in EphA3$^{ki/ki}$ mice

(A) Quantification of the area of anterior and posterior SC functional maps in EphA3$^{ki/ki}$ mice. Data are represented as mean +/- SEM. N = 9.

(B) Quantification of signal strength from anterior and posterior maps in EphA3$^{ki/ki}$ mice. Data are represented as mean +/- SEM. *, P = 0.007, two-tailed student's t-test; N = 9.

(C) Distribution of anterior to posterior amplitude ratios in EphA3$^{ki/ki}$ mice. *bars*, mean +/- SEM; N = 9.

Figure S2. The retinogeniculate and geniculocortical projections are not anatomically duplicated in EphA3$^{ki/ki}$ mice

(A) Whole mount view of the SC after focal injection of DiI in nasal retina. In EphA3$^{ki/ki}$ mice, two TZs (arrowheads) were observed in the central and posterior SC. *dashed area*, SC; *inset*, schematic of retinal injection site; N, nasal; T, temporal; M, medial; P, posterior. N = 8.

(B) Coronal section through the LGN after focal injection of DiI in nasal retina. In EphA3$^{ki/ki}$ mice, a single TZ (arrowhead) was observed in ventral dLGN. *dashed area*, dLGN; D, dorsal; M, medial. N = 8. Images in (A) and (B) are from the same animal.

(C) Image of the cortical surface of V1 (dashed area) prior to intrinsic optical imaging. After imaging, fluorescently tagged CTBs were injected at the indicated locations (green and red dots). A, anterior; L, lateral.

(D) Coronal section through the LGN after focal injection of CTB-594 (red) and CTB-488 (green) in V1. In EphA3$^{ki/ki}$ a single injection in V1 labels dLGN cell somas in a single area. D, dorsal; M, medial. N = 5. Images in (C) and (D) are from the same animal.

Figure S3. Laminar targeting and refinement errors of corticocollicular projections in β2$^{-/-}$ mice

(A) Parasagittal SC section after focal injection of DiI (red) in central V1 and whole eye fill with CTB-488 (green) in the contralateral eye, which labels all RGCs. In WT mice a

single injection gives a single TZ in the central SC. *insert*, schematic of V1 injection site; A, anterior; D, dorsal; *, pretectal nucleus.

(B) Parasagittal SC section after focal injection of DiI (red) in central V1 and whole eye fill with CTb-488 (green) in the contralateral eye, which labels all RGCs. In $\beta2^{-/-}$ mice a single injection gives a single broad TZ in the central SC. *insert*, schematic of V1 injection site; *, pretectal nucleus.

(C) Corticocollicular TZ location expressed as a percent of SC anterior-posterior axis was plotted as a function of V1 injection site expressed as percent of the L-M axis of the cortical hemisphere. Line represents best-fit regression, $R^2 = 0.9118$.

(D) Quantification of TZ area, as a percent of the SC in WT and $\beta2^{-/-}$. Data are represented as mean +/- SEM, N > 7. ***, P < 0.001 vs. WT, Kolmogorov-Smirnov test.

(E) Quantification of TZ overlap with the SC retinal input layer as a percent of TZ area in WT and $\beta2^{-/-}$ mice. Data are represented as mean +/- SEM. *, P < 0.05 vs. WT, Kolmogorov-Smirnov test.

Figure S4. EphA and ephrin-A expression gradients are not altered in the SC of EphA3$^{ki/ki}$ mice

(A & B) Parasagittal SC sections of P8 brains after staining with EphA3-alkaline phosphatase (AP) fusion protein. In WT (A) and EphA3$^{ki/ki}$ (B) mice, there was a high posterior to low anterior gradient of ephrin-A expression. LGN, lateral geniculate nucleus; pt, pretectum; SC, superior colliculus; IC, inferior colliculus; A, anterior; D, dorsal.

(C & D) Parasagittal SC sections after staining with ephrin-A5-AP fusion protein. In WT (C) and EphA3$^{ki/ki}$ (D) mice, there was a high anterior to low posterior gradient of EphA expression.

(E) Parasagittal section after AP only staining. In EphA3$^{ki/ki}$ mice, no significant background staining was observed.

SUPPLEMENTAL REFERENCES

Cheng, H. J., Nakamoto, M., Bergemann, A. D., and Flanagan, J. G. (1995). Complementary gradients in expression and binding of ELF-1 and Mek4 in development of the topographic retinotectal projection map. Cell *82*, 371-381.

Feldheim, D. A., Vanderhaeghen, P., Hansen, M. J., Frisén, J., Lu, Q., Barbacid, M., and Flanagan, J. G. (1998). Topographic guidance labels in a sensory projection to the forebrain. Neuron *21*, 1303-1313.

Supplemental Figure 1

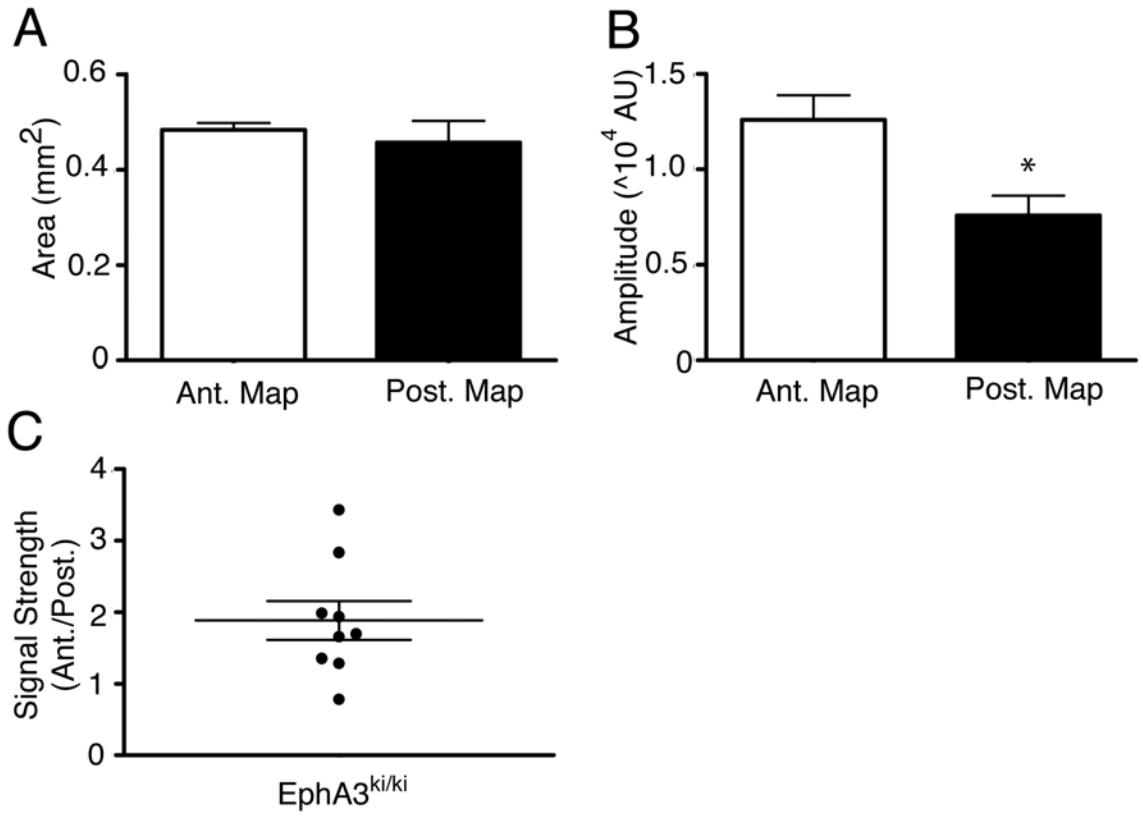

Supplemental Figure 2

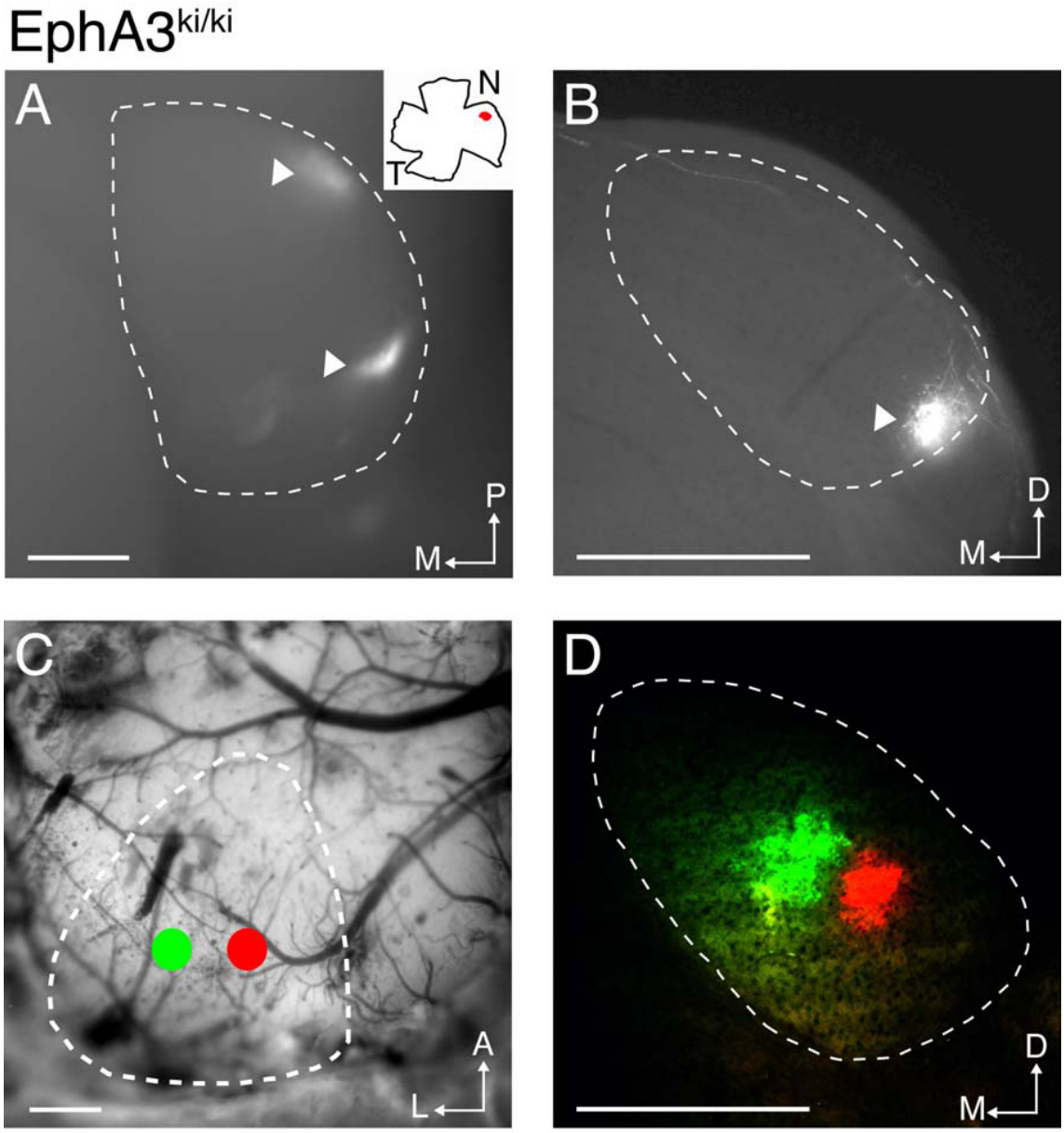

Supplemental Figure 3

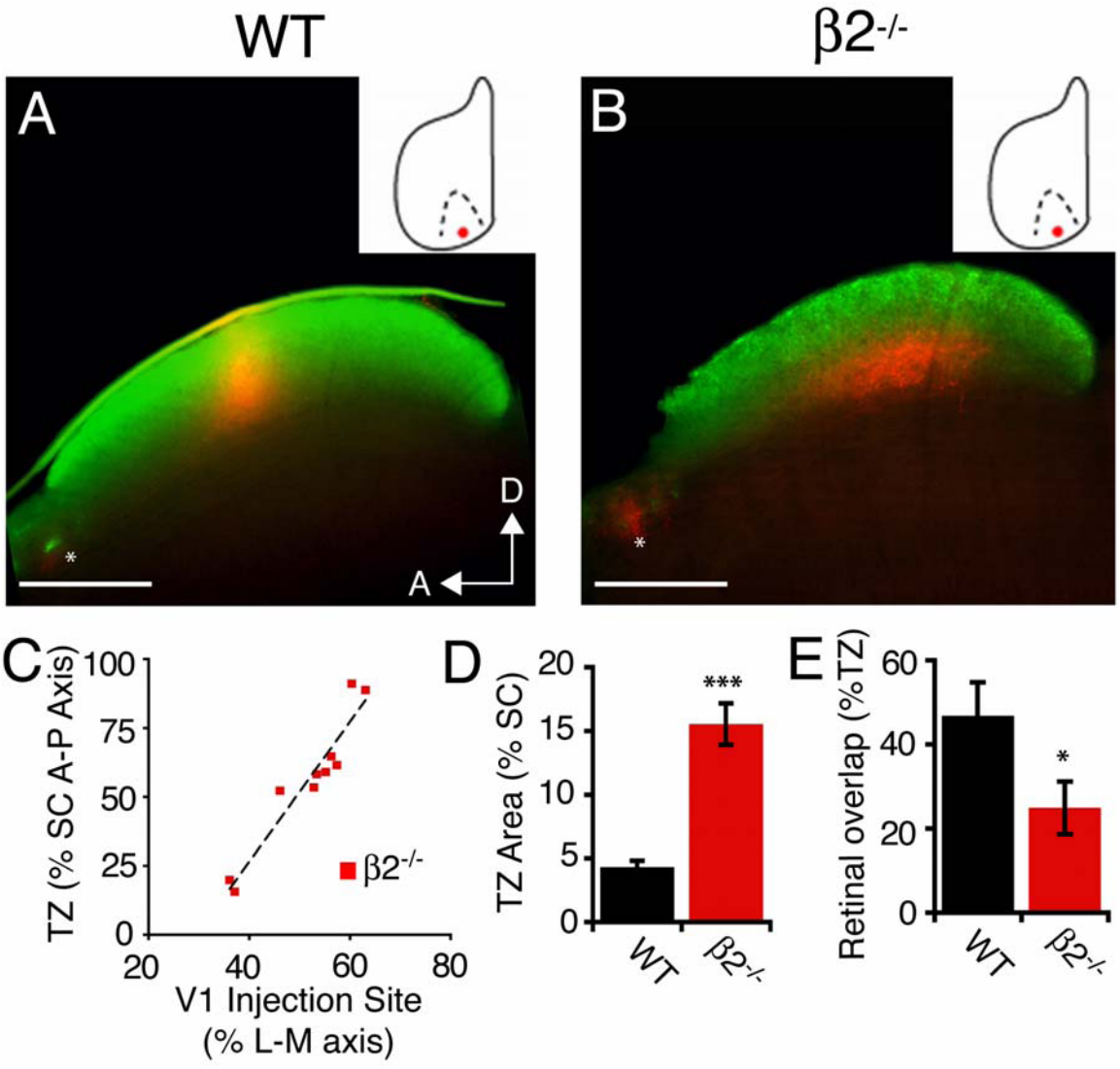

Supplemental Figure 4

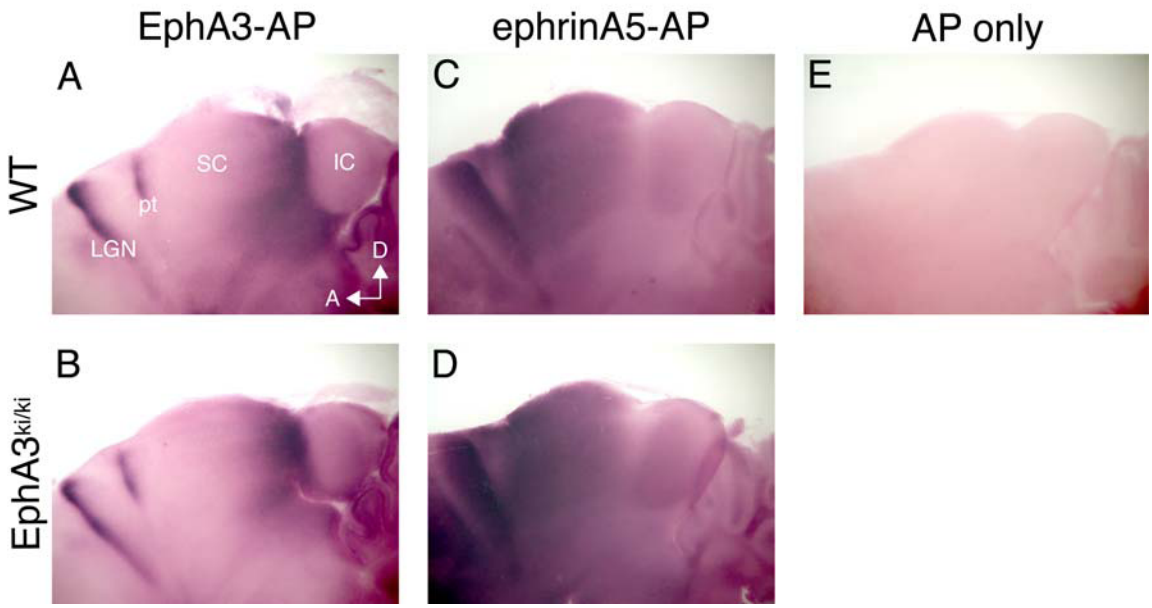

Differences between cortical and collicular map development in *Isl2-EphA3* knock-in mice

SUMMARY

The *Isl2-EphA3*$^{ki/ki}$ mouse has two maps of visual space in the superior colliculus but only one in primary visual cortex. We use anterograde tracing from the retina and retrograde tracing from cortex to find that the lack of a second map begins in the retinal projection to the dLGN.

INTRODUCTION

The processes of map formation in the retinocollicular and retinogeniculocortical projections have much in common, including a dependence on EphA/ephrin-A signaling and patterned retinal activity to order the azimuth axis (Cang et al., 2008b; Cang et al., 2008a). However, in the *Isl2-EphA3*$^{ki/ki}$ mouse, collicular maps in have two separate and coherent maps of space, while the maps in primary visual cortex (V1) only have one (Triplett et al., 2009). This result implies that, despite the many commonalities between cortical and collicular azimuth topographic mapping, in this particular mutant mouse, the processes of map formation in these two brain areas must differ in some profound way. The single map of space in cortex might be a result of either receiving non-duplicated anatomical input or of functionally suppressing of aberrant inputs, similar to what occurs in the “Midwestern” Siamese cat (Kaas and Guillery, 1973). If cortex receives only a single projection from the dorsolateral geniculate nucleus (dLGN), it would also be

interesting to know whether the dLGN is given a single or a duplicated set of inputs from retinal ganglion cells (RGCs).

We use anatomical tracing techniques to show that the origin of the single cortical map is anatomical. There is only a single map of space represented in the set of retinal inputs to the dLGN and therefore in the dLGN inputs to primary visual cortex.

RESULTS

We wanted to know whether the single functional map seen in the primary visual cortex of *Isl2-EphA3*$^{ki/ki}$ mice reflected the anatomy of the underlying inputs or whether the cortex suppressed aberrant inputs during imaging (Kaas and Guillery, 1973). Therefore, we injected the retrograde tracer cholera toxin subunit B (CTB) into the visual cortices of *Isl2-EphA3*$^{ki/ki}$ mice that had been functionally imaged. Two injections were made into each cortex, one of CTB conjugated to a red fluorophore and one of CTB conjugated to a green fluorophore (Fig. 1B). We found that each tracer only ended up labeling one column of cells in the dLGN (n=5 of 5 *Isl2-EphA3*$^{ki/ki}$ mice and n=3 of 3 *Isl2-EphA3*$^{wt/ki}$ mice), implying that the thalamocortical projection in these mice is not doubled (Fig. 1C).

In these animals, the retinal projection to the SC of these animals is doubled (Brown et al., 2000). Therefore, we investigated whether the retinal projection to the dLGN is doubled like the retinocollicular projection or single like the thalamocortical projection. We injected the anterograde tracer DiI into the retinas of several *Isl2-EphA3*$^{ki/ki}$ mice (Fig. 1D). We found that each injection only labeled one column of

terminations in the dLGN (n=8 of 8 *Isl2-EphA3*$^{ki/ki}$ mice), implying that this animal's retinogeniculate projection is also single (Fig.1E).

DISCUSSION

The *Isl2-EphA3* knock-in mouse is valuable for understanding many aspects of topographic map development. We demonstrate that in the *Isl2-EphA3*$^{ki/ki}$ mouse, in both the retinogeniculate and the thalamocortical projections, axons from the source only go to one topographic location in the target, showing that these connections contain only a single map of space. Despite a shared dependence on EphA and ephrin-A signaling, retinogeniculate map formation must be different enough from retinocollicular map formation to allow for the formation of a single map in the dLGN (Cang et al., 2008b; Cang et al., 2005a).

Role of *Isl2* in shaping retinal projections

The *Isl2-EphA3*$^{ki/ki}$ mouse has a doubled functional map in the colliculus because only Isl2^{+} RGCs over-express EphA3; projections from Isl2^{+} and Isl2^{-} cells end up segregated into two separate maps (Brown et al., 2000). The dLGN's single map of space could be a consequence of having only one of these populations of neurons project to the dLGN. *Isl2* is a LIM homeodomain transcription factor that is expressed in the pancreas, spinal cord, and retina and contributes to the determination of cell fate in the nervous system (Thaler et al., 2004; Pak et al., 2004). In the eye, *Isl2* seems to force the RGCs that express it to adopt a contralaterally-projecting fate (Pak et al., 2004). A study has shown that Isl2^{+} neurons densely innervate the dLGN, ruling out the possibility that there

is a single map because only Isl2$^-$ neurons project to the geniculate (Pak et al., 2004). In addition, previous work has found that RGCs that express GFP under the control of the dopamine receptor 4 (DRD4) promoter project to the dLGN (Huberman et al., 2009). Because these cells do not express *Isl2*, we can also discard the possibility that only Isl2$^+$ RGCs project to retina (Feldheim, personal communication).

If both Isl2$^+$ and Isl2$^-$ cells go to the dLGN, why do they not form a doubled map of space, as they do in the colliculus? One possible explanation is that neural activity causes the projections to align. Retinal waves early in life act via Hebbian mechanisms to make the development of smooth topographic maps more likely by encouraging a topographic organization such that neighboring cells in the SC receive input from neighboring cells in the retina (Butts and Rokhsar, 2001; Cang et al., 2005b). In some cases, the effect of retinal activity can overcome the effects of altered mapping caused by the *Isl2-EphA3* knock-in allele and force a duplicated projection to merge into one map (see chapter 4). Compared to the SC, the effect of retinal waves on topography might be stronger or the effect of the EphA3 over-expression weaker, allowing neural activity to collapse the Isl2$^+$ and Isl2$^-$ projections into one map.

Alternatively, it may be that unlike in the colliculus, where both Isl2$^+$ and Isl2$^-$ RGCs project to the same layer, these populations go to distinct layers in the dLGN. In other species, the cells of different dLGN layers form a common single topographic map, with "lines of projection" running through all layers containing the cells that receive inputs and send outputs concerning each point in visual space. In the mouse, it has been shown that one population of Isl2$^-$ cells, the ones that express DRD4, and one population of Isl2$^+$ cells, the ones that express calretinin, project to distinct geniculate laminae

(Huberman et al., 2009). If this finding holds true for all populations of Isl2$^-$ and Isl2$^+$ cells, it may be that Isl2$^-$ and Isl2$^+$ cells do form multiple maps of space, but these maps are physically overlaid on each other in the dLGN instead of being arranged end-to-end along the same axis as in the colliculus. Given that the thalamocortical projection is also single, we can further conclude that the axons of the neurons that receive inputs from the Isl2$^-$ and Isl2$^+$ RGCs must mingle as they travel to the cortex, assuming that both types of targets project to V1.

Conclusions

There is a single map of space in the primary visual cortex of *Isl2-EphA3*$^{ki/ki}$ mice because the retinogeniculate projection is not doubled. The *Isl2-EphA3* knock-in mouse is a useful tool for revealing how *Isl2* expression is associated with specific patterns of projection to the superior colliculus and dLGN.

METHODS

Mice

Isl2-EphA3 knock-in mice were generated and genotyped as previously described (Brown et al., 2000). Mice were maintained on a mixed CD-1/C57Bl6 background. All mice used were adults at least 40 days of age. All mouse protocols were performed in accordance with the University of California Santa Cruz and San Francisco IACUC standards.

Functional imaging and injection of retrograde tracers

Imaging of intrinsic optical signals was performed as described previously (Cang et al., 2005a; Kalatsky and Stryker, 2003). Briefly, mice were anesthetized with isoflurane

supplemented with chlorprothixene (0.003 mg/kg) given intramuscularly. Mice were also given atropine (0.3 mg/kg) and dexamethasone (2 mg/kg) subcutaneously. A craniotomy was made over the left hemisphere. Functional imaging then proceeded as described in (Kalatsky and Stryker, 2003). After imaging, two injections of the retrograde tracer cholera toxin subunit B (CTB) conjugated to Alexa Fluor (Invitrogen, Carlsbad, CA) were made into primary visual cortex using a Nanoject (Drummond Scientific Company, PA) and a glass pipette with a 20–30 μm tip opening. One injection was of CTB-488 (green), and the other of CTB-594 (red). The Nanoject was set to inject 32.2 nl of the dye, which was diluted to 2mg/mL in PBS, but small variations in injection volume were unavoidable. Then, the mouse was allowed to recover for 48 hours before being sacrificed.

Injection of anterograde tracers

Mice were anaesthetized by intraperitoneal injection of 100 mg/kg ketamine and 10 mg/kg xylazine. A small amount of 1,1'-dioctadecyl-3,3,3',3'-tetramethylindocarbocyanine (DiI) (Invitrogen, Carlsbad, CA) was injected at focal regions intraocularly using a handheld picospritzer (Parker Instrumentation, Cleveland, OH) and a pulled glass needle as described previously (Feldheim et al., 2000). Mice were allowed to recover for 4-7 days before being sacrificed.

Fluorescence microscopy

Mice that had undergone anterograde or retrograde tracer injections were sacrificed and intercardially perfused with 4% paraformaldehyde in PBS. The brains were fixed overnight before sectioning coronally at 100 μm using a vibratome (Lancer, MO). Images

of the dLGN were captured using a digital camera through a 2.5X, 5X or 10X objective on an Axioskop 2 Plus microscope (Zeiss).

REFERENCES

Please refer to the global list of references in this dissertation.

Figure 1

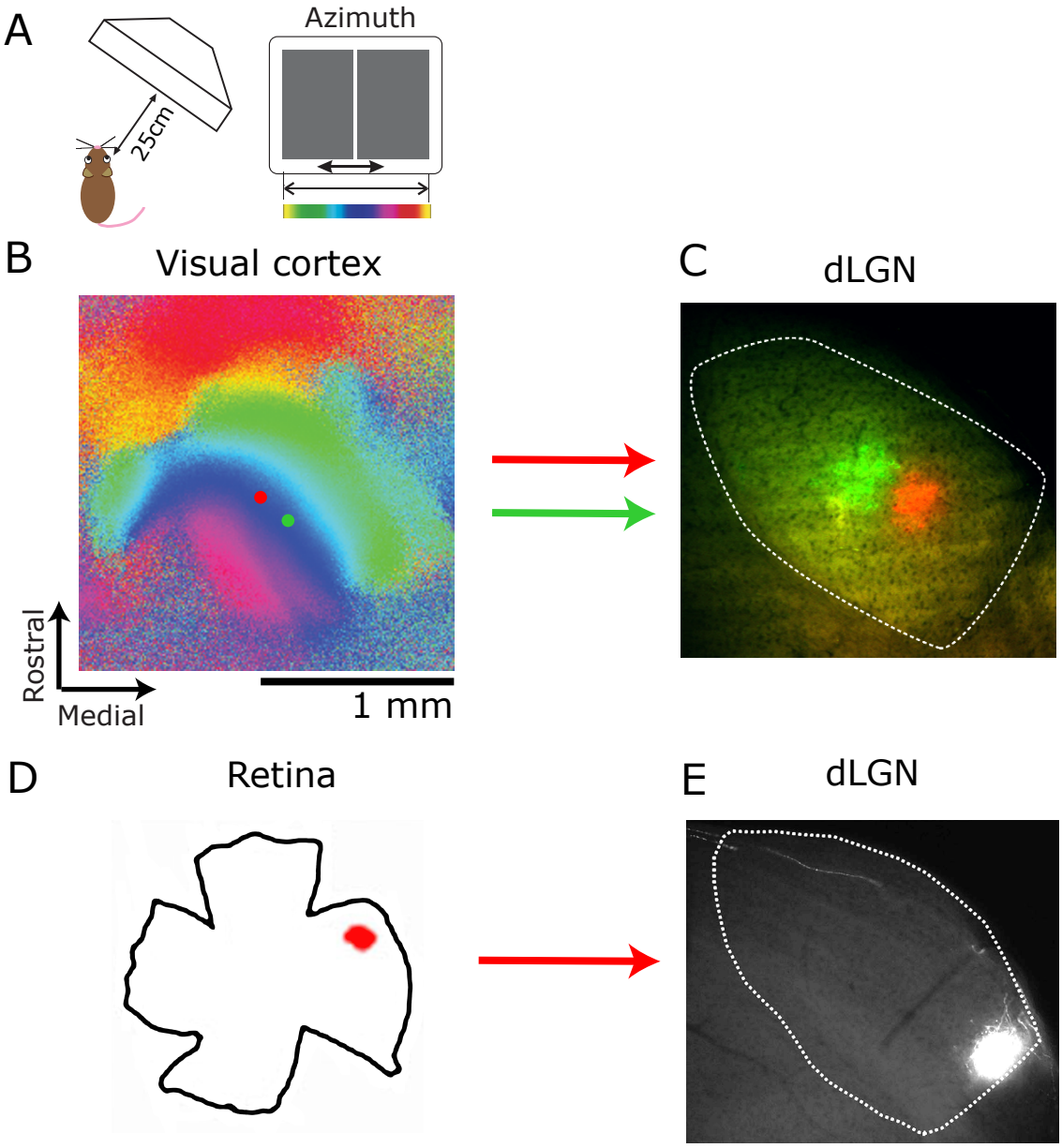

Figure 1: A. For functional imaging, a monitor is placed 25cm away from the mouse on the side contralateral to the hemisphere being imaged. Mice were shown full-field stimuli in azimuth (and elevation; not shown). B. Functional map of the azimuth axis from a representative *Isl2-EphA*$^{ki/ki}$ mouse. The color code is given in panel A. A red and a green dot are overlaid on the map to represent the locations of injections of cholera toxin subunit B (CTB) retrograde tracers conjugated to different fluorophores. C. The dLGN of the mouse whose map is shown in B. The outline of the dLGN is shown in white, and the green and red spots represent the locations labeled by the CTB injections. D. A representation of a flattened retina that has been injected with the anterograde tracer DiI. E. The dLGN of a *Isl2-EphA*$^{ki/ki}$ mouse that underwent a retinal injection. The outline of the dLGN is in white, and the bright spot represents the location labeled by the DiI.

The origins of structural and functional heterogeneity in a topographic map mutant

Melinda T. Owens,[1] Jason W. Triplett,[2] David A. Feldheim[2], and Michael P. Stryker[1]

[1]W.M. Keck Foundation Center for Integrative Neuroscience, Department of Physiology, University of California, San Francisco, San Francisco, CA 94143, USA; [2]Department of Molecular, Cell, and Developmental Biology, University of California, Santa Cruz, Santa Cruz, CA 95064, USA

SUMMARY

The projection from the retina to the superior colliculus (SC) relies on a combination of molecular guidance cues and patterned neural activity to form a smooth, orderly topographic map. Previous work has shown that mice homozygous for the *Isl2-EphA3* knock-in allele over-express EphA3 in a subset of their retinal ganglion cells (RGCs), creating two maps of space in the retinocollicular projection. Here we examine mice that are heterozygous for *Isl2-EphA3* and reveal unexpected variability in the structure of their collicular maps. This heterogeneity cannot be explained by purely genetic factors, since different map structures could be present in one animal or even within one SC. Using functional imaging and computational modeling, we showed that the heterozygous *Isl2-EphA3* knock-in mouse exists at a point of instability: changing the over-expression levels of EphA3 even slightly caused map structures to be much less diverse. Retinal waves were also necessary for the expression of map variability. Our results demonstrate that a precise combination of molecular guidance cues and patterned

neural activity can reveal the stochastic process inherent in map formation and lead to map heterogeneity.

INTRODUCTION

The proper functioning of the adult brain depends on events that happen early in development, when each of the billions of neurons that comprise the nervous system must find and connect to the correct partners. The neuronal connections responsible for processing sensory information are often organized as precise and orderly topographic maps, which preserve in the target the neighbor-neighbor relations that are present in the source. In the visual system, the retina's natural order is maintained in higher visual brain areas as retinotopic maps. A prominent mammalian model for studying how topographic maps are established is the projection of retinal ganglion cells (RGCs) to the superior colliculus (SC), a midbrain integrative center. RGCs project to the most dorsal layer of the SC, the upper stratum griseum superficiale (SGS), and are organized topographically, such that the nasal-temporal (N-T) axis of the retina projects to the anterior-posterior (A-P) axis of the SC and the dorsal-ventral (D-V) axis of the retina projects along the medial-lateral (M-L) axis of the SC.

Collicular maps in wildtype animals are precise and smooth. Much is known how the SC achieves that state along the nasotemporal (azimuth) axis. In mice, RGC axons enter the colliculus during the first week of life and establish topography in a multi-stage process (McLaughlin et al., 2003). Initially, the axons initially overshoot their targets with their primary growth cones and then send out interstitial branches, which are created most densely near the site of the future termination zone (Feldheim and O'Leary, 2010).

The tyrosine kinase receptors EphAs and their ligands the ephrin-As, which form opposing counter-gradients across the nasotemporal axis of the eye and the anterior-posterior axis of the SC, act as positional labels to guide these branches to their approximate positions in the SC (Marcus et al., 1996; Flenniken et al., 1996; Flanagan, 2006). Later on, axon segments and branches in topographically erroneous locations are eliminated, leaving a compact projection in the correct location (Feldheim and O'Leary, 2010). This refinement depends on spontaneous neural activity in the form of type II retinal waves, which act via Hebbian mechanisms so that only the appropriate connections, whose activity patterns are consistent with that of their immediate neighbors, are retained, and the topographic map becomes smooth (Butts and Rokhsar, 2001; McLaughlin et al., 2003). Together, the spontaneous retinal waves and EphA/ephrin-A signaling pattern almost the entire map in the azimuth axis, creating an orderly and predictable map (Cang et al., 2008b).

Wildtype collicular maps are also very stereotyped. Map variability has been demonstrated in such systems as the cortex of the Siamese cat, in which almost all of the RGCs project contralaterally, and the SC of the ephrin-A triple knockout mouse, which is missing all ephrin-A signaling in cortex and SC (Kaas and Guillery, 1973; Cang et al., 2008b). It is not surprising mutants like these have distorted maps. However, it is not known whether animals with less disruptive manipulations of anatomic input or molecular guidance cues can also display variability. If a mutant were found that displayed map variability in spite of, say, having normal retinal waves and only slightly elevated levels of EphA/ephrin-A signaling, it would imply that stochastic events are not something deviant that occurs only under extreme conditions but instead are an inherent

part of map formation that can be revealed under the right conditions. The traditional method of characterizing map mutants, anatomical tracing, is not suited to analyzing or even finding map variability: tracing techniques can sample the projection patterns of only one or two places in each retina, so results from many individual mice must be combined, obscuring any individual variability that might be present (Brown et al., 2000; Bevins et al., 2011; Reber et al., 2004). In contrast, functional techniques such as optical imaging of intrinsic signals (OIS) can show the structure of an entire map at once at a range of length scales (Cang et al., 2008b; Cang et al., 2008a). Therefore, functional imaging of variable maps from a mutant that still retained normal levels of EphA signaling would be ideal for studying the origins of map heterogeneity.

In this paper, we use functional imaging to reveal the existence of great inter-individual map variability in superior colliculus of the *Isl2-EphA*$^{wt/ki}$ mouse. The heterogeneity in this mouse was not predicted by previous anatomical tracing data but is consistent with tracing data considered on an animal-by-animal basis (Brown et al., 2000). This variability does not have a strictly genetic origin and is dependent on patterned retinal activity early in life. Using both functional imaging and computational modeling approaches, we show that the heterogeneity seen in this mutant is a consequence of the exact level of EphA3 over-expression in this mouse, which allows the map to be shaped by stochastic process during development.

RESULTS

Unexpected variability of visual maps in the SC of Isl2-EphA$^{wt/ki}$ mice

The *Isl2-EphA3* knock-in mouse has been used to study the contribution of EphAs and ephrin-As in map development. These mice ectopically express EphA3 from an internal-ribosome-entry-site cDNA expression cassette placed in the 3' untranslated region of the *Islet2* gene, which drives expression in about 40% of RGCs scattered in a salt-and-pepper fashion across the retina (Brown et al., 2000). EphA3 is not normally expressed in the retina, so the RGCs of these mice are divided into an Islet2^{-} population that expresses endogenous EphA levels and an Islet2^{+} population that has EphA3 expression superimposed on top of the endogenous EphA levels. Mice that are homozygous for the *Isl2-EphA3* knock-in allele, called *Isl2-EphA3*$^{ki/ki}$ mice, express more extra EphA3 than mice that are heterozygous for the allele, called *Isl2-EphA3*$^{wt/ki}$ mice. If anterograde tracers are injected into the retina of the homozygous *Isl2-EphA3*$^{ki/ki}$ mice at one location, two locations in the SC will be labeled, showing that *Isl2-EphA3*$^{ki/ki}$ mice have duplicated maps of azimuth: the Isl2^{+} RGCs form one map at the rostral end of the SC, and the Isl2^{-} RGCs comprise another at the caudal end (Brown et al., 2000). Functional imaging has confirmed that these mice have two complete and coherent maps of the visual field in the SC that do not overlap (Triplett et al., 2009). Studies using anterograde tracers in *Isl2-EphA3*$^{wt/ki}$ mice show that in these mice, most Isl2^{+} neurons also tend to project more rostrally and Isl2^{-} neurons more caudally than they would in the wildtype animal. If the data from many mice are combined, it would appear that because of the lower levels of EphA3 in the heterozygote, the areas innervated by the Isl2^{+} and the Isl2^{-} neurons in *Isl2-EphA3*$^{wt/ki}$ mice overlap substantially (Brown et al., 2000). Analysis of the aggregate data implied that much of the SC receives retinal input from two distinct locations in the retina: one located more rostrally that is made up of Isl^{-}

RGCs and one that is more caudal that is comprised of Isl^{+} RGCs. It would also predict that the functional maps of the SCs of these animals would be fuzzy and of poor quality, similar to the functional maps of β2 mutants, in which one location in the SC gets input from many locations in the retina (Cang et al., 2005b).

Surprisingly in the light of these predictions, functional imaging of the maps of *Isl2-EphA3*$^{wt/ki}$ mice actually reveals good maps of high quality. Maps in *Isl2-EphA3*$^{wt/ki}$ mice do not differ from those of wildtype or *Isl2-EphA3*$^{ki/ki}$ littermates in size or peak amplitude, a measure of map quality (n=8 for wildtypes, n=9 for *Isl2-EphA3* mutants) (Fig. 1A- C). Most unexpectedly, maps in individual *Isl2-EphA3*$^{wt/ki}$ mice varied greatly from one another. Out of 26 mice imaged, 7 animals had a doubled map of space (Fig. 2H, I), similar to those seen in *Isl2-EphA3*$^{ki/ki}$ mice (Fig. 2F, G). Another 7 displayed a map with a single map of space (Fig. 2J, K), similar to those of wildtype animals (Fig. 2D, E). These animals were not simply mice with an incompletely revealed doubled map, since the total size of the SC occupied by the single and doubled maps in *Isl2-EphA3*$^{wt/ki}$ mice was the same (Fig. 1D).The remaining 12 mice had maps that are partially doubled and partially single (Fig. 2L,M). Hereafter, this kind of map is called a mixed-type map. Although the maps of azimuth display the most obvious differences, the elevation maps differ as well. In *Isl2-EphA3*$^{ki/ki}$ mice, the elevation maps display a discontinuity that allows each of the maps of space to be coherent (Triplett et al., 2009). This discontinuity is present only in the mice that have doubled or partially doubled maps of azimuth and is absent in the *Isl2-EphA3*$^{wt/ki}$ mice with single maps. This finding implies that the doubled portions of these maps represent a second complete and coherent map of space.

Since EphA and ephrin-A signaling is also crucial for the proper formation of the azimuth axis in the retinogeniculocortical pathway, we also imaged cortical maps in *Isl2-EphA3*$^{wt/ki}$ mice. We found that cortical maps of azimuth and elevation in these mice displayed normal peak amplitudes compared to wildtype and *Isl2-EphA3*$^{ki/ki}$ littermates, showing that they did not have alterations in map quality (Fig.3A, B). In addition, they were all single (n=15 of 15) (Fig. 3E). This cortical phenotype is not surprising given that *Isl2-EphA3*$^{ki/ki}$ mice, which over-express EphA3 more strongly, also have cortical maps of normal quality and structure (Triplett et al., 2009).

Heterogeneity in *Isl2-EphA3*$^{wt/ki}$ functional maps does not have a strictly genetic basis

Why are the maps of space in the *Isl2-EphA3*$^{wt/ki}$ mouse so variable? One possible explanation is that the structures of maps might be determined from the start of development by inter-individual genetic differences. After all, *Isl2-EphA3*$^{ki/ki}$ mice form doubled maps instead of single maps like those seen in their wildtype littermates because their genes tell them to over-express a lot of EphA3 in their Isl2^{+} RGCs. Since the mice we studied were maintained on a hybrid genetic background, it is conceivable that whether an individual *Isl2-EphA3*$^{wt/ki}$ mouse forms a single or a doubled map is determined by exactly how much EphA3 is over-expressed in their Isl2^{+} neurons, which in turn is specified by unknown strain-specific genetic factors. This possibility is unlikely because so many of the maps are of a mixed type (Fig. 2L,M). It is nonetheless conceivable that a mouse could program its RGCs such as all Isl2^{+} RGCs on one side of the retina over-express more EphA3 than all the RGCs on the other side of the retina, giving rise to a doubled map on one side and a single map on the other. Alternatively, the

structures could evolve in response to random events that occur during map formation. The deterministic genetic hypothesis predicts that the structure of the collicular map in one hemisphere should match the structure on the collicular map in the other hemisphere. Therefore, we imaged the both colliculi in *Isl2-EphA3*$^{wt/ki}$ mice. Although some mice had maps of similar structure in both hemispheres, many did not. Several mice had mixed-type structures in both hemispheres, but the maps differed in aspects like where the split occurred or whether the single map appeared laterally or medially (Fig. 4B1-4). One mouse even had a single map in the right hemisphere but a mostly doubled map in the left (Fig. 4C1-4). In total, 44% of mice (4 of 9) had maps of different structures in their left and the right SCs. These results rule out a purely genetic basis for the origin of map heterogeneity in this mutant.

Functional images in individual *Isl2-EphA3*$^{wt/ki}$ mice are consistent with anatomy

A possible explanation for the discordance between the aggregate anatomical tracer data, which implies a messy map, and the individual functional maps, which are variable and of high quality, is that some of the retinal inputs into the SC are being functionally suppressed. Visual maps in primary visual cortex are able to suppress aberrant input from the lateral geniculate nucleus, but the extent to which maps in SC can suppress retinal input is unknown (Kaas and Guillery, 1973). To address the possibility of functional suppression, we imaged *Isl2-EphA3*$^{wt/ki}$ mice while showing them spatially-restricted stimuli. These stimuli would only excite a small part of the retina at once, potentially activating ectopic termination sites that are normally suppressed when full-field stimuli are presented. We focused on *Isl2-EphA3*$^{wt/ki}$ mice with mixed-type maps,

since we would be able to compare in the same SC areas of activation that give a doubled map and areas of activation that give a single map. *Isl2-EphA3*$^{wt/ki}$ mice were shown a series of stimuli consisting of short bars that only took up 5^{O} of visual space in azimuth (Fig. 3B). The areas in SC that each bar activated were combined, and this map was compared to the map derived from conventional full-field stimuli (Fig. 5C-F). In every case (n=4), the map obtained from spatially-restricted stimuli matched the maps obtained with full-field stimulation very well. In particular, stimulating areas of retina that normally project to the "single" portion of the map always gave one band of activation in the SC, not two as the aggregate tracer data would predict. These results confirm the reliability of our imaging method and rule out the possibility of large areas of functional suppression.

In *Isl2-EphA3*$^{wt/ki}$ mice, RGCs from a small area of retina sometimes project to one location in the SC and sometimes project to two (Brown et al., 2000). We wanted to see whether anatomy and function coincided on an individual level, even though it does not seem to do so on the aggregate level. Therefore, we performed functional imaging and retinal injections of anterograde tracers in the same animals. Adult animals over the age of 40 days were injected with a small amount of the anterograde tracer DiI in the retina. Within a week of injection, functional imaging was performed, the animal was sacrificed, and its eye and brain were recovered for histology. We found that, just as in juvenile mice analyzed at 11-12 days of age in previous studies, some tracer injections in the adult *Isl2-EphA3*$^{wt/ki}$ mice labeled two spots in the SC, some labeled one, and some labeled a long "smear" (Fig. 6A-C, respectively) (Brown et al., 2000). The continued existence of this anatomical variability shows that the high-quality functional maps we

see in adult mice are not a result of refining RGC projections after day 12, when retinal projections were measured in earlier studies. We also found that the functional and anatomical results that were consistent in most animals (Fig. 6). Specifically, of mice with a single dye spot in the SC, 64% (7 of 11 mice) had single maps and 27% (3 of 11) had maps that were single on the side of the SC where the dye spot was located; only 1 mouse had a map that was mostly doubled. Of mice with a doubled dye spot, 42% (5 of 12) had doubled or mostly doubled map, 33% (4 of 12) had mixed-type maps, and 25% (3 of 12) had mostly single maps. Of the 4 mice with a "smeared" dyes pot, 1 had a single map, but the other 3 (75%) had a mixed-type map. A chi-squared test shows that maps with single, doubled, and "smeared" dyespots are associated with significantly different distributions of single, doubled, and mixed maps ($p=0.003$). Overall, 67% of mice had maps where the functional imaging results matched with the anatomical tracer data (single spot with single or single on that side map, double spot with doubled map, "smear" with mixed-type map). These results show that the specific anatomy of the RGC projection in an individual gives rise to that individual's functional map.

Exact level of EphA signaling in *Isl2-EphA3*$^{wt/ki}$ makes map formation non-deterministic

The presence of mixed-type maps suggests that in *Isl2-EphA3*$^{wt/ki}$ mice, the process of map formation is somewhat unstable. Unlike in the ephrin-A triple knockout mouse, where RGCs can choose to innervate any place in the SC, the presence of overall gradients of EphAs and ephrin-As in the SC constrains the map somewhat so that nasal RGCs still tend to project more caudally in the SC and temporal RGCs still tend to project more rostrally (Cang et al., 2008b). However, there is not enough guidance from

the EphAs to definitively push maps towards the single state, as in wildtypes, or towards the doubled state, as in the *Isl2-EphA3*$^{ki/ki}$ mouse. One side of the SC can end up as doubled and the other single, as in (Fig. 2L, M). Because there is currently no way to fine-tune the amount of EphA3 over-expression in the *Isl2-EphA3*$^{wt/ki}$ mouse, we cannot determine experimentally what range of levels of EphA3 over-expression allow for such variability in map formation. Previously, however, computational modeling of SC development has been used to validate the results of anatomical tracing in *Isl2-EphA3*$^{ki/ki}$ and *Isl2-EphA3*$^{wt/ki}$ mice (Koulakov and Tsigankov, 2004; Tsigankov and Koulakov, 2010). Here, we use the same mathematical model to replicate *in silico* the variability we see *in vivo*.

In the model proposed by Tsigankov and Koulakov, map formation depends on graded chemical cues and activity-dependent refinement (Tsigankov and Koulakov, 2010; Tsigankov and Koulakov, 2006). The SC is represented by a 100 by 100 matrix to simulate the termination sites for RGC axons. The chemical cues along the N-T axis of the map simulate the graded expression of EphA and ephrin-A in both retina and SC (see Methods for detailed descriptions). The exogeneous EphA3 in the retinas of *Isl2-EphA3*$^{ki/ki}$ and *Isl2-EphA3*$^{wt/ki}$ mice is simulated by adding a fixed factor, ΔR, to the "chemical cue" profile of every other RGC; the ΔR used for modeling *Isl2-EphA3*$^{ki/ki}$ mice is twice as much the one used to model *Isl2-EphA3*$^{wt/ki}$ mice to represent the effect of possessing two *Isl2-EphA3* alleles as opposed to one. Initially, the map is random, but it undergoes a series of optimization steps. At each step, two randomly chosen RGCs are exchanged with the probability $p = 1/[1 + \exp(4*\Delta E)]$, where $\Delta E = \Delta E_{chem} + \Delta E_{act}$ is the change in adhesive energy due to the exchange. In general, ΔE_{chem} is minimized when the

RGC expressing the highest amounts of receptor project to places in the SC expressing the lowest amounts of ligand and vice versa, which makes sense given the repulsive nature of the interaction between the EphAs and ephrin-As. ΔE_{act} is minimized when RGCs that are close to each other in the retina project close to each other in the SC. After 10^7 steps, orderly and organized topographic maps appear. When ΔR is set to zero, simulating map formation in wildtype animals, the maps are always single (Fig 7C, D). When ΔR is set to a high number like 0.70, representing conditions in the *Isl2-EphA3*$^{ki/ki}$ mouse, the maps are always doubled (Fig 7E, F). However, at the intermediate value of ΔR=0.35, different simulation runs give maps of very divergent structures, reminiscent of the maps seen in *Isl2-EphA3*$^{wt/ki}$ mice. Some runs give rise to maps that are almost entirely single (Fig 7G, H) or doubled (Fig 7I, J), and the majority of maps are mixed (Fig 7K, L). These simulations show that we can use the Koulakov and Tsigankov model to successfully simulate the development of variable maps.

In our model, we can set ΔR to be whatever we choose to simulate the effects of different levels of EphA3 over-expression. To model small changes in the amount of EphA3 over-expression, we varied ΔR by 14% up or down, from ΔR=0.35 to ΔR=0.30 or 0.40. Surprisingly, we found that these small alterations in ΔR caused large changes in map structure. All simulations with ΔR=0.40 resulted in maps with two full-length representations of the vertical meridian, which we called doubled maps (n=20) (Fig. 8A, B). Similarly, all simulations with ΔR=0.30 resulted in single maps (n=10) (Fig. 8C, D). It is clear that map formation is sensitive to small changes in the amount of EphA3 over-expression around ΔR=0.35 and that map formation in *Isl2-EphA3*$^{wt/ki}$ mice must proceed

on a knife's edge of instability, with small changes in EphA3 enough to push map development toward a single or a doubled structure.

Map heterogeneity depends on structured retinal activity

Before eye opening, spontaneous activity in the form of correlated bursts of action potentials propagates across the retina in a wave-like manner (Meister et al., 1991; Wong et al., 1993). These retinal waves are thought to drive patterned activity in areas downstream of the retina, allowing Hebbian mechanisms to refine topographic maps, in particularly along the azimuth axis (Butts and Rokhsar, 2001; Cang et al., 2005b). Because retinal waves cause the creation of smooth maps and contribute to the emergence of local structure, we wondered if they had a role in the heterogeneity seen in *Isl2-EphA3*$^{wt/ki}$ mice. Therefore, we crossed the *Isl2-EphA3* knock-in line with the β2 mutant, which has abnormal retinal waves, to make *EphA3*$^{wt/ki}$*/β2*$^{-/-}$ mice (Bansal et al., 2000). As expected from studies on β2$^{-/-}$ single mutants, the azimuth maps in *EphA3*$^{wt/ki}$*/β2*$^{-/-}$ mice have much lower peak amplitudes than the ones in their *EphA3*$^{wt/ki}$*/β2*$^{+/-}$ littermates (p=0.0002, n=10 for *EphA3*$^{wt/ki}$*/ β2*$^{+/-}$ and n=5 *EphA3*$^{wt/ki}$*/β2*$^{+/-}$) (Fig. 9A), and the peak amplitudes of the elevation maps were somewhat lower as well (p=0.002) (Fig 9B) (Cang et al., 2005b). All *EphA3*$^{wt/ki}$*/β2*$^{-/-}$ mice had single maps (n=10) (Fig. 9E, F). Even in the two mice that had azimuth maps that were too degraded to evaluate, the elevation maps did not display the mid-map discontinuity that is the hallmark of having two separate maps of space (compare Fig. 9E to Fig. 2G, I and Fig 9D). Their *EphA3*$^{wt/ki}$*/β2*$^{+/-}$ littermates retained the ability to make variable maps: only 60% (3 of 5) of them had single maps (Fig. 9C, D). The fact that all

maps from all *EphA3*$^{wt/ki}$/*β2*$^{-/-}$ mice had a similar structure shows that normal retinal waves are necessary for the expression of map variability.

DISCUSSION

The development of orderly and predictable topographic maps relies on both gradients of molecular cues, such as those made by the EphAs and ephrin-As, and patterned activity early in life, like that provided by type II retinal waves. In this paper, we used functional imaging to discover that a well-known map mutant, the heterozygous *Isl2-EphA3* knock-in mouse, displays significant variability in its collicular maps. This variability was not predicted by aggregate anatomical tracer data, but an individual's anatomical projection phenotype correlated well with its phenotype as assessed by functional imaging. The source of this heterogeneity was not strictly genetic, as an animal's two colliculi could have different map structures. We inferred from functioning imaging and then confirmed with computational modeling that the exact level of over-expression of EphA3 was crucial for map variability. Patterned retinal activity in the form of retinal waves was also necessary for the expression of map heterogeneity.

Instability in map formation

The formation of the collicular map is a prolonged, multi-stage process involving exuberant over-extension of branches followed by massive reorganization and pruning (Feldheim and O'Leary, 2010). It is easy to imagine how randomly choosing to prune one set of branches and not another could greatly influence the eventual shape of the map. However, maps in wildtype mice are highly stereotyped, suggesting that in normal

animals, the forces of molecular cues and neural activity can adjust for any deviations that may occur. Previous studies have shown that map variability can occur when these factors are disrupted or when the input to a map is too abnormal to accommodate within that map's normal structure. An example of the former is the ephrin-A triple knockout mouse, which is missing all ephrin-A signaling in SC and has essentially random large-scale retinocollicular projection patterns (Cang et al., 2008b). An example of the latter is found in the Siamese cat, in which a grossly altered retinogeniculate projection pattern causes the dLGN to send very abnormal input to primary visual cortex. In response, the cortical topographic maps of space in the primary visual cortex of these cats organize into one of two different ways (Kaas and Guillery, 1973). The variability in these maps, then, is a result of extremely disruptive manipulations. In contrast, the present study finds heterogeneity in a map mutant with a relatively subtle molecular phenotype. The *Isl2-EphA3*$^{wt/ki}$ mouse still possesses normal background levels of EphAs and ephrin-As. The overall effect of this allele on mapping is so mild that the maps in the V1 of these mice are of normal structure. Indeed, a slightly stronger manipulation, giving a mouse two *Isl2-EphA3* alleles instead of one, restores a fixed map pattern in the colliculus, albeit at the cost of making the entire collicular map abnormal all the time instead of just in some individuals (Triplett et al., 2009). The fact that map heterogeneity can still appear in the absence of large-scale manipulations suggests that a certain small amount of randomness is present in the mechanisms that create the map of the azimuth axis, a stochasticity that can be revealed under the right conditions.

What factors cause the map in an individual *Isl2-EphA3*$^{wt/ki}$ mouse to become single or doubled? One possibility is that the individual level of over-expression of

EphA3 biases map formation from the start. We do show that small changes in the amount of EphA3 over-expression can influence map structure, and there is natural variability in protein transcription and translation. So, mice with single maps, for example, might just be mice that happen to over-express EphA3 to a lesser extent than normal. Although we cannot rule out the possibility that some mice have the maps they do because they stochastically made more or less of the EphA3 than other mice, it is unlikely that the structure of most maps are determined in this way. After all, the most common type of map seen both *in vivo* and in our simulations is the mixed type, which by definition developed in a range of EphA3 over-expression that was conducive to map instability. It is more likely that the structures of individual *Isl2-EphA3*$^{wt/ki}$ mice evolve gradually in response to random decisions made early during the process of map formation.

Relating functional imaging to anatomical data

Most studies of the development of the retinocollicular connection, and most studies of map development in general, rely on techniques using anatomical tracers. It seems likely that if many individual projections displayed altered mapping, it would cause disruptions in the large-scale function of the SC as well. Indeed, mutants missing single or multiple ephrin-As have both ectopic termination zones anterior or posterior to the correct site of termination and disorganized functional maps of azimuth (Cang et al., 2008b; Feldheim et al., 2000). Because it not possible to trace the projections from more than one or two places in the retina, when trying to infer the structure of a large-scale map from tracing data, one can only combine the data from many mice and assume that

the sum of the data gives an accurate view of the map. Unfortunately, this strategy only works if the map in every mouse is the same, and in this paper, we found out that maps in *Isl2-EphA3*$^{wt/ki}$ mice are actually quite diverse. The lab that generated the *Isl2-EphA* allele has since used it in combination with other genetic manipulations of EphA levels, such as knocking out various EphAs, to further probe retinocollicular development (Bevins et al., 2011; Reber et al., 2004). Given the presence of map variability in *Isl2-EphA3*$^{wt/ki}$ mice and its dependence on the exact level of EphA3 over-expression, it would be interesting to know if these new multiple mutants also display map variability. In particular, studies of the *Isl2-EphA3*$^{wt/ki}$ mouse in a background lacking other EphAs would disclose whether map variability is a function of absolute amounts of EphA3 or over-expression levels relative to the background levels of EphAs.

A few of the animals we studied appeared to lack concordance between their individual anatomic tracing data and their functional map structure. We believe this is because our functional imaging techniques do not reveal the entirety of the SC: the caudal-most portion of the SC lies beneath or behind the sinuses below the lambda suture, and removing these sinuses is not feasible. Therefore, some of the tracer injections projected to places on the SC that were not imaged. Since our imaging and simulation data both show that *Isl2-EphA3*$^{wt/ki}$ maps can have different types of structure within the same SC, it is possible that the discordant projections ended up in unimaged locations with a different local map structure.

Role of patterned retinal activity

We found that *EphA3*$^{wt/ki}$*/β2*$^{-/-}$ double mutants always displayed a single map, suggesting that retinal waves play an important role in causing map variability. The β2 mutant is a global knockout of the β2 subunit of the nicotinic acetylcholine receptor, however, and it is possible that the lack of map variability is caused by some other role of β2 in the retina or colliculus. However, previous studies have shown that interfering with the retinal waves using other methods, such as injection of the cholinergic agonist epibatidine, disrupts visual map formation similarly to the β2 knockout (Cang et al., 2005b). It is also clear that β2 mutants have fragile and abnormal retinal waves, although the exact nature of the wave phenotype *in vivo* is not clear (Bansal et al., 2000; Sun et al., 2008). Thus, the most likely mechanism for how the knockout of β2 affects map variability is through its effects on the retinal waves.

The wave-like bursts of activity in the retina during the first week of life produce neural activity with the property that cells that are physically close to each other have more correlated activity than do cells that are far away from each other. In activity-dependent mapping models, neurons with similar activity patterns are more likely to synapse on the same or adjacent target cells than are neurons with different activity patterns (Butts and Rokhsar, 2001; Debski and Cline, 2002). Therefore, retinal waves makes the development of smooth topographic maps more likely by encouraging a topographic organization such that neighboring cells in the SC receive input from neighboring cells in the retina. In the *Isl2-EphA3*$^{wt/ki}$ mouse, it is likely that the retinal waves, in acting to make the map smooth, are inadvertently be forcing the map to "choose" at any given point along the azimuth axis whether to be either single or doubled. In *EphA3*$^{wt/ki}$*/β2*$^{-/-}$ mice, which lack retinal waves, fine-scale refinement does not occur,

lowering the quality of the map. In addition, neighboring cells in the SC do not feel any pressure to receive input from neighboring RGCs, and RGCs choose where to project strictly on the basis of the levels of EphAs and ephrin-As present in the retina. As the collicular EphA/ephrin-A gradients in this mouse are still monotonic and single, the functional maps in *EphA3*$^{wt/ki}$*/β2*$^{-/-}$ mice are single too.

Overall model of retinocollicular mapping

The findings of the present experiments are consistent with an account of map formation that involves two main processes. First, each RGC branch terminal seeks its optimal position in the fixed ephrin-A gradients of the superior colliculus according to its own level of EphA expression. Second, each RGC also tries to terminate next to its retinal neighbors so that their combined activity at the peaks of the retinal waves is most effective at driving SC cells. In wildtype mice, these two goals are in harmony: neighboring RGCs have similar EphA expression levels as well as similar activity. In the knock-in *Isl2-EphA3* mice, however, the EphA expression levels of Isl2^{+} RGCs are quite distinct from those of their Isl2^{-} neighbors, even though their activity patterns are still nearly identical. If the difference in EphA expression is sufficiently great to separate the two populations completely or nearly completely initially during the activity-independent phase of growth, as it is in the *Isl2-EphA3*$^{ki/ki}$ mouse, each of the two maps of space can independently further refine under the influence of retinal activity. The effect of this refinement is to make each map isotropic, giving rise to a discontinuity in the representation of elevation between the rostral and caudal maps. Overall, activity-

dependent refinement contributes positive feedback to the process of map formation, making it metaphorically autocatalytic.

On the other hand, if the EphA levels of neighboring Isl2^{+} and Isl2^{-} RGCs are not very distinct, their initial activity-independent projections will overlap extensively. The influence of correlated activity would easily triumph over the weak EphA differences, driving the formation of a wildtype-like single map.

The outcome for map formation can only go either way when the amount of EphA over-expression in the Isl2^{+} RGCs is at a certain critical level, as it is in the *Isl2-EphA3*$^{wt/ki}$ mouse. In these mice, Isl2^{+} and Isl2^{-} projections initially overlap to a moderate degree. Development could then proceed in one of two possible ways. The projections could begin to separate, and the positive feedback of correlated activity within each RGC population would drive them to form separate, orderly isotropic maps similar to the ones found in *Isl2-EphA3*$^{ki/ki}$ animals. Alternatively, the influence of correlated activity could overcome the EphA distinctions and drive the formation of a single map. At this critical level of EphA3 over-expression, stochastic events like small changes in the level of EphA3 expression or the overall strength of EphA/ephrin-A signaling would be enough to push the outcome towards either a single or a double map. Once a structure begins to coalesce, activity-dependent refinement would encourage neighboring RGCs to organize themselves in accordance with the emerging map, solidifying it. Interestingly, if the refinement begins simultaneously at different points in the SC, it is possible for this process to produce a single map in one half of the SC and a doubled map in the other half, a result that was repeatedly observed *in vivo*. In the absence of correlated activity, the variability of the maps would disappear, as it actually does in *EphA3*$^{wt/ki}$*/β2*$^{-/-}$ mice.

The present experimental observations and their complete confirmation and extension in the mathematical model provide overwhelming support for this account of collicular map formation.

Conclusions

We demonstrate that topographic maps in *Isl2-EphA3*$^{wt/ki}$ mice are variable, suggesting that this level of EphA signaling brings the process of map formation close to a point of instability. Normal patterns of activity in the retina early in life are necessary for expressing map heterogeneity. Our data illustrate how using functional measures of topographic mapping complements the use of traditional anatomical tracers in elucidating map structure and development.

METHODS

Mice

Isl2-EphA3 knock-in and *nAChR-β2* mutant mice were generated and genotyped as previously described (Brown et al., 2000; Xu et al., 1999). Mice were maintained on a mixed CD-1/C57Bl6 background. All mice used in this paper were adults at least 40 days of age. All mouse protocols were performed in accordance with the University of California Santa Cruz and San Francisco IACUC standards.

Functional imaging

Imaging of intrinsic optical signals was performed as described previously (Cang et al., 2008a; Kalatsky and Stryker, 2003). Briefly, adult mice older than P40 were anesthetized with intraperitoneal injections of urethane (1.0 g/kg in 10% saline solution) supplemented

with chlorprothixene (0.03 mg/kg). Animals were also given atropine (0.3 mg/kg) and dexamethasone (2 mg/kg) subcutaneously. A tracheotomy was performed, and a craniotomy was made along the midline and lambda sutures of the left hemisphere. In some animals, we then performed functional imaging of cortical maps. Afterwards, the cortex overlying the superior colliculus was aspirated, and we imaged maps of the SC. Electrophysiological studies demonstrate that ablating or silencing visual cortex does not change receptive field properties of superficial SC neurons (Drager and Hubel, 1976; Schiller et al., 1974). Optical images of the cortical intrinsic signal were obtained at the wavelength of 610 nm, using a Dalsa 1M30 CCD camera (Dalsa, Waterloo, Canada) controlled by custom software. A high-refresh-rate monitor (Nokia Multigraph 4453, 1024 × 768 pixels at 120 Hz) was placed 25 cm away from the animal where it subtended 70° of the contralateral visual field. Drifting thin bars (2° width) were displayed on the monitor. Most experiments used bars the length of the full screen, but some experiments used shorter bars the length of 5° of visual angle. Animals were presented with horizontal or vertical bars drifting orthogonal to the axis corresponding to either the dorsal-ventral or nasal-temporal axis of the animal in order to stimulate constant lines of elevation or azimuth, respectively. After imaging, in some cases, an additional craniotomy would then be made over the right hemisphere to image the other superior colliculus.

RGC axon tracing and fluorescent microscopy

Mice were anaesthetized by intraperitoneal injection of 100 mg/kg ketamine and 10 mg/kg xylazine. A small amount of 1,1'-dioctadecyl-3,3,3',3'-tetramethylindocarbocyanine (DiI) (Invitrogen, Carlsbad) was injected at focal regions intraocularly using a handheld picospritzer (Parker Instrumentation, Cleveland) and a

pulled glass needle as described previously (Feldheim et al., 2000). Between one and two weeks after injection, animals were imaged as described above. After imaging, animals were immediately sacrificed and intracardially perfused with ice-cold 4% paraformaldehyde (PFA) in PBS. Brains were dissected out, fixed overnight, and embedded in 2% agarose in PBS. Whole mounts of the superior colliculus were imaged using a digital camera through a 2.5X, 5X or 10X objective on an Axioskop 2 Plus microscope (Zeiss).

Analysis of retinotopic maps

The peak amplitude of maps was measured directly. The size of topographic maps were analyzed using custom software in Matlab. Size was taken to be the response area of the elevation map within 15% (for SC) or 30% (for V1) of the peak magnitude. Statistical tests were performed as indicated in the figure legends.

Modeling of retinotopic map formation

We followed the modeling studies of (Tsigankov and Koulakov, 2006) and (Tsigankov and Koulakov, 2010) to simulate map formation in the SC. Briefly, the SC is represented by an N by N matrix (N=100), which is the termination sites for the RGC axons. The initial map is random. On each step of the optimization procedure, we choose two RGC axons in SC randomly and exchange them with the probability $p = 1/[1 + \exp(\Delta E)]$, where ΔE is the change in adhesive energy due to the exchange. The formation of retinotopic map in SC depends on two components, graded chemical guidance cues (ΔE_{chem}) and activity dependent refinement (ΔE_{act}), in the following form: $\Delta E = \Delta E_{chem} + \Delta E_{act}$.

The contribution of chemical guidance cues is modeled by the following formula:

$E_{chem} = \Sigma_i \alpha*R_A(i)*L_A(r_i) - \beta*R_B(i)*L_B(r_i)$, where $R_A(i)$ represents the EphA receptor level of point (i) in retina and $L_A(r_i)$ represents ephrin-A ligand level in its target point in SC; $R_B(i)$ and $L_B(r_i)$ simulate levels of receptors and ligands that have graded expressions and are required for map formation along dorsoventral axis; and $\alpha=\beta=120$ describe the strength of contributions.

The expression levels of these components are simulated following the original model found in (Tsigankov and Koulakov, 2006):

$R_A(x) = \exp(-x/N)- \exp(x/N - 2)$ and

$L_A(x) = \exp(x/N - 1) - \exp(-1 - x/N)$, where $x = 1…N$ is the coordinate along the N-T axis.

$R_B(y) = \exp(-y/N)$; $L_B(y) = \exp(-y/N)$, where y is the D-V coordinate.

To model the contribution of the extra EphA3 expressed in the retinas of *Isl2-EphA3* knock-in mice, a factor ΔR was added to R_A to every other cell in the retinal matrix. Following (Tsigankov and Koulakov, 2010), the value of ΔR was set to 0.70 to model the homozygous *Isl2-EphA3* knock-in and to 0.35 to model the heterozygote.

The contribution of activity-dependent process is modeled as:

$E_{act} = -\gamma/2\Sigma_{i\,j}C_{ij}U(r_i - r_j)$, where $\gamma = 0.30$ is the strength parameter; $C_{i\,j}$ is the cross-correlation of neuronal activity between two RGCs during retinal waves; and U simulates the overlap between two SC cells. Here, we use $C_{i\,j} = \exp(-r/R)$, where r is retinal distance between axons i and j and $R = 0.11*N$ and $U(r) = \exp(-r^2/(2d^2))$, where r is the distance between two SC points and $d = 5$ is the range of Hebbian attraction in the SC.

REFERENCES

Please refer to the global list of references in this dissertation.

ACKNOWLEDGEMENTS

This work was supported by grants from the NIH (R01-EY014689 to D.A.F. and R01-EY02874 to M.P.S.) J.W.T. was supported by an NIH National Research Service Award Postdoctoral Fellowship (F32- EY18531). M.T.O was supported by a NSF Graduate Research Fellowship and an NIH Training Program for the Visual Sciences (T32-EY007120). We thank Greg Lemke (R01-NS031249) for his creation of the *Isl2-EphA3* knock-in mice. We also thank Sam Pleasure, Erik Ullian, and members of the Feldheim and Stryker labs for discussion and critical reading of the manuscript.

Figure 1

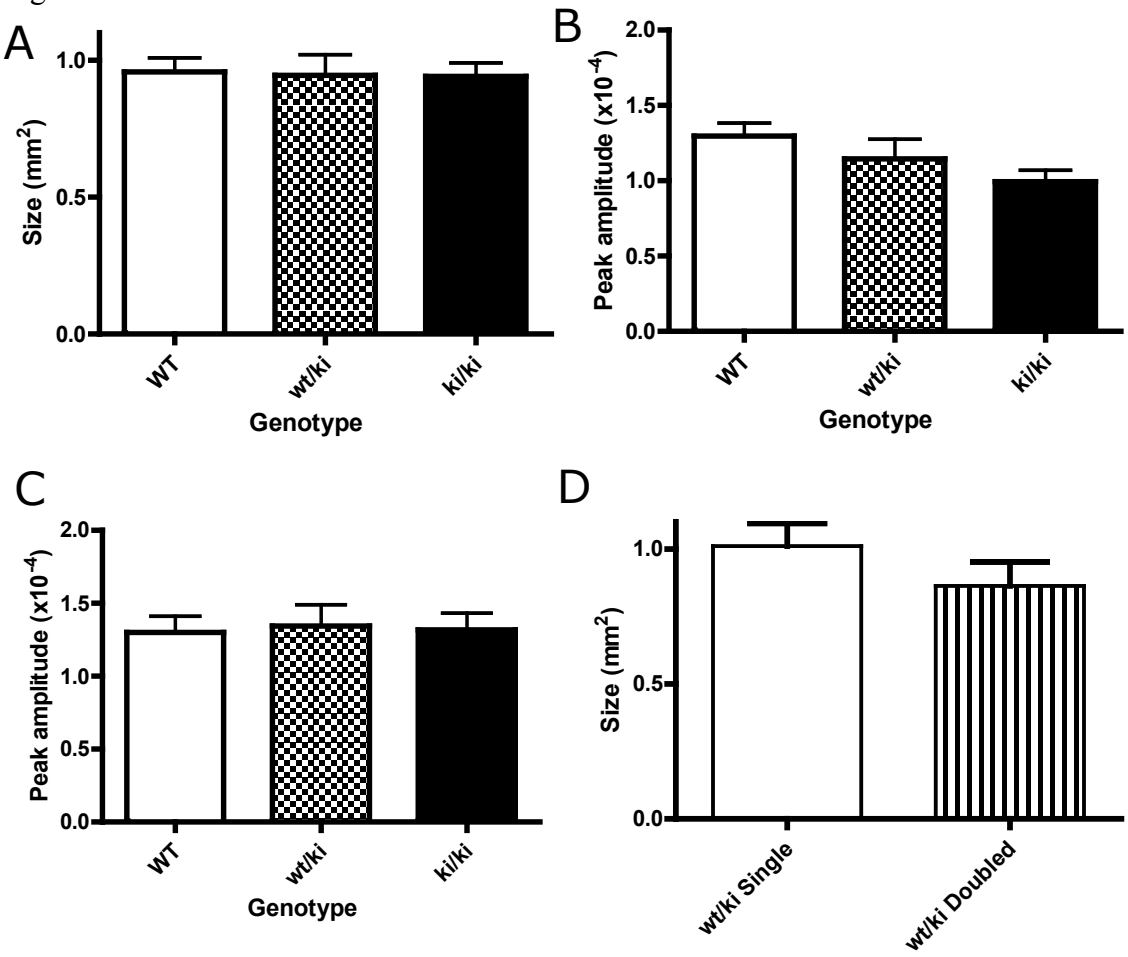

Figure 1: A. Size of SC map in wildtype (WT), *Isl2-EphA3*$^{wt/ki}$ (wt/ki), and *Isl2-EphA3*$^{ki/ki}$ (ki/ki) mice. B-C. Peak amplitude of the azimuth (B) and elevation (C) maps as a fractional change in reflection in WT, wt/ki, and ki/ki mice. D. Size of the SC map in *Isl2-EphA3*$^{wt/ki}$ mice with single or doubled maps of space in the SC. A-C analyzed with a one-way ANOVA with a Bonferroni multiple comparisons test. D analyzed with a two-tailed Student's t-test.

Figure 2

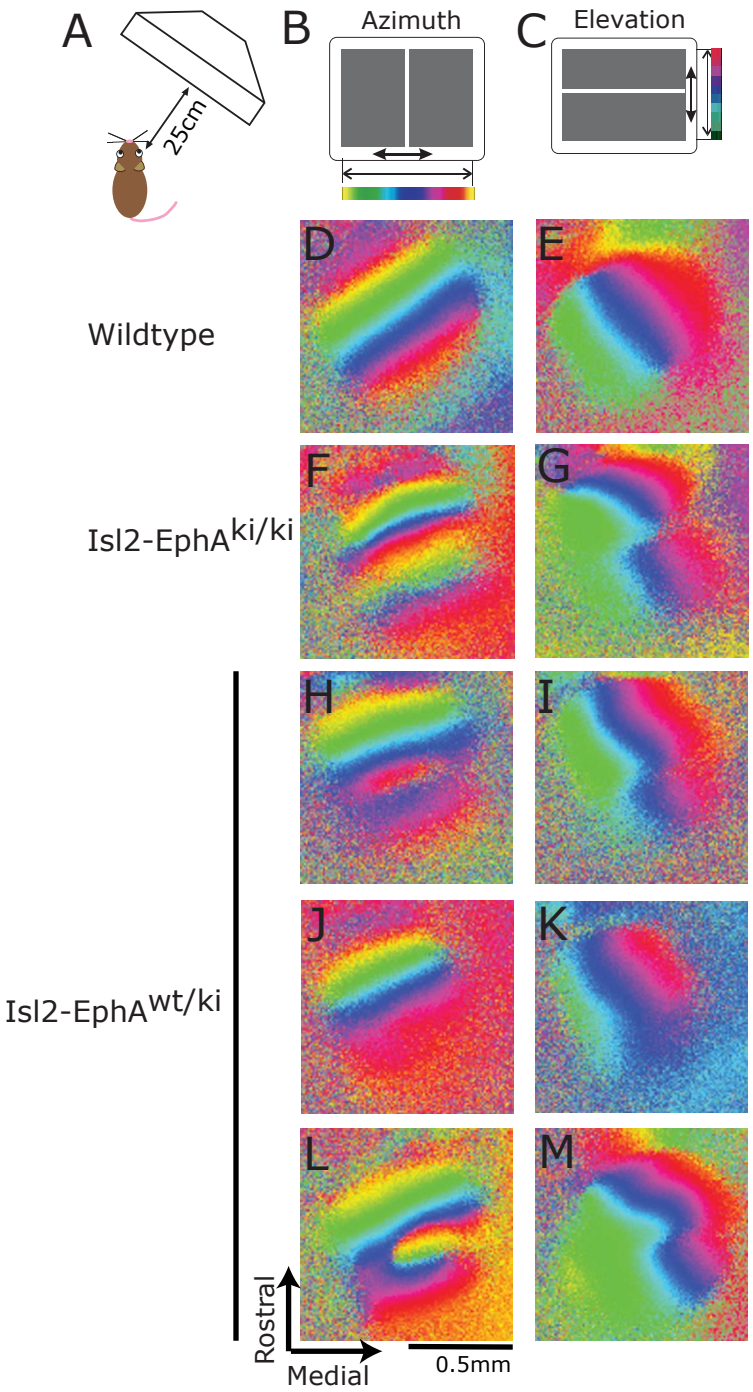

Figure 2: A. A stimulus monitor is placed 25cm away from the anesthetized mouse contralateral to the hemisphere being imaged. B-E. Collicular azimuth (D) and elevation (E) maps of a wildtype mouse. The color code used to represent positions of different lines on the stimulus monitor is illustrated in panel B for azimuth and C for elevation. F, G. Maps of azimuth (F) and elevation (G) from an *Isl2-EphA*$^{ki/ki}$ mouse. H-M. Azimuth (H, J, L) and elevation (I, K, M) maps from individual *Isl2-EphA*$^{wt/ki}$ mice. Each row shows maps from the same mouse.

Figure 3

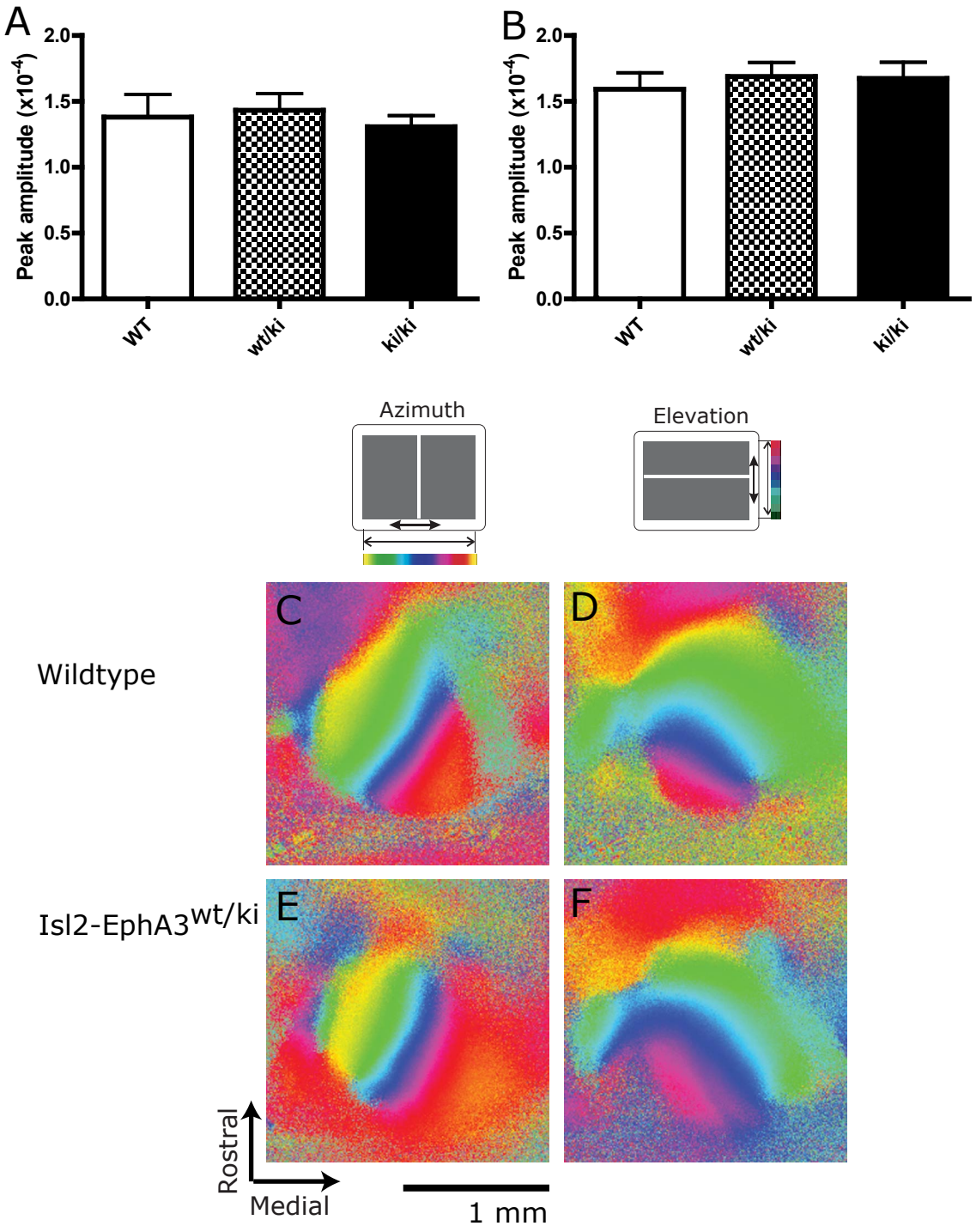

Figure 3: A, B. Peak amplitude of the azimuth (A) and elevation (B) maps as a fractional change in reflection in wildtype (WT), *Isl2-EphA3*$^{wt/ki}$ (wt/ki), and *Isl2-EphA3*$^{ki/ki}$ (ki/ki) mice. C, D. Azimuth (C) and elevation (D) maps of primary visual cortex from a representative wildtype animal. E, F. Azimuth (E) and elevation (F) maps of primary visual cortex from a representative *Isl2-EphA3*$^{wt/ki}$ animal.

Figure 4

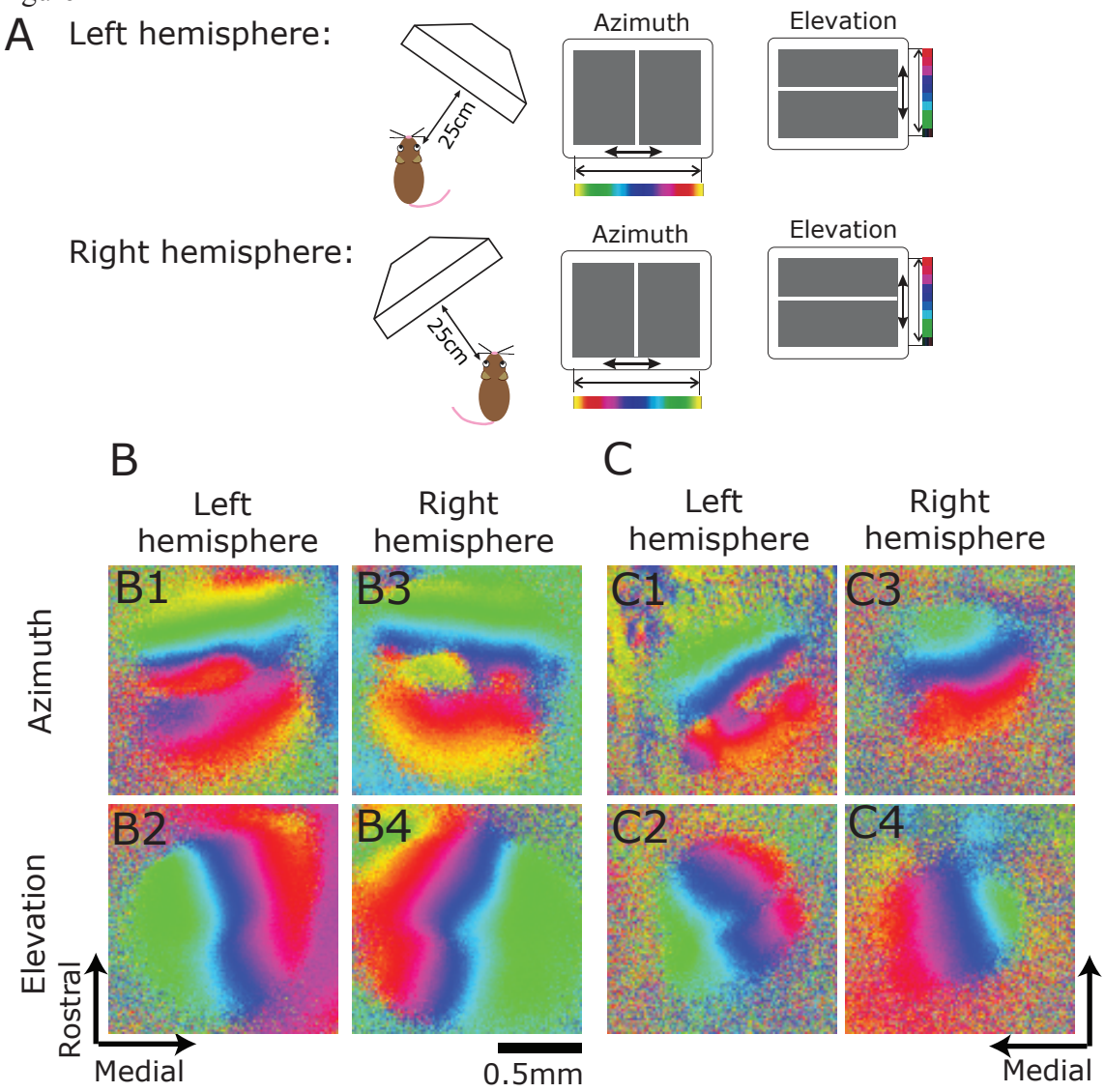

Figure 4: A. Setups for imaging left and right hemispheres. Note that the color code for the azimuth maps in the right hemisphere have been reversed. This change preserves the relationship between color and location along the nasotemporal axis of the retina, with green representing more nasal locations and red representing more temporal ones. The color code for the elevation maps is the same. B. Maps from the left (B1, B2) and right (B3, B4) hemisphere colliculi of one mouse. B1 and B3 are of azimuth and B2 and B4 of elevation. C. Maps from the left (C1, C2) and right (C3, C4) hemisphere colliculi of another mouse. C1 and C3 are of azimuth and C2 and C4 of elevation.

Figure 5

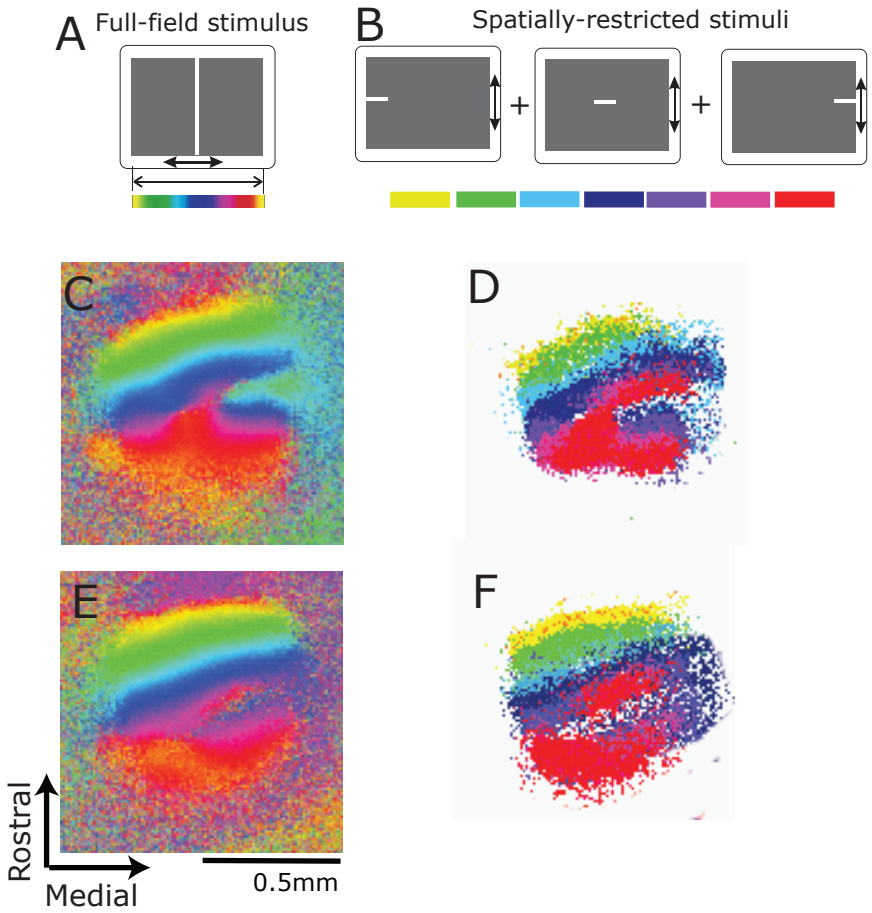

Figure 5: A. The full-field stimulus is a single bar the length of the entire screen. B. Spatially-restricted stimuli are bars of length 5^{o} sampling small areas of azimuthal space. Each animal was shown seven different short-bar stimuli that together covered the whole visual field. C, E. Full-field azimuth maps of two *Isl2-EphA3*$^{wt/ki}$ mice. The color code used to illustrate the maps is shown in panel A. D, F. Azimuth maps derived from spatially-restricted stimuli. The area that each short-bar stimulus activated in the SC was color-coded as shown in panel B, and the activation areas from the seven stimuli were combined. D is from the same mouse as C, and F from the same mouse as E.

Figure 6

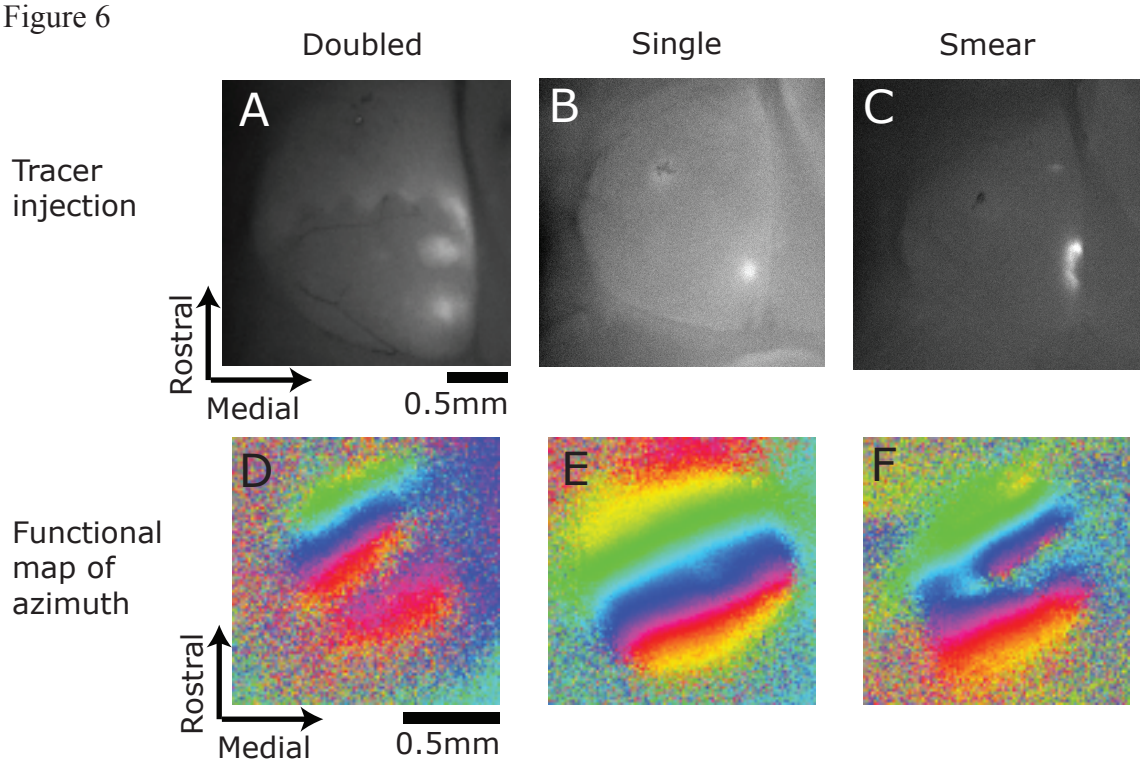

Figure 6: A-C. Colliculi of mice injected with anterograde tracer DiI in retina. D-F. Functional maps of azimuth from the same animals. Each column represents matching tracer/functional imaging results from an individual animal.

Figure 7

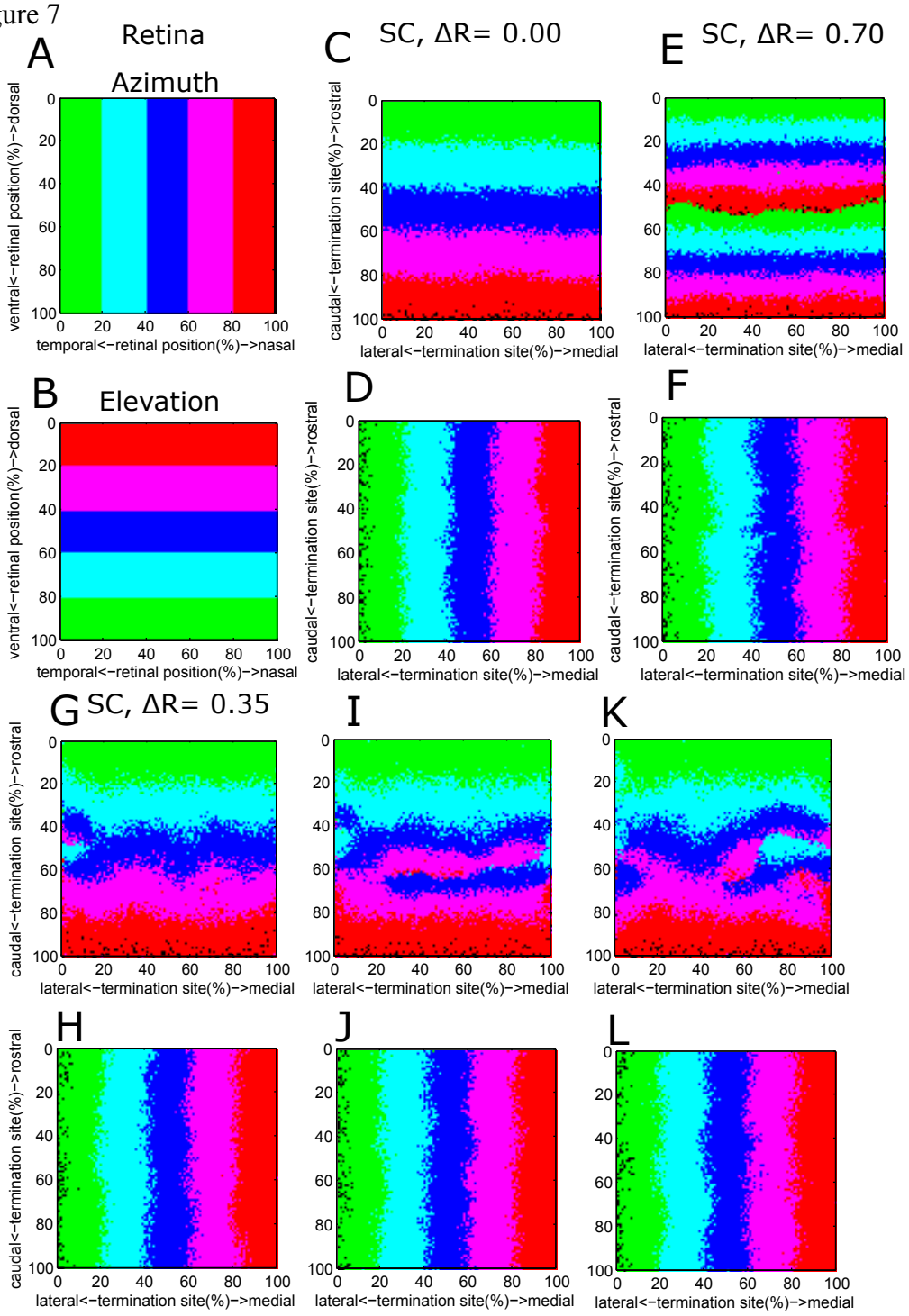

Figure 7: The SC is represented by a 100 × 100 matrix, which are the termination sites for RGC axons. C, D. Simulated map with ΔR=0, representing wildtype development. C is map in azimuth and D is map in elevation. Color codes shown in A (azimuth) and B (elevation). E, F. Simulation with ΔR=0.7 in azimuth (E) and elevation (F), representing map in *Isl2-EphA*$^{ki/ki}$ mice. G, H; I, J; K, L. Simulations with ΔR=0.35 in azimuth (G, I, K) and elevation (H, J, L), representing maps of *Isl2-EphA*$^{wt/ki}$ mice.

Figure 8

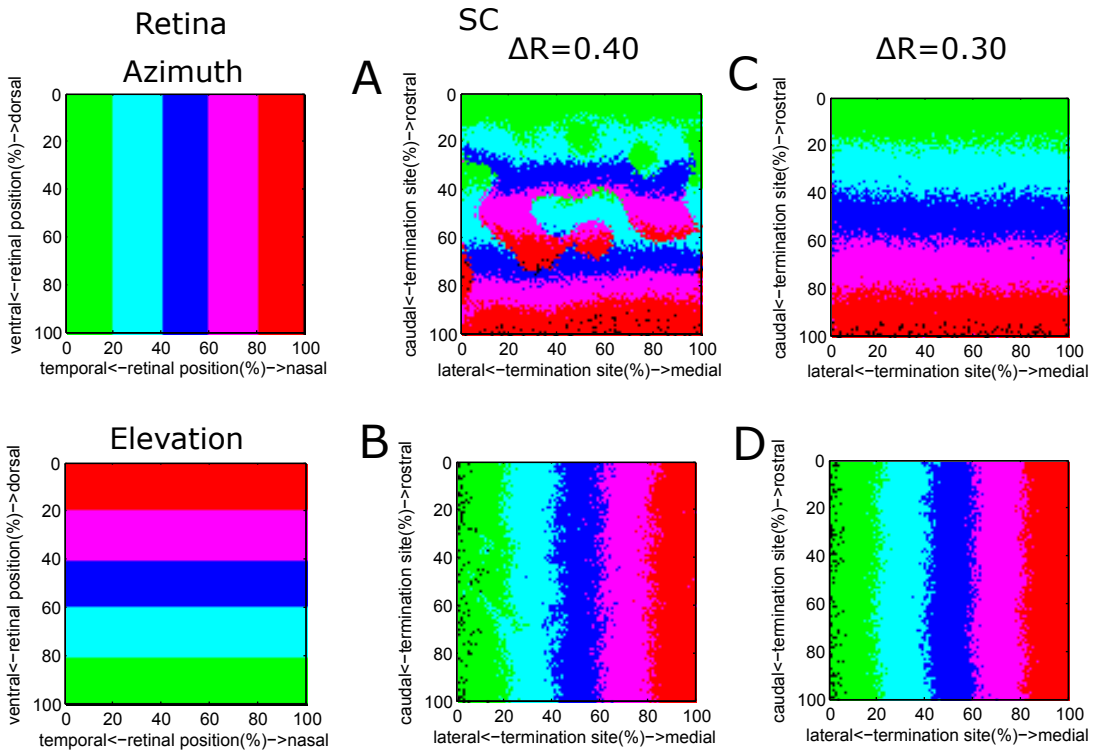

Figure 8: A, B. Azimuth (A) and elevation (B) map of a representative simulation with ΔR=0.4. C, D. Azimuth (C) and elevation (D) map of a representative simulation with ΔR=0.3.

Figure 9

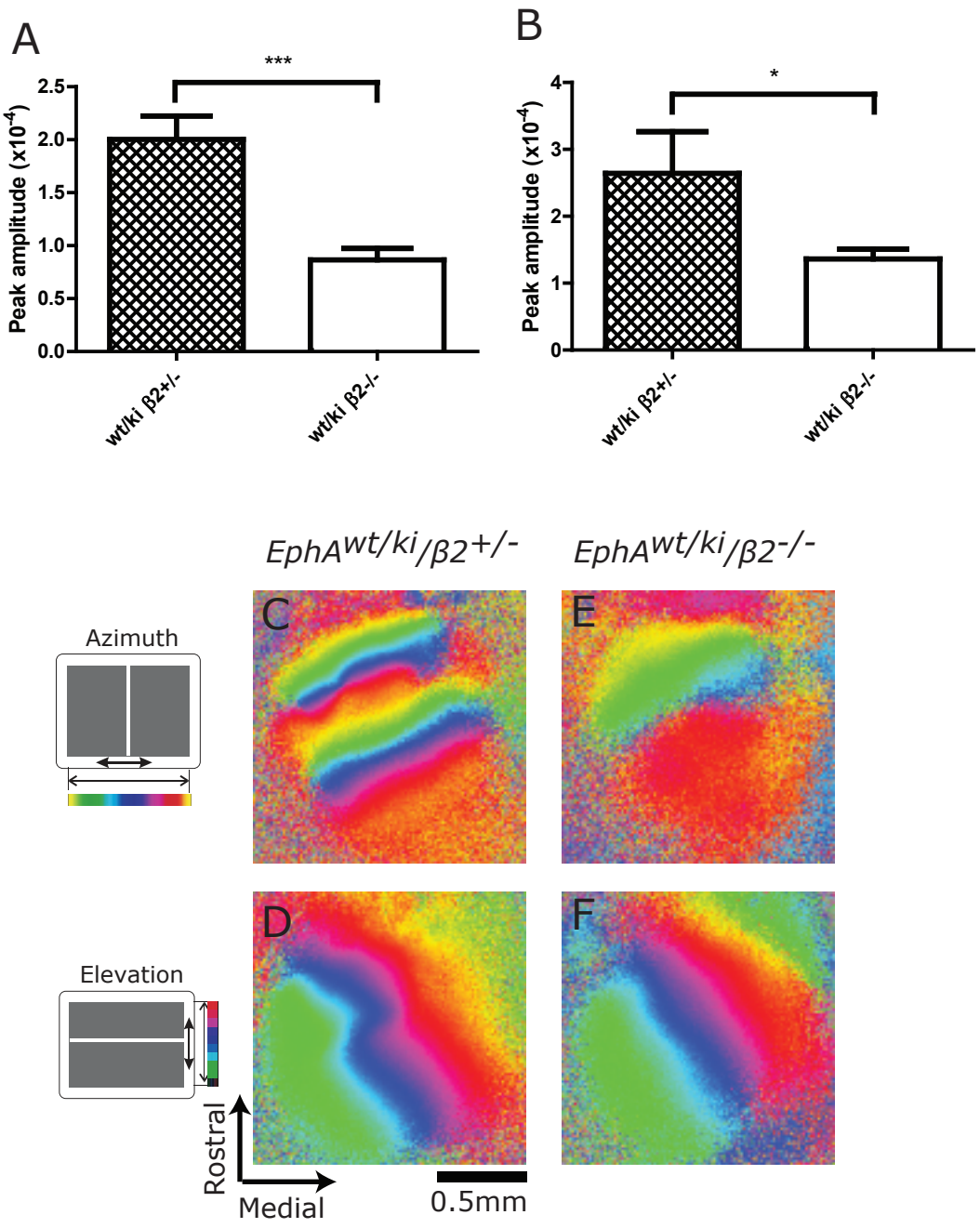

Figure 9: A, B. Peak amplitude as a fractional change of reflection in the azimuth (A) and elevation (B) maps of *EphA*$^{wt/ki}$/*β2*$^{+/-}$ and *EphA*$^{wt/ki}$/*β2*$^{-/-}$ double mutants. ***: p<0.005; *: p<0.05. C,D. Azimuth (C) and elevation (D) maps from a *EphA*$^{wt/ki}$/*β2*$^{+/-}$ mouse that happened to have a doubled map. E,F. Azimuth (E) and elevation (F) maps from a representative *EphA*$^{wt/ki}$/*β2*$^{-/-}$ mouse.

Conclusions

The proper functioning of the adult brain depends on events that happen early in life, when each of the billions of neurons that comprise the nervous system must find and connect to the correct partners. The way visual brain areas arrange their connections into orderly, precise, and smooth topographic maps is a model not only for how other sensory pathways self-organize but also for neural development in general.

Two factors have emerged as organizing principles in the development of topographic maps. The first is molecular guidance cues. As Roger Sperry postulated in his chemoaffinity hypothesis, axons make connections between areas in a way that matches graded labels between the source and the target (Sperry, 1963). During the time visual system projections are forming, opposing counter-gradients of various molecules are present across the nascent retina, superior colliculus (SC), and primary visual cortex (V1). The molecular cues whose roles have been studied the most during visual system development are the tyrosine kinases the EphAs and their ligands the ephrin-As, which are present in gradients that are consistent with mapping the azimuth axis of space, which corresponds to the nasotemporal axis of the retina (Marcus et al., 1996; Flenniken et al., 1996; Flanagan, 2006; Cang et al., 2005a). Altering relative concentrations of either the EphAs or the ephrin-As can cause drastic changes in the organization of visual maps on both an anatomical and a functional level (Cang et al., 2005a; Cang et al., 2008b; Brown et al., 2000; Triplett et al., 2009).

The second organizing principle is neural activity. In 1949, Donald Hebb proposed that as a general rule, neurons preferentially strengthen their connections to other neurons that have matching activity patterns (Hebb, 1949). In the visual system,

spontaneous bursts of activity sweeps across the retina during the first week of life, when the connections to the SC and the dorsolateral geniculate nucleus (dLGN) form (Bansal et al., 2000; McLaughlin et al., 2003). These type II retinal waves produce neural activity with the property that retinal ganglion cells (RGCs) that are physically close to each other and therefore respond to similar regions of space have more correlated activity than RGCs that are far away from each other. In activity-dependent mapping models based on Hebb's rule, neurons with similar activity patterns are more likely to synapse on the same or adjacent target cells than are neurons with different activity patterns (Butts and Rokhsar, 2001; Debski and Cline, 2002). Therefore, retinal waves act to refine maps and cause them to be locally smooth. Interfering with the waves either pharmacologically or by knocking out the β2 subunit of the nicotinic acetylcholine receptor alters formation of the azimuth map anatomically and functionally in the SC and V1 and can alter visual behavior in the azimuth axis (Cang et al., 2005b; McLaughlin et al., 2003; Wang et al., 2009). It is the pattern and not the mere presence of neural activity that is required for map formation. Although the exact nature of the wave phenotype of the β2 knockout mouse *in vivo* is not clear, even the studies that claim the strongest effects *in vitro* show that the β2 knockout's RGCs are still active (Bansal et al., 2000; Sun et al., 2008). Therefore, it is the specific pattern of activity that these waves produce that is important for making smooth maps.

In this dissertation, I study how the patterned retinal activity and molecular guidance cues the Ephs and ephrins shape topographic projections and maps in a number of different visual system models: the retinocollicular projection, the retinogeniculo-cortical pathway, and the corticocollicular projection. Using optical intrinsic signal

imaging, I characterize for the first time the functional topographic maps of several different mutant mice with altered Eph and ephrin signaling. By crossing some of those mutants with β2 knockout mice, I can analyze how those Eph and ephrin mutations affect mapping in the presence and absence of retinal waves. I combine these results from functional imaging with those from anatomical tracing techniques and computational modeling to form a more complete picture of topographic map development.

The retinocollicular projection

The growth of the projection from the retina to the superior colliculus, which is called the optic tectum in non-mammalian animals, is one of the most widely studied models of neural development. RGCs from nasal retina project to the caudal part of the SC, and RGCs from temporal retina project to the nasal part (Feldheim and O'Leary, 2010). Previous studies have shown that both EphA/ephrin-A signaling and retinal waves are critical for patterning the azimuth map, which is represented rostrocaudally in the SC. Absence of both of these factors nearly obliterates retinotopic order in this axis (Cang et al., 2008b). In particular, it is known that changes in relative levels of EphAs in the retina are sufficient for restructuring the azimuth map. Mice with the *Isl2-EphA3* knock-in allele mouse over-express EphAs in a spatially random subset of their RGCs, the ones that also express *Isl2*; this over-expression encourages $Isl2^+$ neurons, on average, to project more rostrally than $Isl2^-$ RGCs. Previous work has shown that there is a duplicated representation of azimuth in mice that are homozygous for this allele (*Isl2-EphA3*$^{ki/ki}$ mice), and in chapter 2 I show that the $Isl2^+$ and $Isl2^-$ RGCs form two completely separate, coherent maps of space in colliculus (Brown et al., 2000; Triplett et al., 2009).

In chapter 4, I go on to discover that maps in mice that are heterozygous for this allele (*Isl2-EphA*$^{wt/ki}$ mice) display unexpected variability. Some animal's maps are doubled, as in the *Isl2-EphA3*$^{ki/ki}$ mouse; some are single, as in wildtype mice; and some show a combination of the two structures in different sections of the SC. This heterogeneity does not arise from inter-individual genetic differences but rather is a result of stochastic processes present during map formation. Using a computational model, I show that the *Isl2-EphA*$^{wt/ki}$ mouse exists at a point of instability: changing the over-expression levels of EphA3 even slightly causes map structures to be much less diverse. I also conclude that patterned neural activity must work together with the EphA3 over-expression to cause this variability, since mice that are heterozygous for the *Isl2-EphA3* allele but lack retinal waves do not have variable maps.

My findings, along with previous work concerning retinocollicular development in wildtype *Isl2-EphA3*$^{ki/ki}$ mice, and are consistent with an account of map formation that involves the two main factors of molecular guidance cues and neural activity. First, each RGC branch terminal seeks its optimal position in the fixed ephrin-A gradients of the superior colliculus according to its own level of EphA expression. Second, each RGC also tries to terminate next to its retinal neighbors so that their combined activity at the peaks of the retinal waves is most effective at driving SC cells. In wildtype mice, these two goals are in harmony: neighboring RGCs have similar EphA expression levels as well as similar activity. In the knock-in *Isl2-EphA3* mice, however, the EphA expression levels of Isl2^{+} RGCs are quite distinct from those of their Isl2^{-} neighbors, even though their activity patterns are still nearly identical. If the difference in EphA expression is sufficiently great to separate the two populations completely or nearly completely

initially during the activity-independent phase of growth, as it is in the *Isl2-EphA3*$^{ki/ki}$ mouse, each of the two maps of space can independently further refine under the influence of retinal activity. The effect of this refinement is to make each map isotropic, giving rise to a discontinuity in the representation of elevation between the rostral and caudal maps. Overall, activity-dependent refinement contributes positive feedback to the process of map formation, making it metaphorically autocatalytic.

On the other hand, if the EphA levels of neighboring Isl2^{+} and Isl2^{-} RGCs are not very distinct, their initial activity-independent projections will overlap extensively. The influence of correlated activity would easily triumph over the weak EphA differences, driving the formation of a wildtype-like single map.

The outcome for map formation can only go either way when the amount of EphA over-expression in the Isl2^{+} RGCs is at a certain critical level, as it is in the *Isl2-EphA3*$^{wt/ki}$ mouse. In these mice, Isl2^{+} and Isl2^{-} projections initially overlap to a moderate degree. Development could then proceed in one of two possible ways. The projections could begin to separate, and the positive feedback of correlated activity within each RGC population would drive them to form separate, orderly isotropic maps similar to the ones found in *Isl2-EphA3*$^{ki/ki}$ animals. Alternatively, the influence of correlated activity could overcome the EphA distinctions and drive the formation of a single map. At this critical level of EphA3 over-expression, stochastic events like small changes in the level of EphA3 expression or the overall strength of EphA/ephrin-A signaling would be enough to push the outcome towards either a single or a double map. Once a structure begins to coalesce, activity-dependent refinement would encourage neighboring RGCs to organize themselves in accordance with the emerging map, solidifying it. Interestingly, if the

refinement begins simultaneously at different points in the SC, it is possible for this process to produce a single map in one half of the SC and a doubled map in the other half, a result that was repeatedly observed *in vivo*. In the absence of correlated activity, the variability of the maps would disappear, as it actually does in *Isl2-EphA3*$^{wt/ki}$ mice lacking β2.

The collicular map is also ordered in the elevation (dorsoventral) axis; RGCs from the ventral retina go to the medial SC, and RGCs from the dorsal retina go the lateral SC (McLaughlin and O'Leary, 2005). Much less is known about mapping in this system. Axons in the optic tract are already somewhat presorted along the elevation but not the azimuth axis (Plas et al., 2005). For the retinal projection to the SC/optic tectum, in which the elevation axis is represented mediolaterally, there is evidence that a mediolateral gradient of Wnt3a controls mapping through the Ryk and Frizzled receptors, that a gradient of Sema3 encourages RGCs to terminate laterally, and that interfering with either the cell adhesion molecule ALCAM or its receptor L1's interaction with ankyrin causes ectopic, laterally-located termination zones in mice with normal retinas (Schmitt et al., 2006; Liu et al., 2004; Buhusi et al., 2008; Buhusi et al., 2009). However, by far the most popular hypothesis has been that elevation signaling is controlled by signaling through EphBs and their ligands, the ephrin Bs. Mice express ephrin-B1, EphB1, EphB2, and EphB3 in a mediolateral gradient across the developing SC, consistent with a role in elevation mapping (Hindges et al., 2002). Mice that are deficient in EphB1, EphB2, and/or EphB3 may exhibit ectopic laterally-located termination zones in the SC in early life, showing that loss of the molecules affects RGC branching within the colliculus (Hindges et al., 2002; McLaughlin et al., 2009). To test this hypothesis, in chapter 1, I

imaged the SCs of various mutant mice with compromised EphB or ephrin-B signaling. Contrary to expectations, I found no quantitative change in the precision of topographic maps of the superior colliculus of animals with even severe disruptions of EphB signaling. However, knocking out most of the animal's EphBs did alter the angles that the vertical and horizontal meridians made with each other. Therefore, my results strongly oppose a role for signaling by the molecular guidance cues EphBs and ephrin-Bs in the precision of map topography but suggest that EphBs may be involved in the overall structure of the SC map.

The retinogeniculocortical pathway

Retinotopy is preserved as information is passed from the retina to the dorsolateral geniculate nucleus (dLGN) and on to the cortex, with neurons in the medial part of V1 receiving input from the nasal retina and neurons in the caudal part of V1 receiving input from the ventral retina (Kalatsky and Stryker, 2003). Mapping in the retinogeniculocortical pathway shares many similarities with retinocollicular mapping, including a dependence on EphA-signaling and retinal waves. The combination of these two factors patterns almost the entirety of the azimuth axis of cortex, just like it does in the SC (Cang et al., 2008a; Cang et al., 2008b). Similarly, I show in chapter 1 that EphB signaling plays similar roles in the SC and cortex. Mice missing even four of the five EphBs had cortical maps of normal topographic quality, showing that EphBs are not important for topographic precision. However, some mice missing multiple EphBs had elevation maps that were rotated abnormally far towards the midline. The penetrance of this phenotype increased as more signaling was disrupted through the loss of more EphBs,

and its presence depended most on the loss of ephrin-B1 and kinase activity from EphB2. This data suggests that, like in SC, EphBs in cortex guide the formation of the visual map as a whole.

Curiously, while cortical elevation maps in EphB mutants are rotated towards the midline, cortical maps in mice missing all cortical ephrin-A signaling are rotated abnormally in the opposite direction (Cang et al., 2005a). My findings are consistent with the hypothesis that the normal alignment of visual maps is a compromise between distinct molecular gradients for the azimuth and elevation axes that are not at right angles. Under the influence of neural activity, such a map would become coherent and assume an intermediate orientation.

I did not find that all aspects of mapping in the retinocollicular and retino-geniculocortical pathways were the same, however. In chapters 2 and 4, I saw that the *Isl2-EphA3*$^{ki/ki}$ and *Isl2-EphA3*$^{wt/ki}$ mice have only a single map of normal quality in cortex despite possessing a variety of mapping phenotypes in the SC. Since it is known that EphA signaling is important for proper cortical mapping, these results in *Isl2-EphA3* knock-in mice imply that the retinogeniculocortical pathways of these mice somehow compensate for the retinal EphA3 over-expression (Cang et al., 2005a). Thus, in chapter 3, we further examined retinogeniculocortical mapping in these mutants by performing retrograde tracing from cortex to dLGN and anterograde tracing from retina to dLGN in *Isl2-EphA3*$^{ki/ki}$ mice, which consistently have doubled collicular maps of space. We found that in this mouse, the relationship between points on the retina, dLGN, and cortex is always one-to-one-to-one, implying that the cortical map is single because the retinogeniculate projection only contains a single map of space. More investigation is

needed to understand whether the single geniculate map arises from the map-collapsing properties of retinal waves or the way molecular cues in the dLGN guide incoming $Isl2^{+}$ and $Isl2^{-}$ RGCs.

The corticocollicular projection

Higher visual brain areas also make connections with each other, but little is known about how topographic maps from these brain regions are merged. The SC receives input from many sensory areas, including the retina, as discussed previously, and V1. RGCs project to the dorsal-most layer of the SC, the upper stratum griseum superficiale (SGS), while axons from V1 terminate in a deeper layer called the lower SGS (May, 2005). This corticocollicular projection provides a link between the two major streams of visual processing, the retinocollicular pathway, used for some reflexive visual behaviors, and the retinogeniculocortical pathway involved in conscious vision. The axons from V1 arrange themselves so that they are in register with the topography of the retinocollicular map (Dräger and Hubel, 1976). In chapter 2, we investigated which of the two major factors was responsible for the alignment of the V1 projection with collicular topography. If gradients of molecular guidance cues were responsible, it would mean that RGC and V1 axons independently use the same graded labels, most probably the EphAs and ephrin-As, expressed in the SC to specify each map. Therefore, both temporal RGCs and lateral V1 projection neurons, say, would project to the same A-P location in the SC because they express similar amounts of EphA receptors. On the other hand, if activity-dependent were responsible, it would mean that Hebbian-type mechanisms are used to match up V1 and RGC neurons that monitor the same location in

space (Hebb, 1949). The retinocollicular map would be established first, and V1 axons would then form synapses with SC neurons onto which RGCs that share common activity patterns or cell surface molecules synapse. Support for this model comes from previous studies that showed that in retinal input can be instructive for the alignment of auditory and visual maps in the owl optic tectum and ferret SC (King et al., 1988; Knudsen and Brainard, 1991). In wildtype animals, the results of either model coincide, since both the V1 and the SC have similar gradients of EphAs and ephrin-As and receive similar input from the retina. However, in the *Isl2-EphA3*$^{ki/ki}$ mouse, these models can be distinguished: while this manipulation does not affect the molecular gradients present in the SC and V1, it does change the retinal input so that each point in the retina sends input to one place in visual cortex but two places in the SC. We found that the development of the corticocollicular projection occurs after the bulk of retinocollicular development is done, consistent with the activity-dependent model. Further support for that model came from examining the *Isl2-EphA3*$^{ki/ki}$ mouse, where we found a duplicated corticocollicular projection, matching the doubled maps of space in the SC. Altering retinal activity patterns by knocking out β2 in a *Isl2-EphA3*$^{ki/ki}$ background revealed that cortical projections no longer doubled, showing that retinal waves are necessary for the aligning the V1 projection. However, in mice that lacked or had greatly reduced retinal input to both structures because of enucleation or a lack of the Math5 transcription factor, which is essential for RGC differentiation, rough corticocollicular topography remains. In all, these results suggest that although some molecular cues must be present that guide V1 axons to their approximate locations, retinal activity is instructive for the precise alignment of the V1 and SC maps.

Conclusion

Overall, this dissertation shows how patterned neural activity and molecular guidance cues shape topographic maps throughout the visual system. Each chapter combines the fruits of different techniques, including functional imaging, anatomical tracing, and computational modeling, to provide a more complete understanding of map development.

List of References

Allen Developing Mouse Brain Atlas (2009) [Internet]. Seattle (WA): Allen Institute for Brain Science.

Bansal A, Singer JH, Hwang BJ, Xu W, Beaudet A, Feller MB (2000) Mice lacking specific nicotinic acetylcholine receptor subunits exhibit dramatically altered spontaneous activity patterns and reveal a limited role for retinal waves in forming ON and OFF circuits in the inner retina. J. Neurosci. 20:7672-7681.

Bevins N, Lemke G, Reber M (2011) Genetic dissection of EphA receptor signaling dynamics during retinotopic mapping. J Neurosci. 31:10302-10310.

Brown A, Yates PA, Burrola P, Ortuno D, Vaidya A, Jessell TM, Pfaff SL, O'Leary DD, Lemke G (2000) Topographic mapping from the retina to the midbrain is controlled by relative but not absolute levels of EphA receptor signaling. Cell 102:77-88.

Buhusi M, Demyanenko GP, Jannie KM, Dalal J, Darnell EP, Weiner JA, Maness PF (2009) ALCAM regulates mediolateral retinotopic mapping in the superior colliculus. J Neurosci. 29:15630-15641.

Buhusi M, Schlatter MC, Demyanenko GP, Thresher R, Maness PF (2008) L1 interaction with ankyrin regulates mediolateral topography in the retinocollicular projection. J Neurosci. 28:177-188.

Butts DA, Rokhsar DS (2001) The information content of spontaneous retinal waves. J. Neurosci. 21:961-973.

Cang J, Kaneko M, Yamada J, Woods G, Stryker MP, Feldheim DA (2005a) Ephrin-As guide the formation of functional maps in the visual cortex. Neuron 48:577-89.

Cang J, Niell CM, Liu X, Pfeiffenberger C, Feldheim DA, Stryker MP (2008a) Selective disruption of one Cartesian axis of cortical maps and receptive fields by deficiency in ephrin-As and structured activity. Neuron 57:511-523.

Cang J, Renteria RC, Kaneko M, Liu X, Copenhagen DR, Stryker MP (2005b) Development of precise maps in visual cortex requires patterned spontaneous activity in the retina. Neuron 48:797-809.

Cang J, Wang L, Stryker MP, Feldheim DA (2008b) Roles of ephrin-As and structured activity in the development of functional maps in the superior colliculus. J Neurosci 28:11015-11023.

Chandrasekaran AR, Furuta Y, Crair MC (2009) Consequences of axon guidance defects on the development of retinotopic receptive fields in the mouse colliculus. The Journal of Physiology 587:953-963.

Cowan CA, Henkemeyer M (2002) Ephrins in reverse, park and drive. Trends Cell Biol 12:339-346.

Davy A, Aubin J, Soriano P (2004) Ephrin-B1 forward and reverse signaling are required during mouse development. Genes Dev 18:572-583.

Debski EA, Cline HT (2002) Activity-dependent mapping in the retinotectal projection. Curr Opin Neurobiol 12:93-99.

Dhande OS, Hua EW, Guh E, Yeh J, Bhatt S, Zhang Y, Ruthazer ES, Feller MB, Crair MC (2011) Development of single retinofugal axon arbors in normal and β2 knock-out mice. J Neurosci 31:3384-3399.

Drager UC, Hubel DH (1976) Topography of visual and somatosensory projections to mouse superior colliculus. J Neurophysiol 39:91-101.

Dravis C, Henkemeyer M (2011) Ephrin-B reverse signaling controls septation events at the embryonic midline through separate tyrosine phosphorylation-independent signaling avenues. Dev Biol 355:138-151.

Dravis C, Yokoyama N, Chumley MJ, Cowan CA, Silvany RE, Shay J, Baker LA, Henkemeyer M (2004) Bidirectional signaling mediated by ephrin-B2 and EphB2 controls urorectal development. Dev Biol 271:272-290.

Feldheim DA Personal communication.

Feldheim DA, Kim Y, Bergemann AD, Frisén J, Barbacid M, Flanagan JG (2000) Genetic analysis of ephrin-A2 and ephrin-A5 shows their requirement in multiple aspects of retinocollicular mapping. Neuron 25:563-574.

Feldheim DA, O'Leary DD (2010) Visual map development: Bidirectional signaling, bifunctional guidance molecules, and competition. Cold Spring Harb Perspect Biol 2:a001768.

Flanagan JG (2006) Neural map specification by gradients. Curr Opin Neurobiol 16:59-66.

Flenniken AM, Gale NW, Yancopoulos GD, Wilkinson DG (1996) Distinct and overlapping expression patterns of ligands for eph-related receptor tyrosine kinases during mouse embryogenesis. Dev Biol 179:382-401.

Genander M, Halford MM, Xu N, Eriksson M, Yu Z, Qiu Z, Martling A, Greicius G, Thakar S, Catchpole T, Chumley MJ, Zdunek S, Wang C, Holm T, Goff SP, Pettersson S, Pestell RG,

Grubb MS, Rossi FM, Changeux J, Thompson ID (2003) Abnormal functional organization in the dorsal lateral geniculate nucleus of mice lacking the [beta]2 subunit of the nicotinic acetylcholine receptor. Neuron 40:1161-1172.

Hebb D (1949) *The organization of behavior: A neurophysiological theory.* Wiley: New York.

Henkemeyer M, Frisén J (2009) Dissociation of EphB2 signaling pathways mediating progenitor cell proliferation and tumor suppression. Cell 139:679-692.

Henkemeyer M, Orioli D, Henderson JT, Saxton TM, Roder J, Pawson T, Klein R (1996) Nuk controls pathfinding of commissural axons in the mammalian central nervous system. Cell 86:35-46.

Hindges R, McLaughlin T, Genoud N, Henkemeyer M, O'Leary DDM (2002) EphB forward signaling controls directional branch extension and arborization required for dorsal-ventral retinotopic mapping. Neuron 35:475-487.

Huberman AD, Wei W, Elstrott J, Stafford BK, Feller MB, Barres BA (2009) Genetic identification of an on-off direction- selective retinal ganglion cell subtype reveals a layer-specific subcortical map of posterior motion. Neuron 62:327-334.

Kaas JH, Guillery RW (1973) The transfer of abnormal visual field representations from the dorsal lateral geniculate nucleus to the visual cortex in Siamese cats. Brain Res 59:61-95.

Kalatsky VA, Stryker MP (2003) New paradigm for optical imaging: Temporally encoded maps of intrinsic signal. Neuron 38:529-545.

King AJ, Hutchings ME, Moore DR, Blakemore C (1988) Developmental plasticity in the visual and auditory representations in the mammalian superior colliculus. Nature 332:73-76.

Knudsen EI, Brainard MS (1991) Visual instruction of the neural map of auditory space in the developing optic tectum. Science 253:85-87.

Koulakov AA, Tsigankov DN (2004) A stochastic model for retinocollicular map development. BMC Neurosci 5:30.

Liu Y, Berndt J, Su F, Tawarayama H, Shoji W, Kuwada JY, Halloran MC (2004) Semaphorin3D guides retinal axons along the dorsoventral axis of the tectum. J Neurosci 24:310-318.

Lopez-Bendito G, Molnar Z (2003) Thalamocortical development: How are we going to get there? Nat Rev Neurosci. 4:276-289.

Marcus RC, Gale NW, Morrison ME, Mason CA, Yancopoulos GD (1996) Eph family receptors and their ligands distribute in opposing gradients in the developing mouse retina. Dev Biol 180:786-789.

May PJ (2006) The mammalian superior colliculus: Laminar structure and connections. In: Progress in brain research (J.A. Büttner-Ennever, ed), pp321-378. Elsevier.

McLaughlin T, Lim Y-, Santiago A, O'Leary DDM (2009) EphB receptors in retinal ganglion cells direct dorsal-ventral retinotopic mapping by specific guidance of branches. Program 411.10. Neuroscience Meeting Planner (Online) .

McLaughlin T, O'Leary DDM (2005) Molecular gradients and development of retinotopic maps. Annu Rev Neurosci 28:327-355.

McLaughlin T, Torborg CL, Feller MB, O'Leary DDM (2003) Retinotopic map refinement requires spontaneous retinal waves during a brief critical period of development. Neuron 40:1147-1160.

Meister M, Wong R, Baylor D, Shatz C (1991) Synchronous bursts of action potentials in ganglion cells of the developing mammalian retina. Science 252:939-943.

Mesulam MM (1998) From sensation to cognition. Brain 121:1013-1052.

Orioli D, Henkemeyer M, Lemke G, Klein R, Pawson T (1996) Sek4 and nuk receptors cooperate in guidance of commissural axons and in palate formation. EMBO J 15:6035-6049.

Pak W, Hindges R, Lim Y, Pfaff SL, O'Leary DDM (2004) Magnitude of binocular vision controlled by islet-2 repression of a genetic program that specifies laterality of retinal axon pathfinding. Cell 119:567-578.

Pitulescu ME, Adams RH (2010) Eph/ephrin molecules- a hub for signaling and endocytosis. Genes Dev 24:2480-2492.

Plas DT, Dhande OS, Lopez JE, Murali D, Thaller C, Henkemeyer M, Furuta Y, Overbeek P, Crair MC (2008) Bone morphogenetic proteins, eye patterning, and retinocollicular map formation in the mouse. J Neurosci 28:7057-7067.

Plas DT, Lopez JE, Crair MC (2005) Pretarget sorting of retinocollicular axons in the mouse. J Comp Neurol 491:305-319.

Reber M, Burrola P, Lemke G (2004) A relative signalling model for the formation of a topographic neural map. Nature 431:847-853.

Schiller PH, Stryker M, Cynader M, Berman N (1974) Response characteristics of single cells in the monkey superior colliculus following ablation or cooling of visual cortex. J Neurophysiol 37:181-94.

Schmitt AM, Shi J, Wolf AM, Lu CC, King LA, Zou Y (2006) Wnt-ryk signalling mediates medial-lateral retinotectal topographic mapping. Nature 439:31-37.

Shimoyama M, Matsuoka H, Nagata A, Iwata N, Tamekane A, Okamura A, Gomyo H, Ito M, Jishage K, Kamada N, Suzuki H, Tetsuo Noda T, Matsui T (2002) Developmental expression of EphB6 in the thymus: Lessons from EphB6 knockout mice. Biochem Biophys Res Commun 298:87-94.

Sperry R (1963) Chemoaffinity in the orderly growth of nerve fiber patterns and connections. Proc Natl Acad Sci USA 50:703-710.

Sun C, Warland DK, Ballesteros JM, van der List D, Chalupa LM (2008) Retinal waves in mice lacking the β2 subunit of the nicotinic acetylcholine receptor. Proceedings of the National Academy of Sciences 105:13638-13643.

Thaler JP, Koo SJ, Kania A, Lettieri K, Andrews S, Cox C, Jessell TM, Pfaff SL (2004) A postmitotic role for isl-class LIM homeodomain proteins in the assignment of visceral spinal motor neuron identity. Neuron 41:337-350.

Triplett JW, Owens MT, Yamada J, Lemke G, Cang J, Stryker MP, Feldheim DA (2009) Retinal input instructs alignment of visual topographic maps. Cell 139:175-185.

Tsigankov DN, Koulakov AA (2006) A unifying model for activity-dependent and activity-independent mechanisms predicts complete structure of topographic maps in ephrin-A deficient mice. J Comput Neurosci 21:101-114.

Tsigankov DN, Koulakov AA (2010) Sperry versus Hebb: Topographic mapping in Isl2/EphA3 mutant mice. BMC Neurosci 11:155.

Wang HU, Chen Z, Anderson DJ (1998) Molecular distinction and angiogenic interaction between embryonic arteries and veins revealed by ephrin-B2 and its receptor eph-B4. Cell 93:741-753.

Wang L, Rangarajan KV, Lawhn-Heath CA, Sarnaik R, Wang B, Liu X, Cang J (2009) Direction-specific disruption of subcortical visual behavior and receptive fields in mice lacking the β2 subunit of nicotinic acetylcholine receptor. J Neurosci 29:12909-12918.

Williams SE, Mann F, Erskine L, Sakurai T, Wei S, Rossi DJ, Gale NW, Holt CE, Mason CA, Henkemeyer M (2003) Ephrin-B2 and EphB1 mediate retinal axon divergence at the optic chiasm. Neuron 39:919-935.

Wong RO, Meister M, Shatz CJ (1993) Transient period of correlated bursting activity during development of the mammalian retina. Neuron 11:923-938.

Xu W, Orr-Urtreger A, Nigro F, Gelber S, Sutcliffe CB, Armstrong D, Patrick JW, Role LW, Beaudet AL, De Biasi M (1999) Multiorgan autonomic dysfunction in mice lacking the β2 and the β4 subunits of neuronal nicotinic acetylcholine receptors. J Neurosci 19:9298-9305.

Yokoyama N, Romero MI, Cowan CA, Galvan P, Helmbacher F, Charnay P, Parada LF, Henkemeyer M (2001) Forward signaling mediated by ephrin-B3 prevents contralateral corticospinal axons from recrossing the spinal cord midline. Neuron 29:85-97.

Publishing Agreement

It is the policy of the University to encourage the distribution of all theses, dissertations, and manuscripts. Copies of all UCSF theses, dissertations, and manuscripts will be routed to the library via the Graduate Division. The library will make all theses, dissertations, and manuscripts accessible to the public and will preserve these to the best of their abilities, in perpetuity.

I hereby grant permission to the Graduate Division of the University of California, San Francisco to release copies of my thesis, dissertation, or manuscript to the Campus Library to provide access and preservation, in whole or in part, in perpetuity.

September 6th, 2011

Author Signature Date